ELSEVIER

Advances in Colloid and Interface Science
67 (1996) 1–118

ADVANCES IN COLLOID AND INTERFACE SCIENCE

Electrokinetic properties, colloidal stability and aggregation kinetics of polymer colloids[1]

R. Hidalgo-Álvarez[a]*, A. Martín[a], A. Fernández[a], D. Bastos[a], F. Martínez[a], F.J. de las Nieves[b]

[a] *Biocolloid and Fluid Physics Group, Department of Applied Physics, Faculty of Sciences, Campus Fuentenueva, University of Granada, Granada 18071, Spain*

[b] *Group of Complex Fluid Physics, Department of Applied Physics, Faculty of Sciences, University of Almeria, Almeria, Spain*

Abstract

The purpose of this article is to present some important advances in the electrokinetic and colloidal characterization of polymer colloids. Special attention is paid to the new electrokinetic techniques: diffusiophoresis, dielectric dispersion and electro-acoustic. Also the most recent theoretical approaches are reviewed with respect to the electrokinetic properties of polymer colloids. Recently there has been intense discussion concerning electrokinetic processes and the theories used for data interpretation. Several concerns have been raised relating to the inability of the different processes and theories to yield the same electrokinetic potential. The most important explanations (shear plane expansion, preferential ion adsorption, osmotic swelling, crossing of the mobility/ζ-potential and anomalous surface conductance) to the electrokinetic behaviour of polymer colloids are discussed and analyzed. Also the effect of heat treatment on the electrokinetic properties of different types of polymer colloids is extensively considered.

With regard to the colloidal stability of polymer colloids, three- and two-dimensional aggregations are presented. First, the stability factor W is introduced using the classical theory DLVO and the values obtained of Hamaker constant compared with the theoretical values estimated from the Lifshitz theory. The differences usually found by several authors are explained as due to the hydrodynamic interaction. Special attention is paid

1 This review is dedicated to Professor Johannes Lyklema on the occasion of his retirement from the Physical and Colloid Chemistry Department of the Agricultural University, Wageningen, The Netherlands

* Corresponding author

0001-8686/96/$32.00
PII: S0001-8686(96)00297-7

to the extended DLVO theory for studying homocoagulation of polymer colloids in three dimensions and to the new expressions for the van der Waals, electrostatic and structural forces that must be deduced to study the colloidal stability of polymer colloids in two dimensions. Also, the heterocoagulation of polymer colloids with different sign of surface charge density and particle size is reviewed, and a new definition of the heterocoagulation stability factor is given.

The aggregation kinetics of polymer colloids in three dimensions is analyzed using the Smoluchowski theory (in terms of the reaction kernels k_{ij}) in the cases where the Smoluchowski's equation is analytically solvable (constant, sum, product kernel and linear combinations thereof). The dynamic scaling in aggregation phenomena with polymer colloids is studied using the classification scheme for homogeneous kernels due to Van Dongen and Ernst based on the relative probabilities of large clusters sticking to large clusters, and small clusters sticking to large clusters. The techniques (multiparticle and single particle detection) enabling us to provide cluster-size distribution of aggregating polymer colloids are also presented.

Finally, the aggregation kinetics of two dimensional aggregation of polymer colloids is studied on the basis of the fractal dimension of the aggregates.The different scaling theories for two-dimensional aggregation are also considered.

Contents

1. Introduction

Polymer colloids play an important role in many industrial processes. These include the manufacture of synthetic rubber, surface coatings, adhesives, additives in paper, textiles and many others. The rapid increase in the utilisation of latices over the last two decades is due to a number of factors. Water-based systems avoid many of the environmental problems associated with organic-solvent based systems; latices can be designed to meet a wide range of application problems; emulsion polymerization on a large scale proceeds smoothly for a wide range of monomers.

The spherical shape of many polymer beads and their narrow size distribution makes them most suitable for fundamental studies requiring well-defined monodisperse systems. The particles can be useful e.g., as size standards for instrumental calibration and as carriers in antibody diagnostic tests. They provide valuable experimental systems for the study of many colloidal phenomena and recently have been used as model systems for the simulation of molecular phenomena, including nucleation, crystallization and the formation of glasses. The long time scale of the motion of polymer colloids enables us to make real time observations on various phenomena, which have been impossible for atomic and molecular systems. Since the polymer colloids are much smaller than the bubbles, and can be dispersed "monomolecularly" in liquids (namely, not in contact with each other as was the case with the bubbles), the thermal motion can be visualized. Thus, the polymer colloids are a much more realistic model for atoms and molecules than the bubble rafts.

Polymer colloids are often treated as "model" particles: monodisperse, amorphous microspheres with smooth, uniform surfaces and rigidly attached, well-defined surface functional groups. Their sphericity, monodispersity, and virtually zero dielectric constant in comparison to water made them particularly suitable for fundamental electrokinetic and colloidal aggregation studies. Electrokinetic processes are widely used to determine the electrical charge on the slipping plane of a polymer colloid. Electrokinetic is closely related to the slipping process, the ζ-potential being the potential at the slipping plane. Very recently, Lyklema [1] considered this very aspect in a very interesting paper.

The preparation of uniform polymer microspheres via emulsion polymerization has been extensively reviewed by Ugelstad [2]. Parameters such as particle size, surface charge density and type of charge group can be controlled by varying the conditions of the polymerization,

allowing latices to be "designed" for specific end uses. For these reasons, polymer colloids have been widely used as model systems in investigations into electrokinetic and colloidal stability phenomena. However, it has been in the area of electrokinetics that the polymer colloids have failed to live up to much of the initial expectation. One particular disappointment has been the failure to find a convincing explanation for the behaviour of the ζ-potential of polymer colloids as a function of electrolyte concentration, which has brought the ideality of the system into serious question.

The aggregation of polymer colloids is a phenomenon which underlies many chemical, physical, and biological processes. Currently, it is believed that there are two limiting regimes of irreversible colloidal, or cluster aggregation [3]. Diffusion-limited cluster aggregation (DLCA) occurs when every collision between diffusing clusters results in the formation of a bond. The rate of aggregation is then limited by the time it takes the clusters to diffuse towards one another. Reaction-limited cluster aggregation (RLCA) occurs when only a small fraction of collisions between clusters results in the formation of a bond. Here, the aggregation rate is limited not by diffusion, but by the time it takes for the clusters to form a bond. The precise range of experimental conditions which result in DLCA and RLCA is a topic of current research [4–7].

Little experimental work has been done to determine the form and time dependence of the cluster–size distributions that arise during colloidal aggregation [8]. Determining the detailed form of these size distributions is important since many of the physical properties of a colloidal suspension of a polymer matrix depend on this distribution. Moreover, it is essential to know the form of the size distribution in order to properly interpret static and dynamic light scattering measurements on colloidal aggregation. In this review, we describe measurements of cluster–size distribution and dynamic scaling which arise during salt-induced aggregation of polymer colloids. The topic is advancing rapidly at the present time, synthetically with the preparation of new materials and physically with the development of new techniques for their characterization. These recent advances will be reviewed and extensively discussed in this paper.

2. Purification of polymer colloids

Polymer colloids prepared by emulsion polymerization can have different electrokinetic and stability properties according to the type of mono-

mers and procedures used during synthesis. However, the development of methods for the preparation of polymer latices containing monodisperse particles, particularly in the absence of surface active agents, has led to their widespread use in the testing of theories of colloidal phenomena. After preparation, a cleaning procedure is required to remove salts, oxidation products, oligomeric materials and any remaining monomers from the latex. A worrying feature of the cleaning and characterization procedures is that different authors, using similar recipes for the latex preparation, have observed different surface groups. For example, Vanderhoff [9–10] using mixed-bed ion-exchange resins to remove ionic impurities have concluded that only strong-acid groups, i.e., sulphate groups arising from the initiator fragments, are present on the latex surface; their conclusion was based on the single end point observed in conductometric titration. Other authors [11–12], particularly those using dialysis as a cleaning procedure, have detected the presence on the surface of weak-acid groupings in addition to the strong-acid groupings. In fact, weak-acid groups could be produced by the hydrolysis of surface sulphate groups to alcohol (hydroxyl) groups followed by oxidation to carboxyl groups [11]. Moreover, Lerche and Kretzschmar [13] have shown that the surface charge density of several latex samples depended on the cleaning method used, and that the ion-exchange and dialysis was not able to remove charged oligomeric material from the particle surfaces completely. Thus, a very key question has arisen as to which set of results is correct and which cleaning procedure should be used by preference when preparing clean latices for fundamental investigations. It has been found that serum replacement is an as reliable and easy method to clean latex suspensions [14]. Nevertheless, the ion form of the latices cleaned by serum replacement is only achieved after ion-exchange with resins. A cycle of several centrifugation/redispersion might probably be the only method able to remove oligomer chains from the surface of polymer colloids [15]. The different methods for preparing clean latices do provide polymer colloids with quite different electrokinetic and stability properties. Cleaning of polymer colloids is of paramount importance for electrokinetic and stability studies. The removal of polymeric impurities is essential in order to have both control over the surface charge and of the supporting electrolyte concentration.

Also, the deionization of latex suspensions plays a decisive role in the formation of fluid-like, crystalline, or amorphous interparticle structure [16].

3. Surface characterization of polymer colloids

Once clean polymer colloids have been prepared, it is necessary to determine their surface characteristics. The surface structure and characteristics of polymer colloids are important for many reasons. They determine the stability of the colloidal dispersion, the adsorption characteristics of surfactants, latex film formation mechanisms, and the properties of these films obtained from latex. They also provide information on the emulsion polymerization mechanisms, especially when structured beads are synthesized. The techniques suitable for surface analysis of polymer colloids are numerous. Conductometric titration of polymer colloids is considered a basic technique for surface-charge determination [17–24]. Other classical methods include soap titration [25–27], and contact angle measurements [28–30]. Moreover, surface topography of polymer beads is usually studied by electron microscopy (transmission electron microscopy) [30]. The problems associated with the surface characterization of polymer colloids have been studied by several authors [17–18,20,31–36]. Labib and Robertson [32] have shown that conductometric titration of polymer beads is more difficult to interpret than conductometric titration of free acids, and proposed a method to determine the stoichiometric end-points in an appropriate and reliable manner. Hlavacek et al. [37] have demonstrated that the variation in the composition of the liquid phase which occurs during acid–base titrations of polymer colloid suspensions can be explained by a mechanism involving weak acid or base ion-exchange reactions coupled with surface ionization. Identification of the sites involved and their thermodynamic constants allows a good quantitative prediction of experimental results, gives an explanation for the influence of ionic strength on the pH curves and an indication of the state of the solid surface. Also, Gilany [38] determined the surface charge density of polystyrene beads by using the concentration and activity of a binary electrolyte added to the latex dispersion. The distribution of ions was calculated by means of the non-linearized Poisson–Boltzmann equation and the cell model. The effective charge of latex beads was found to be smaller than the analytical charge. It was concluded that a small effective charge cannot be explained with specific binding of counter ions to the polymer colloids.

The hydrophobic or hydrophilic character of the polymer surface may have a certain influence on the surface structure of the polymer colloids [30]. The hydrophobic surface of polymer colloids plays a crucial role in the ion distribution in the interfacial region. Contact angle is a measurement

of the hydrophobicity of the polymer–solution interface, and has been used to obtain information on the surface structure of core-shell and block polymer colloids [28–30,39]. To determinate the water of hydration around charged polymer beads, Grygiel and Starzak [40] have studied the interfacial properties of carboxylated polymer beads using environment-sensitive laser excitation spectroscopy of the Eu^{3+} ion. This ion spectroscopy technique uses the changes in the electronic properties of the ion in different molecular environment to elucidate the structure and properties of those environments. Lifetime measurements show when binding to a highly charged surface (32.3 $\mu C\ cm^{-2}$) that the ion loses about half its waters of hydration while energy transfer from Eu^{3+} for these highly charged surfaces gives an ion separation (7.1 Å) that is consistent with the known average separation of the surface sites (7.1 Å). For lesser charged beads (15.1 and 2.6 $\mu C\ cm^{-2}$, respectively), the energy transfer separation distance is smaller than the surface site–site separation indicating energy transfer between surface-bound and interfacial ions. For lesser charged beads an ion separation of about 9.6 and 9.7 Å is found, indicating that bound ions retain most of their water of hydration. Using osmotic pressure measurements Rymdén [35] has observed that the ion binding in aqueous polymer colloids depends on the surface charge density of carboxylated latex beads.

4. Electrokinetic background

Electrokinetic phenomena is a generic term applied to effects associated with the movement of ionic solutions near charged interfaces. Determination of the detailed structure of the electric double layer (e.d.l.) of polymer colloids is of primary importance in problems of stability and rheology of disperse systems, electrokinetic processes, filtration and electrofiltration, desalting of liquids on organic membranes, etc. Calculating ζ-potential of the polymer–solution interface is important when looking for an accurate microscopic explanation of electrokinetic phenomena.

To describe the structure of the e.d.l., information is needed on three potentials: the surface potential (Ψ_0), the potential of the Stern layer (Ψ_s) and the diffuse potential (Ψ_d). In the absence of organic impurities and polyelectrolytes adsorbed on the latex surface the Ψ_d-potential can be equated to the potential in the electrokinetic slipping plane (ζ-potential). In some cases, one can take Ψ_0 to be approximately equal to Ψ_s with indifferent electrolyte, and thus a detailed study of the structure

of the e.d.l. only requires a knowledge of the Ψ_0- and ζ-potentials. Extensive reviews [41–49] testify to the strong interest which has been shown in the electrokinetic phenomena during the past few decades.

Typical electrokinetic phenomena used to characterize polymer colloids are:

(1) *Electrophoresis*: where a uniform electric field is applied and the particle velocity is measured [17–20,49–107].

(2) *Streaming potential*: where a liquid flux is allowed to pass through a porous medium and the resulting electric potential difference is measured [103,108–114].

(3) *Electro-osmosis*: where an electric field is applied to a porous medium and the resulting volumetric flow of fluid is measured [54,115, 116].

(4) *Diffusiophoresis*: where a gradient of a solute in solution is applied and the migration of suspended colloid particles is measured [43,117–127]. Much of the early theoretical and experimental work on diffusiophoresis was on gaseous systems. Recent work, however, has focused on diffusiophoresis in liquid systems involving charged particles and electrolytes in solution.

(5) *Dielectric dispersion*: this technique involves the measurement of the dielectric response of a sol as a function of the frequency of an applied electric field. The complex dielectric constant [62,83,128–140] and/or electrical conductivity [141–147] of a suspension are measured as a function of frequency. The presence of dispersed particles generally causes the conductivity of this dispersion to deviate from the conductivity of the equilibrium bulk electrolyte solution

(6) *Electro-acoustic phenomena*: where alternating pressure fields are applied and the resulting electrical fields are measured [85,148–154]. When an alternating voltage is applied to a colloidal dispersion, the particles move back and forth at a velocity that depends on their size, ζ-potential and the frequency of the applied field. As they move, the particles generate sound waves. This effect was predicted by Debye [155] in 1933.

(7) *Electroviscous effects* in colloidal suspensions and electrolyte flows through electrically capillaries under a pressure gradient. The presence of an e.d.l. exerts a pronounced effect on the flow behaviour of a fluid. These effects are grouped together under the name of electroviscous effects [156–162].

In all cases there is a relative motion between the charged surface and the fluid containing the diffuse double layer. There is a strong coupling between velocity, pressure, electric, and ion concentration fields.

5. Calculation of zeta-potential

5.1. Electrokinetic phenomena

The literature pertaining to the study of electrokinetic properties of polymer colloids has a long and confusing history. We note specifically: (a) experimental electrokinetic data performed in different laboratories on ostensibly identical systems often conflict; (b)minor changes (cleaning procedure, surface charge, and particle size) may result in major differences in the measured electrokinetic data and (c) the ζ potentials obtained using the various electrokinetic processes on the same dispersions are quite different in values. These studies are difficult due to the complex interactions involved.

5.1.1. Electrophoretic mobility

Recent development of laser-based instrumentation for electrophoretic mobility experiments has made it possible to determine the zeta potential (ζ) of particles suspended in liquid media for systems that were difficult or impossible to study using classical techniques. The new instruments use electrophoretic light scattering (ELS) to measure electrophoretic mobilities. ELS allows direct velocity measurements for particles moving in an applied electric field by analyzing the Doppler shift of laser light scattered by the moving particles [65]. Recently Kontush et al. [163] designed a setup for studying nonlinear electrophoresis.

It is found that electrophoretic mobility curves pass through a minimum (anionic latex beads) or a maximum (cationic latex beads) as a function of increasing ionic strength. From a theoretical point of view, calculation of the ζ-potential from electrophoretic mobility data encounters a number of difficulties as a result of the polarization of e.d.l. The term "polarization" implies that the double layer around the particles is regarded as being distorted from its equilibrium shape by the motion of the particle. In general, for $\kappa a \leq 30$ it is necessary to account for e.d.l. polarization when calculating ζ [50,81,83,107]. There are several theoretical treatments to convert electrophoretic mobility (μ_e) data into ζ-potential under polarization conditions. Monodisperse spherical polymer latices have proved to be a very useful model system for testing the most recent theoretical approaches [50–51,68,70,107]. As most of the theories deal with spherically shaped particles of identical size, the introduction of monodisperse latices appeared to offer excellent chances for experimental verification of these theories. However, growing evidence

of anomalous behaviour of the ζ-potential as a function of 1:1 electrolyte concentration has appeared in the literature [17–19,21,50,68–71,79,83–91]. The standard electrophoretic theories used for the conversion of mobility into ζ-potential give rise to a maximum in ζ potential as well. This behaviour contradicts the Gouy–Chapman model which predicts a continuous decrease in potential. Various explanations for this maximum have been proposed [17,18,22,28,50,68,70,71,74,83,97,107], and some authors [112] have even pointed out that a maximum mobility value does not necessarily imply a maximum in ζ-potential, indicating that the conversion of mobility into ζ-potential of polystyrene microspheres/electrolyte solution interface should be done by means of a theoretical approach which takes into account all possible mechanisms of double layer polarization. Other authors, on the contrary, have pointed out that the appearance of a minimum (or maximum) in the ζ-potential is unimportant since the e.d.l. around polymer colloids, even with 1:1 electrolytes, cannot be explained on the basis of the Gouy–Chapman model. They proposed the use of a dynamic Stern layer [55] or an electric triple layer model [152] instead.

Overbeek [104] and Booth [105] were the first to incorporate polarization of the e.d.l. into the theoretical treatment. They assumed that the transfer and charge redistribution processes only involved the mobile part of the e.d.l. Also, O'Brien and White [57], starting with the same set of equations as Wiersema [106], have more recently published a theoretical approach to electrophoresis, which takes into account any combination of ions in solution with the possibility of very high ζ-potentials (up to 250 mV), far enough from the values to be expected in most experimental conditions. In simple terms, the theory of O'Brien and White predicts the measured electrophoretic mobility of a colloidal particle in an applied electric field to be the sum of three forces, viz: (1) an electric force propelling the particle, due to the charged nature of the particle, (2) a drag force due to hydrodynamic drag, and (3) a relaxation force due to an electric field induced in the opposite direction to the applied field as a result of the induced polarization within the diffuse layer of ions surrounding the particle.

It predicts the electrical force propelling the particle to be proportional to ζ and the retarding forces to be proportional to ζ^2. A maximum in the conversion of mobility to zeta potential is thus predicted for particles size and ionic strength conditions such that $5 < \kappa a \leq 100$.

The most striking features of O'Brien and White's theoretical treatment results are:

(a) For all values of $\kappa a \geq 3$, the mobility function has a maximum which becomes more pronounced at high κa values.

(b) The maximum occurs at $\zeta = 5$–7 (i.e. $\zeta \approx 125$–175 mV).

(c) Their computer solution is much more rapid than the earlier theoretical treatments used in the conversion of mobility into ζ-potential (up to 250 mV).

A simplified version and analytical form for the mobility equation, accurate to order $1/\kappa a$ and valid for our purposes for $\kappa a > 10$, can be expressed as [45]:

$$\tilde{\mu}_e = \frac{3\tilde{\zeta}}{2} - \frac{6\left[\frac{\tilde{\zeta}}{2} - \frac{\ln 2}{z}\left(1 - \exp(z\tilde{\zeta})\right)\right]}{2 + \frac{\kappa a}{1 + \frac{3m}{z^2}} \exp\left(-\frac{z\tilde{\zeta}}{2}\right)} \tag{1}$$

where m is the dimensionless ion drag coefficient given by

$$m = \frac{2\varepsilon_0 \varepsilon N_a^2 kT}{3\eta z \Lambda_0} \tag{2}$$

All the above cited theoretical approaches to convert mobility into ζ-potential assume the absence of ionic conduction inside the shear plane. In an attempt to account for this phenomenon theoretically, Semenikhin and Dukhin [61] developed an equation incorporating both the dimensionless ζ-potential, and the dimensionless diffused Ψ_d-potential. The mobility μ_e for a spherical particle with a thin e.d.l. ($\kappa a > 25$) in a 1:1 electrolyte is then a function of:

$$\mu_e = f(\zeta, \kappa a, m, g_1, g_2) \tag{3}$$

where

$$g_1 = f(p, \Psi_d, \zeta)$$
$$g_2 = f(p, \Psi_d, \zeta) \tag{4}$$

p is the ratio of the counterion diffusion coefficient near the particle to its value in the bulk solution and m is the dimensionless ionic drag coefficient.

If $\tilde{\zeta}$ and $\tilde{\Psi}_d$ are larger than 2, Eq. (3) can be simplified as:

$$\tilde{\mu}_e = \frac{3}{2}\tilde{\zeta}\left[\frac{1 + \mathrm{Rel}\left(\dfrac{4 \ln \cosh \tilde{\zeta}/4}{\tilde{\zeta}}\right)}{1 + 2\,\mathrm{Rel}}\right] \tag{5}$$

where

$$\mathrm{Rel} = \frac{\lambda_s}{\lambda a} = \frac{\exp(\tilde{\psi}_d/2) + 3m \exp(\tilde{\zeta}/2)}{\kappa a} \tag{6}$$

Dukhin [49] introduced the dimensionless relaxation parameter Rel as a measure of the effect of surface conductance on electrokinetic phenomena. It is noted that Rel can be used with two meanings, viz. in indicating the degree of e.d.l. polarization (non-equilibrium degree) for curved surfaces and in indicating the relative contribution of surface conductance to the total conductance in non-polarized systems (equilibrium states). An increase in the surface conductance and/or decrease in the radius results in an increase in Rel and thus in the polarization field in the direction of the induced electromigration current. We can distinguish two different mechanisms of electrical conduction: surface conduction associated with tangential charge transfer through the mobile portion of the e.d.l. (normal conduction taken into account in the Overbeek–Booth–Wiersema theory); and anomalous surface conduction, which is related to the tangential charge transfer between the slipping plane and the particle surface. The Semenikhin and Dukhin theory [61] considers only a particular case of anomalous conduction associated with the presence of a boundary layer. Figure 1 shows the variation of adimensional electrophoretic mobility as a function of adimensional ζ-potential for different electrokinetic radius values obtained by Eq. (5) for cationic latex particles. The differences with the O'Brien and White theory are quite clear.

The induced tangential ionic flow near the surface has to be provided for by radial ionic migration, diffusion and convection from beyond the e.d.l. where co- and counterion concentration can differ considerably from those near the surface. The concentration polarization results in an angular dependence of the ion concentration and the potential. Semenikhin and Dukhin [73] derived analytical formulae that express these dependencies for the cross section of the thin diffuse e.d.l. of a spherical particle. Contrary to the mathematical procedures employed

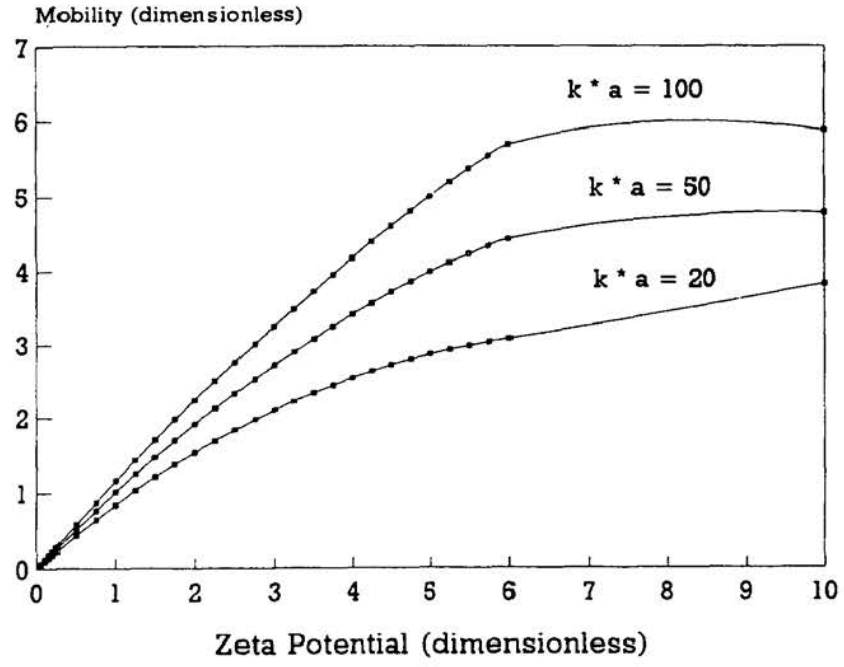

Fig. 1. Variation of dimensionless electrophoretic mobility as a function of dimensionless ζ-potential for different electrokinetic radius obtained by Eq. (5).

by Overbeek [104], Booth [105] and Wiersema [106], the main advantage of Dukhin and Semenikhin approach is the possibility of taking into account the effect of anomalous conduction on polarization.

The Semenikhin–Dukhin theory assumes that there is no contribution to the electrical conduction by any Stern layer ions, and that the PBE applies up to the outer Helmholtz plane. The diffuse layer ions between the shear plane and the outer Helmholtz plane do conduct a current and this anomalous surface conductance (inside the shear plane) dramatically reduces the mobility for a given value of ζ-potential. Consequently, for a description of electrophoresis under condition $R_{el} > 1$, not only the effect of diffusion flows must be taken into consideration, but also the change in the polarization potential across the thin diffuse layer [49].

Comparative studies using different theoretical treatments of mobility data for ζ-potential determination have been accomplished by various authors [51,68,83,99,162]. This kind of study is closely related to the determination of the detailed structure of the e.d.l. of colloidal particles.

This way, Baran et al. [68] have been successful in describing the structure of the e.d.l. for polystyrene latices. They used potentiometric titration, conductometry and electrophoresis to determine the surface charge, Ψ_0, Ψ_s, ζ-potentials and the surface conductivity of monodisperse particles of a polystyrene latex in solutions of alkali metal chlorides. Until rather recently, only Ψ_0 and ζ-potentials could be determined. Even here, the extensive data that are available on the ζ-potential cannot be regarded as a quantitative characteristic of the e.d.l., since any strict interpretation of electrokinetic data encounters at least three obstacles: polarization of the e.d.l. by an external field, the possible existence of a boundary layer with reduced mobility, and the significant roughness of the surface of solid particles.

There are no direct methods for the measurement of Ψ_s. In most studies, this potential has been taken equal to the ζ-potential, on the assumption that the slip boundary coincides with the boundary of the Stern layer. In some cases it has been assumed that $\Psi_s = \Psi_0$. Finally, some authors have attempted to estimate Ψ_s by using the Eversole and Boardman's method. Baran et al. [68] have calculated Ψ_s from relative electrical conductivity measurements, and have shown that the dependencies of Ψ_0 and Ψ_s on κa are identical. Hence, $\Psi_s = \Psi_0$ for the polystyrene latex particles. Baran et al. [68] have accomplished this by using the tables of Wiersema et al. [106], together with Semenikhin and Dukhin's equation [61]. For comparison, they also calculated ζ using Smoluchowski's equation.

The ζ-potential calculated with allowance for e.d.l. polarization, all the way up to $\kappa a \leq 60$, is substantially greater than the ζ-potential obtained from the Smoluchowski's equation. This effect was not taken into account in the second case of retarding action of the induced dipole created by polarization of the e.d.l. These differences are gradually smoothed out as the e.d.l. becomes thinner, as would be expected. The greater values of $\zeta_{S\text{-}D}$ in comparison with ζ_w are readily explained on the basis that the S-D theory takes the contribution for polarization into account for all ions of the diffuse layer, whereas Wiersema et al. account only for the ions of the hydrodynamically mobile part of the e.d.l. As the e.d.l. is compressed, the contribution from surface conduction drops substantially and with $C \geq 5\ 10^{-2}$ M, it becomes negligibly small. As a consequence, the difference between the values of ζ_{sm}, ζ_w and $\zeta_{S\text{-}D}$ disappears. Figure 2 shows the values of diffuse and ζ-potentials as a function of electrokinetic radius for anionic polystyrene latex particles. In this case the O'Brien and White and Semenikhin and Dukhin theories were used.

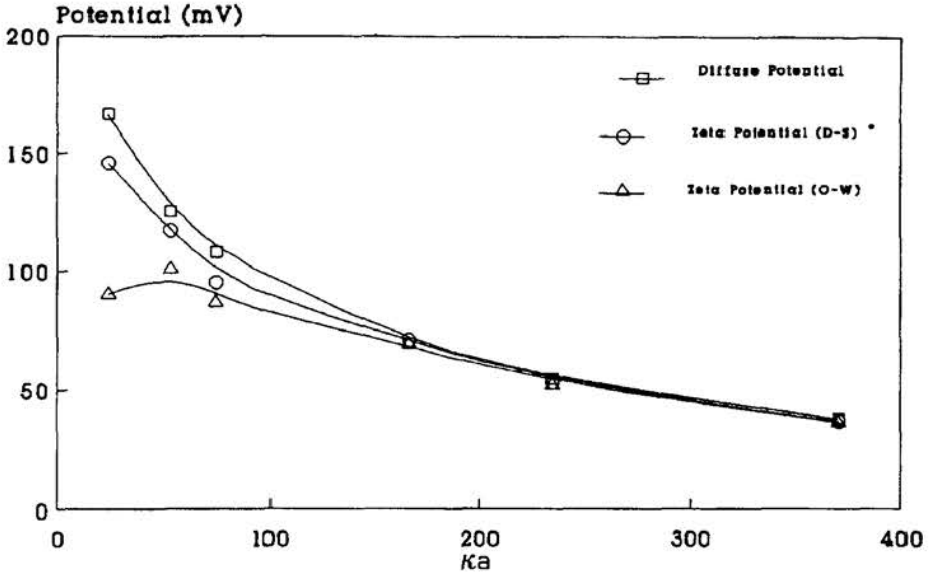

Fig. 2. Diffuse (□) and ζ-potential (○, Semenikhin–Dukhin; △, O'Brien–White) as a function of electrokinetic radius for an anionic polystyrene latex [162].

The ζ-potentials obtained by applying the Smoluchowski, Henry, Overbeek, Booth and O'Brien–White theoretical treatments of electrophoresis to experimental data of electrophoretic mobility of negatively charged polystyrene particles have been analyzed by several authors [81]. The results obtained applying the Overbeek and Booth's theories are compared with those obtained by O'Brien and White's numerical method. Important differences were found for non symmetrical electrolyte and small electrokinetic radius. Midmore and Hunter [83] have compared the ζ-potential values obtained from mobility data applying different theories (O'Brien–White, Semenikhin–Dukhin and Henry). Electrophoresis experiments were performed on two different negatively charged polystyrene latices, using potassium fluoride, chloride, bromide, and iodide as indifferent electrolytes. They found little or no difference in the mobility data for the various co-ions, which seems to indicate that co-ions are not specifically adsorbed onto the polystyrene surface.

O'Brien and White's theory [57] assumes the absence of ionic conduction inside the shear plane. Hence, in the opinion of Midmore and Hunter [83] this theory is not applicable to latex/electrolyte systems below electrolyte concentrations of about 0.01 M. Recently, however,

Russell et al. [107] have concluded that the O'Brien and White theory correctly predicts the relaxation term in electrophoretic mobility measurements which implicates that deviations from theory observed in previous studies cannot be attributed to an incorrect relaxation term. By definition, it also negates the presence of surface conduction (ion mobility by the electrokinetic shear plane) for highly charged sulphonate/styrene latices. This is an interesting observation in itself since highly charged latices are generally viewed to be nonideal in this sense.

An important result from the combined measurements carried out by various authors [68,91,112,162] is that even if the ζ-potential is corrected for the e.d.l. polarization, it is smaller than Ψ_d over a wide range of electrolyte concentrations (10^{-4} to 10^{-2} M), regardless of the method by which Ψ_d is determined. This may be due to the formation of a liquid layer with low hydrodynamic mobility on the particle surface, in which the ions retain high mobility. The thickness of this layer decreases with increasing ionic strength [48,68]. It is also possible that the relationship experimentally found by some authors is a consequence of the surface roughness of latex particles due to the presence of strongly bound (chemisorbed) oligomer molecules [50,69,70,108].

5.1.2. Streaming current and potential

According to the theory of Levine et al. [164] the streaming current in capillaries is related to the ζ potential by the following equation:

$$\frac{I_s}{\Delta P} = \frac{\varepsilon\zeta}{\eta C}\,[1 - G(\kappa a, \zeta)] \tag{7}$$

where G (κa, ζ) is the correction factor to the Helmholtz–Smoluchowski equation and C is the cell constant.

The streaming current data are obtained by multiplication of experimental streaming potential and a.c. conductance data. This way the effect of the polarization of the electrodes and their variable nature on electrokinetic signals is avoided, as is shown by van der Linde and Bijsterbosch [165]. Special attention has been paid to the preparation of homogeneous isotropic plugs of polystyrene spheres. The plugs have to be mechanically stable and completely wetted in order to avoid structural changes during electrokinetic investigations. The most successful preparation technique employs centrifugation, as also used for measurements of coagulation forces. During centrifugation, at specified

speed and ionic strength, the latex concentration at the bottom of the centrifuge tube increases. The lowest layers start to coagulate so that the non-coagulated sediment decreases in mass till the critical coagulation force is reached. In this case streaming potential experiments are performed at pressure differences up to 30 cm Hg. Even at this pressure no changes in the structure of the plug are observed indicating a close-packing of the particles in the plugholder.

To determine the influence of surface conductance in concentrated dispersions, the cell constant C is determined according to Brigg's empirical method. The ratio between C and the electric resistance of the plug (R) provides the effective electric conductivity.

Van der Put and Bijsterbosch [141] have reported data on streaming potential and streaming current for plugs of monodisperse spherical polystyrene particles in aqueous solutions. Streaming current data calculated according to Smoluchowski's and Levine's theories as a function of electrolyte concentration were shown. Due to the constant charge in the system, a levelling off of I_s was predicted at low concentrations. It is worth mentioning that this effect is not present in the classical Smoluchowski's approach. Nevertheless, the curves predicted by Levine's theory were not in agreement with the experimental streaming current data. It was particularly striking that at intermediate concentrations all experimental curves passed through a maximum and that the nearly constant values of I_s at low ionic strength were far below the calculated values. Recently, Van der Linde and Bijsterbosch [165] have shown that streaming current measurements may lead to large errors depending on the type of electrode used. Therefore, ζ-potentials calculated by Levine's theory decrease monotonously with ionic strength when a.c. conductance is employed in the calculation of ζ-potentials. Thus, in order to obtain accurate data, they recommend to measure streaming potential and the conductance at sufficiently high frequency. In fact, the trends of variation in the experimental streaming potential data and the data calculated using Levine's theory are similar [163], although quantitative differences exist between both sets.

In a comparative study of the ζ-potential obtained from streaming potential (Levine theory) and electrophoretic mobility (Semenikhin–Dukhin theory), Hidalgo-Álvarez et al. [112] have shown that when a.c. conductance is used in the calculation of the ζ-potential a better agreement between both methods is obtained. The results obtained with a cationic latex can be seen in Fig. 3.

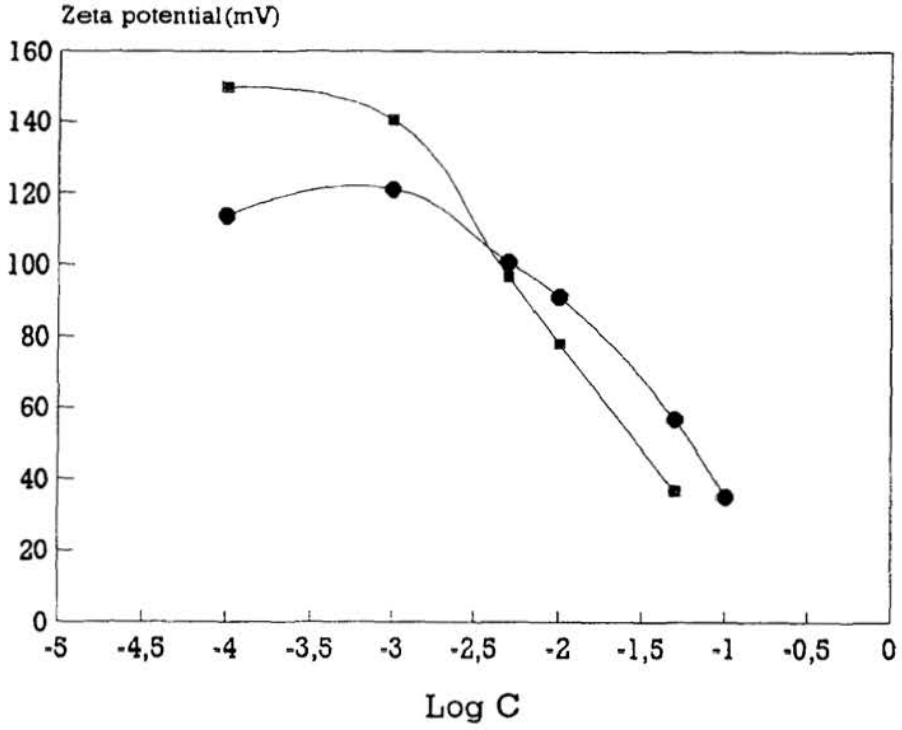

Fig. 3. ζ-potentials obtained from streaming potential (●) and electrophoretic mobility (■) of a cationic polystyrene latex (pH 8).

5.1.3. Electro-osmosis

O'Brien [115] has developed a theoretical treatment for electro-osmosis in a porous material composed of closely-packed spheres immersed in an electrolyte solution. The equations obtained for the electro-osmotic flow are valid if the e.d.l. thicknesses is much thinner than the particle radius. The total electro-osmotic flow is given by the sum of two contributions: one is identical to Smoluchowski's result, with the other one due to each component of the slip velocity, that is

$$J_v = \frac{\varepsilon k T}{\eta e} (\zeta [1 + 3\phi f(0)] - [\zeta - \gamma] g(\beta)) E_f \quad (8)$$

where f(0) is a function of the volume fraction, and takes the values of –0.418, –0.384, and –0.378 for spheres in simple, body centred, and face-centred cubic arrays, respectively. γ is a quantity which has the

same sign of the ζ-potential, but is independent of it. For a symmetric electrolyte, $\gamma = (2/z)\ln 2$.

The computed values for the non-dimensional function $g(\beta)$ can be found in O'Brien's work [115]. β characterizes the relative importance of the tangential flux of counterions.

With the aid of (8), it is possible to calculate the electro-osmotic flow for any ζ-potential. For the simple cubic array, the error in applying Smoluchowski's result rises quite rapidly with ζ, from 15% at $\zeta = 3$ to 50% at $\tilde{\zeta} = 5.5$.

The ζ-potential obtained from (8) has been compared with those obtained using electrophoretic mobility and concentrated and dilute conductivity results. This was applied to Van der Put and Bijsterbosch's streaming current measurements [108].

Electro-osmosis and streaming current/streaming potential yield the same values for the ζ-potential if errors due to resistance measurement are avoided. This agreement, as well as the independence of the ζ-potential on the applied voltage (in the case of electro-osmosis) and on the hydrostatic pressure (in the case of streaming potential/ streaming current), points out that the potential at the boundary immobile/diffuse layer can be determined. These theories call for more reliable experimental data sets.

5.1.4. Diffusiophoresis

Diffusiophoresis is the migration of a suspended colloid particle resulting from the gradient of a solute in solution. The phenomenon was discovered by Aitken [166] and first reported for liquid systems by Derjaguin et al. [117]. Derjaguin et al. analyzed this phenomenon and obtained an approximate expression for the particle velocity. The underlying fluid mechanical theory of diffusiophoresis was later established on a proper theoretical basis by Anderson, Prieve and co-workers in a series of recent papers [118–122,167].

Recent work has focused on diffusiophoresis of particles in liquid systems and has involved charged particles and electrolytes in solution [125,126,167–169]. The essential ingredients for particle motion are a gradient of interacting solute and a diffuse particle/solute interaction (hence the term diffusiophoresis). For instance, in electrolyte diffusiophoresis the diffuse interaction between a charged particle and ions in solution occurs within the e.d.l. adjacent to the particle surface. The theoretical and experimental advances in diffusiophoresis are closely related to deposition of latex particle onto various surfaces.

In a system of charged particles and electrolyte in an aqueous medium, there are two major component effects of diffusiophoresis, chemiphoresis and diffusion potential. These effects are a result of the interaction that occurs between the charges on the surface of the particle and the electrolyte. Expressions for the velocities of these two effects have already been developed from theoretical considerations [125,126]

$$\vec{V}_{DP} = \frac{\varepsilon\, kT}{\eta e}\, \zeta\, \tilde{D}\, \vec{\nabla} \ln C_2 \tag{9}$$

$$\vec{V}_c = \frac{\varepsilon\, \zeta^2}{8\eta}\, \vec{\nabla} \ln C_2 \tag{10}$$

where

$$\tilde{D} = \frac{D_+ - D_-}{Z_+ D_+ - Z_- D_-} \tag{11}$$

and C_2 is the electrolyte concentration.

Equation (9) uses the Smoluchowski equation relating electrophoretic velocity and electric field, and is strictly applicable only for infinitely thin e.d.l., while Eq. (10) is strictly applicable only for infinitely thin e.d.l. and small ζ-potential (D–H approximation). Nevertheless, a numerical solution has been developed to cover all e.d.l. thicknesses and ζ-potentials [170]. However, sometimes, it is preferable to have the particle velocity in a good approximation as an analytical expression, the limiting condition being that the ζ-potential is small and the e.d.l. is thin relative to the particle radius, that is

$$U_{DF} = 2\, \frac{kT}{\eta}\, (\kappa^{-1})^2 \left\{ \tilde{D}\, \tilde{\zeta} + 4 \ln \left[\cosh \left(\frac{\tilde{\zeta}}{4} \right) \right] \right\} \nabla C_2 \tag{12}$$

Note that particle velocity is independent of particle radius, and proportional to the square of the e.d.l. thickness. Furthermore, the velocity is not necessarily proportional to C_2 since κ^{-1} and $\tilde{\zeta}$ are concentration-dependent.

Taking into account the net diffusiophoretic velocity given by

$$\vec{\nabla}_{DF} = \frac{\varepsilon}{\eta} \left[\tilde{D}\, \frac{kT}{e}\, \zeta + \frac{1}{8}\, \zeta^2 \right] \vec{\nabla} \ln C_2 \tag{13}$$

and the diffusiophoretic diffusivity D_{12} (particle = 1, electrolyte = 2) given by

$$D_{12} = \frac{C_1 V_{DF}}{\vec{\nabla} C_2} \tag{14}$$

it follows that

$$D_{12} = -\frac{C_1 \varepsilon}{\eta C_2}\left[\tilde{D}\frac{kT}{e}\zeta + \frac{1}{8}\zeta^2\right] \tag{15}$$

Therefore, by measuring D_{12} or $\vec{V}_{DF}$ for a system consisting of particles and electrolyte in liquid solution, the ζ-potential can be determined using the theories for diffusiophoretic velocity. Lechnick and Shaeiwitz [169] have experimentally demonstrated that $\vec{V}_{DF}$ is independent of particle concentration, which is fully in agreement with theory. Furthermore, the same authors have also studied the electrolyte concentration dependence of diffusiophoresis in liquid [169]. The results obtained suggest that if the ratio between the endpoints of the range of electrolyte concentrations is less than two, then the electrolyte concentration dependence is not very important. Further results suggest that the agreement between the experimental and theoretical diffusion potential is best at electrolyte concentration above 10^{-3} M, in accordance with the infinitely thin double layer and low surface potential assumptions made. However, there have been few quantitative experimental studies of electrolyte diffusiophoresis, and even fewer studies of nonelectrolyte diffusiophoresis. The difficulty in making measurements of particle velocities is to devise an experiment which is capable of giving direct measurements of diffusiophoresis free of all other colloidal phenomena. Recently, Staffeld and Quin [125,126] have reported on a novel experimental device which can provide direct observations of diffusiophoretic movement.

This new experimental technique — the stopped-flow diffusion cell (SFDC) — allows two particle suspensions to be brought into intimate contact while providing an initially step, well-defined solute gradient at the junction between the suspensions. With this technique the manifestation of diffusiophoresis is the spontaneous formation of a concentrated band of particles, a band that moves in response to the transient decay of the initial step-function solute gradient. The ζ-potentials for the polystyrene–aqueous solution interface obtained with this new technique

and those obtained from mobility measurements are in a reasonable agreement [168]. Moreover, this technique is able to carry out measurements of non-electrolyte diffusiophoresis.

On the other hand, Pawar et al. [167] have also analyzed the effects of polarization of the double layer on the diffusiophoretic mobility of spherical, uniformly charged particles in electrolyte gradients. The theory is linear in the macroscopic gradient of electrolyte concentration and hence the diffusiophoresis depends only on ζ and λ. The authors derived an analytical expression for this dependence for the case of a symmetrically charged electrolyte, which provides excellent results for $\kappa a > 20$.

5.1.5. Dielectric dispersion

When a colloidal dispersion is subjected to an alternating electric field (E cos wt) the macroscopic electric current which results has a phase and amplitude which in general depend on the frequency w of the applied field. The macroscopic electric current is of the form

$$\lambda E \cos wt - w \varepsilon E \sin wt \tag{16}$$

In general, λ and ε depend on the angular frequency of the applied field. The dielectric dispersion is related to both electrical conductivity and dielectric permittivity measurements. It is this frequency dependence that is referred here as dielectric dispersion [128]. The frequency dependence of the conductivity and the dielectric response occurs physically as a result of the inability of the polarized double layer to respond rapidly enough to the applied field at higher frequencies. Polymer colloid dispersions exhibit dielectric dispersion in two distinct frequency ranges: one around $\omega = D/a^2$, where D is the ion diffusivity, and the other around $\omega = \lambda^\infty/\varepsilon$, where λ^∞ and ε are the conductivity and permittivity of the background electrolyte. These frequencies typically lie in the kHz (low-frequency) and MHz (high-frequency) ranges, respectively.

(a) Dielectric constant measurements

The dielectric response of a colloidal dispersion at low-frequency [171] and at high-frequency [172] can be also a powerful tool to determine the ζ-potential of polymer–liquid interfaces. In principle, this electrokinetic technique is applicable to dilute as well as concentrated dispersions. Both cases show very large dielectric dispersions at low frequency [173] which cannot be justified in terms of the Maxwell–Wagner theory [174]. From a theoretical point of view the Schwarz–Schurr theory [175–177]

has been successfully applied to aqueous polystyrene suspensions [177]. This theory, however, ignores the relaxation of the diffuse part of the e.d.l.. The Schwarz–Schurr theory is based on the polarization of the counterion cloud around the charge surface of the dispersed particles. It is the displacement of counterions in the e.d.l. by an external electrical field that is responsible for the dielectric dispersion. In the Schwarz–Schurr theory the dispersed particle with e.d.l. is considered to be a sphere with a certain complex dielectric constant suspended in an electrolyte solution with a different complex dielectric constant. The substantial discrepancies between the polarization mechanisms of Schwarz–Schurr and that of Dukhin–Shilov [128] are due to the different kinetic model for the e.d.l., and so their respective qualities depend on the quality of the model assumptions. Lyklema et al. [178] have developed a new theoretical and experimental treatments of low-frequency dielectric dispersion (at frequencies of order D/a^2). According to these authors there are two ways in which a double layer can be polarized by an external field E(w): by polarization of the diffuse part of the e.d.l. and by polarization of the bound charge. They derived equations for the dielectric dispersion $\Delta\varepsilon(w)$ and the static permittivity $\varepsilon(0)$ for these two cases.

For the diffuse-layer polarization the contribution of the particles to ε can be written as

$$\Delta\varepsilon(w) = \Delta\varepsilon(0)\,\frac{1 + W + W^2}{(1 + W)^2 + W^2(1 + A_{21}W)^2} \tag{17}$$

where

$$W^2 = \frac{wa^2}{2D_{eff}} \tag{18}$$

and

$$D_{eff} = \frac{D_+D_-(Z_+ + Z_-)}{D_+Z_+ + D_-Z_-} \tag{19}$$

is the effective coefficient of diffusion.

$$A_{21} = \frac{A_2}{A_1} \tag{20}$$

and A_1 and A_2 are functions of Z_+, Z_-, the electrolyte concentration, sphere radius, Ψ_d and ζ [130]. The ζ-potential occurs because of convection currents due to electroosmosis are accounted for, whereas Ψ_d is the diffuse double layer potential determining conduction and diffusion in the diffuse e.d.l. part.

The low-frequency dielectric increment $\Delta\varepsilon(0)$ can also be expressed in function of the parameters A_1 and A_2 and two other parameters, a_1 and a_2, both dependent on Z_+, Z_- and Ψ_d

$$\Delta\varepsilon(0) = \frac{9}{4}\,\phi\,\varepsilon_r\,(\kappa a)^2\,\frac{(A_1 a_2 - A_2 a_1)}{A_1^2} \tag{21}$$

The bound-layer mechanism is expected to apply only if there are bound counterions without significant exchange. In that case, a different polarization phenomenon applies, and the low frequency dielectric dispersion obeys.

$$\Delta\varepsilon(0) = \frac{9}{4}\,\phi\,\varepsilon_r\,(\kappa a)\,\frac{\left[\dfrac{\sigma_0\,\kappa}{4\,F_c} - \sinh\left(\dfrac{F\,\psi_d}{2N_A\,kT}\right)\right]}{M} \tag{22}$$

with

$$M = 1 + \frac{2}{\cosh\left(\dfrac{F\,\psi_d}{N_A\,kT}\right)}\left[\frac{\sigma_0\kappa}{4\,F_c} - \sinh\left(\frac{F\,\psi_d}{2N_A\,kT}\right)\right] \tag{23}$$

In the Schwarz–Schurr theory M = 1, since there is no diffuse d.l. part. However, introduction of the diffuse part is necessary to account for the screening of the bound charges. Therefore, Ψ_d enters in the equations derived by Lyklema et al. [178]. These authors have compared the theoretical and experimental low-frequency dielectric increment. The first conclusion is that the high experimental values found for $\Delta\varepsilon(0)$ and its continuous rise with κa can never be quantitatively accounted for by the modified Schwarz–Schurr theory. This confirms that polarization of the diffuse d.l. part is the leading feature. Quantitative discrepancies remain between theory and experiment, due to surface- and colloid-chemical peculiarities of the polystyrene latices as pointed

out by Springer et al. [130]. There is ample evidence that an anomalous surface conductance mechanism is responsible for the peculiar electrokinetic behaviour of polystyrene latices [132,179].

Originally, the low-frequency dielectric dispersion observed in dispersions was interpreted on the basis of the idea that the lateral transport of the counter-ions of the Stern layer plays the main role in forming the induced dipole moment of a dispersed particle [177]. Shilov and Dukhin [174] suggested an alternative mechanism. Theoretical [128,175] and, then, experimental [130,178] studies showed that the greatest dielectric increment $\Delta\varepsilon$ is caused by the concentration polarization of the e.d.l. under the condition of free exchange between the double layer and the surrounding electrolyte concentration. One approach to study relaxation of double layers around charged particles is to apply dielectric spectroscopy to dilute colloidal dispersions. The dielectric response represents the conductive and the capacitive parts of the electric current flowing through the sol. The electric field will distort the ionic atmosphere around particles so that the double layer become polarized. It is relatively simple to relate the extent of this polarization to the dielectric response. The induced dipole moment itself is very sensitive to the ionic current flows around the particle, which are strongly dependent on the equilibrium double layer structure. Therefore, dielectric spectroscopy in the proper frequency range enables us to study relaxation processes in the double layer as well as its equilibrium structure. Razilov et al. [133] have developed a quasi-equilibrium theory for the concentration polarization in an e.d.l. and the low-frequency dielectric dispersion, including the concentration polarization in the dense part of the double layer (Stern layer), under the condition of free ion exchange between the diffuse layer and the Stern layer. The application of this theory to low-frequency dielectric dispersion data obtained with polymer colloids might open new possibilities in the explanation of the electrokinetic behaviour of these colloidal systems.

(b) Electrical conductivity measurements

The frequency response of the polymer colloid dispersions is due to the sum of the polarizabilities of the e.d.l. around the particles. The d.l. charge cloud is polarized due to the influence of the external field which is realized as the particle-dependent conductance increment and a very large effective dielectric response.

According to the value of volume fraction of solid particles in colloidal suspensions, we can have concentrated or dilute suspensions of charged

particles in a continuous phase (liquid medium). In both cases, the application of an electric field to such a suspension cause the ions and particles to migrate, giving rise to an electric current. Our aim is to determine the relationship between the applied field and the measured electric current. Electrical conductivity may be measured in a steady electric field (static conductivity) or in an alternating electric field (dielectric response measurements). This second possibility has been exhaustively reviewed by O'Brien [180]. In our case, we are especially interested in reviewing the conductivity of suspensions as this electrokinetic technique enables us to provide information on electrical state of polymer colloid–liquid interfaces.

Precise measurements of conductivity are difficult to perform experimentally. The precision can easily be lost many possible artifacts. Effects like electrode polarization have still not been thoroughly accounted for from a theoretical point of view. Electrode polarization is present at low frequency, at high frequency there are stray capacitance and inductance effects. The modelling of these effects in order to extract the true sample signal is difficult as the polarization and stray effects are up to orders of magnitude greater than the sample signal.

The theory describing the conductivity of suspensions of charged particles is based on the bulk or averaged properties at a finite, but small, particle volume fraction. In this way, it is very different from the theory of electrophoresis, which is concerned with the motion of a single particle at infinite dilution. The counterions which balance the charge on the particle are assumed to diffuse far away from the particle hence not affecting the background ionic strength. In the theory of conductivity, the counterions which balance the charge on the particles do add to the background ionic strength and thus to the suspension conductivity. Since the theory of electrophoresis is based on single particles at infinite dilution and the theory of conductivity of suspensions on data obtained by these averaged properties at finite particle concentration, comparison of ζ-potentials calculated from two experimental techniques provides an excellent test for the completeness of the electrokinetic models employed [48,68,112,116,134,147]. Provided that the physical assumptions of the theory are valid, both processes should yield the same ζ-potential. Here, it is assumed that in the low volume fraction limit the suspension conductivity, K^*, can be written [57,181]:

$$K^* = K^\infty(1 + \phi\,\Delta K^\infty(\zeta, \kappa a)) \tag{24}$$

where K is the dispersion conductivity, K^∞ is the bulk electrolyte

conductivity (outside the e.d.l.), $\phi(0 < \phi < 0.05)$ is the volume fraction of particles in suspension, κa is the electrokinetic radius and ΔK^* is the conductivity increment. As with the electrophoresis, conventional models relate the conductivity increment to a single interfacial property, the ζ-potential [134,146,147].

The experimental evaluation of ΔK^* is performed by measuring the conductivity as a function of the volume fraction. L.P. Voegtli and Zukoski [182] have found that at low volume fractions the conductivity of a latex suspension dialysed against 10^{-4} M HCl becomes a linear function of the volume fraction.

The O'Brien conductivity model [183] provides values of $[(K^*/K^\infty) - 1]/\phi$ much lower than those experimentally obtained by Watillon and Stone-Masui [184]. This is not however, the only case in which conductivity measurements yield different results compared to those obtained by other electrokinetic techniques. For instance, ζ-potentials calculated from electrophoretic mobility and conductivity measurements [185–188] have displayed significant differences. Various interpretation have been offered to justify those differences [68,188]. One of the difficulties is the dearth of data on well-defined systems where the tenets of theory can be tested.

The ζ-potential calculated from the conductivity increment approaches the ζ-potential calculated from the mobility both at high and low salt concentrations but is substantially larger at intermediate ionic strengths. It is apparent that the ζ-potentials calculated from ΔK^* are systematically higher than those from the electrophoretic mobility with the absolute magnitude of these deviations being at its largest (50–60) mV at intermediate salt concentration. In agreement with Zukoski and Saville [185–188] these differences are due to inadequacies in electrokinetic theory applied to polymer colloids. The results obtained by these authors suggest a transport process occurring at the particle surface which is not taken into account in the extant electrophoretic theories. They proposed a model using a dynamic Stern layer. Using the model they have shown that for a fixed ζ-potential, ionic transport behind the shear plane can increase the conductivity increment and depress the electrophoretic mobility [185].

In the opinion of Saville [189], the theories for the electrical conductivity of dilute dispersions fail to take proper account of the effects of non-specific adsorption, which alters the concentration of ions in regions outside the e.d.l., and counterions derived from the particle charging processes. This might explain the poor agreement between theoretical

and experimental data. Dunstan and White [146], however, have found that the volume fraction dependence of the supporting electrolyte concentration potentially explains the discrepancies between the mobility and the conductance-predicted ζ potentials reported by other authors previously. The electrolyte concentration in latex dispersions changes markedly with the volume fraction of the particles and this explains the different ζ-potential values obtained using mobility and conductivity measurements. This work suggests that the observed electrokinetic behaviour is general to colloidal dispersions and not intrinsic to polymer colloids.

Ideal electrokinetic behaviour has been found by Gittings and Saville [190] of a polystyrene latex sample stabilized by sulfate charges (–1.06 $\mu C/cm^2$) with a diameter of 156 nm (measured by TEM) and a hydrodynamic size of 160 nm (measured by PCS). Using the standard model of electrokinetics of electrophoretic mobility and low-frequency dielectric response these authors have found a good agreement between the ζ-potentials of the O'Brien–White and Delacey–White theories, respectively. It seems that lowly charged polystyrene beads with diameters smaller than 200 nm are closer to the ideal colloidal system. There is a good agreement between the conclusions derived by Gittings and Saville [190] and Russell et al. [107].

High-frequency dielectric dispersion

On the other hand, polymer colloids in the Smoluchowski limit ($\kappa a >> 1$) can exhibit another type of dielectric dispersion at higher frequencies (of order κ^2 D). O'Brien [171] has described the high-frequency dielectric dispersion in terms of the complex conductivity $K^*(w)$ for concentrated and dilute colloidal dispersion. From an electrokinetic point of view the relationship found between the surface conductance and ζ using the standard e.d.l. model is very interesting.

The aim of the high-frequency conductivity and dielectric response experiments is to find the complex conductivity of the suspension as well as that the background electrolyte in the frequency regime 0.1–40 MHz.

Experimentally, the complex conductivity of a suspension is obtained by measuring the admittance of a capacitor filled with the suspension in question. The admittance $Y(\omega)$ is converted into the complex conductance $K^*(\omega)$ [129] using

$$Y = C_c K^* \tag{25}$$

where C_c is the geometrically cell constant.

The complex conductivity of the suspension can be expressed in terms of the conductivity $\Delta K(\omega)$ and the dielectric response $\Delta\varepsilon'(\omega) + i\Delta\varepsilon''(\omega)$ due presence of the polymer colloids,viz [129]

$$K^* = K^*_{el} + \phi[\Delta K - i\omega/4\pi(\Delta\varepsilon' + \Delta\varepsilon'')] \quad (26)$$

Alternatively, the complex conductivity of the suspension can be expressed in terms of the complex dipole strength $C_0(\omega)$ [129].

$$K^* = K^*_{el}\,[1 + 3\phi C_0(\zeta)] \quad (27)$$

Depending on the frequency range of interest one of these expression is used. The choice is related to the structure of C_0, $\Delta\varepsilon'$, and $\Delta\varepsilon''$ when plotted against frequency. At low frequency, the real and imaginary parts of C_0 are approximately constant whereas at high frequency these curves possess greater structure, exhibiting well-defined maxima and minima for frequencies beyond 0.1 MHz. In the case of $\Delta\varepsilon'$ and $\Delta\varepsilon''$, all of the structure in the curves is observed at low frequency with relaxation of $\Delta\varepsilon'$ occurring around 1 MHz and $\Delta\varepsilon''$ decreases sharply to zero after reaching a maximum around 0.1 MHz. Very recently, Russell et al. [140] have studied the high-frequency dielectric response of highly charged sulfonate/stryrene latices, they analyzed K* in terms of the real and imaginary parts of the dipole strength using Eq. (27). Most earlier studies in this field were concerned with low-frequency dielectric response and so analyzed their experimental data in terms of $\Delta\varepsilon'$ and $\Delta\varepsilon''$. Russell et al., however, used the high-frequency regime (0.1 to 40 MHz), and since the theoretical dipole strength is a function of the ζ-potential, a comparison of experimental and theoretical data will yield a ζ-potential. The experimental curves were compared to theoretical curves computed at various ζ-potential using the numerical electrokinetic theory of Mangelsdorf and White [55]. The ζ-potentials derived from this study were compared to those obtained from electrophoretic measurements, and a very good correlation between the two electrokinetic processes was observed. This work shows that high-frequency dielectric dispersion usually produces good fits to theory in contrast to dispersion at lower frequencies [182,185].

Dielectric dispersion of concentrated dispersion

The problem of calculating the electrical conductivity of a porous plug is considerably more difficult than the apparently related problem of determining the conductivity of a granular material composed of purely conducting phases. The difficulty arises from the fact that the current

in a porous plug (concentrated colloidal dispersion) is carried by electrolyte ions, rather than electrons. In order to determine the current density at a point in the electrolyte it is necessary to determine not only the local electric field, but also the local ion density gradients and fluid velocity; for in addition to the component of current due to the electric field, there are also components due to the Brownian motion and convection of the ions with the neighbouring fluid. To calculate the total current passing through a plug it is therefore necessary to determine the distribution of ions, electrical potential, and flow field in the pores. This involves the solution of a set of partial differential equations. O'Brien and Perrin [191] have solved those equations and thereby theoretically determined the conductivity of a porous plug. The plug is assumed to be composed of closely packed spheres of uniform ζ-potential, and the Stern layer ions are assumed to be immobile. Besides, the particle radius a has to be much larger than the e.d.l. thickness κ^{-1}. According to the procedure of O'Brien–Perrin, the electrical conductivity of a porous plug is given by:

$$\frac{\lambda}{\lambda_0} = 1 + 3\phi \left[f(0) + \frac{e^2 z_i^2 u_i n_i^0}{\lambda_0} (f(\beta) - f(0)) \right] \tag{28}$$

where the subscript i refers to the counterion of highest charge. In this case, it is assumed that there is only one species of highly charged counterion. β is a variable which relates the net tangential flux of ions entering a portion of the e.d.l. to the flux passing out to the bulk electrolyte, and $f(\beta)$ is a complicated function of β which in turn depends on the geometrical distribution of particles constituting the porous plug (simple, body-entered and free-entered cubic arrays).

The computed values of the function $f(\beta)$ are shown in [191].

By using Eq. (28) together with the $f(\beta)$ values, we can compute the conductivity of the three cubic arrays for any electrolyte. In most practical applications, the conductivity is known through measurement and it is the ζ-potential which must be calculated. In this case one would first calculate the conductivity of the plug over a range of ζ-potential by the above procedure and then interpolate to find the ζ-potential corresponding to the measured conductivities. This method for ζ-potential calculation has been tested and compared with values experimentally obtained by Van der Put and Bijsterbosch [141]. The agreement between the theoretical and experimental ζ-potential values is quite satisfactory when conductivity data of concentrated and dilute polystyrene suspen-

sions are used, but again ζ-potential from conductivity measurement are much larger than those from mobility measurements. Following a slightly different approach to the method used by O'Brien–Perrin [191], Midmore and O'Brien [193] have developed a cell-model formula for the low frequency conductivity of a concentrated suspension of spheres with thin double layers. In this model, the effect of surrounding spheres on a reference sphere is approximated by taking the reference sphere to be at the centre of a larger sphere. From the solution to this problem, we find

$$f(\beta) = \frac{2\beta - 1}{(1 - 2\beta)\,\phi + (2 + 2\beta)} \tag{29}$$

As the volume fraction approaches zero, Eq. (29) reduces to

$$f(\beta) = \frac{(2\beta - 1)}{(2 + 2\beta)} \tag{30}$$

So that, for a symmetric two-species electrolyte, in which the ionic diffusivities are equal, we find

$$\lim_{\phi \to 0} \frac{\left(\frac{\lambda}{\lambda^{\infty}}\right) - 1}{\phi} = -\frac{3}{2}\left[1 - \frac{3\beta}{2\beta + 2}\right] \tag{31}$$

This expression can be used for the unequivocal determination of β.

A new application of conductivity measurements is the experimental determination of the diffuse charge density (σ_d). If the diffuse layer charge is high, which is generally the case for polystyrene latices, the contribution to the charge by the negative adsorption will be small compared to that by the positive adsorption, so that

$$\sigma_d = \frac{\left[\lambda_s F - \left(\frac{2\varepsilon N a kT \sigma_{el}}{\eta z_+}\right)\right]}{\Lambda_+} \tag{32}$$

σ_{el} may be determined from the ζ-potential, and λ_s from conductivity measurements since

$$K = \frac{\lambda_s}{a\lambda_s^{\infty}} = \frac{\beta}{2} \tag{33}$$

when the electrolyte is symmetrical in terms of both charge and ionic diffusivity (e.g. KCl). Also, K can be calculated for any electrolyte from high-frequency and low-frequency conductivity, measurements by means of more complicated formulas.

Midmore and O'Brien [193] found that the diffuse charge density for polystyrene latices ranged from 4.1 and 4.4 μC cm^{-2}, whereas by titration a value of 2.8 μC cm^{-2} was obtained. Once more, conductivity measurements yielded larger values for the electrokinetic parameters. Midmore et al. [194] have examined the effect of temperature, and co-ion and counterion type on the diffuse layer charge of monodisperse polystyrene latices. After an extensive analysis they concluded that conductivity measurements provide a better method for studying the e.d.l. in latex systems.

Finally, conductance measurements have allowed to determine the effective charge number of monodisperse polystyrene spheres [195]. The fraction of free macroions and/or gudgeons in deionized suspension is close to but smaller than unity for spheres having several and several tens analytical valency.

5.1.6. Electro-acoustic phenomena

The electroacoustical methods for determining the ζ-potential of particles are based on the so-called Debye effect [155]. In an electrolytic solution, ultrasonic waves produce alternating potentials between points separated by a phase distance other than an integral multiple of the wavelength. This effect occurs when cations and anions of the electrolyte have different effective masses and frictional coefficients and is a consequence of the resulting differences in the amplitudes and phases of the displacements of the cations and anions. When the anion is lighter than the cation the former is more displaced by the ultrasonic pressure amplitude than the latter. Thus, a region (A) will be charged positively with respect to the another region (B).

If inert metal probes are placed in A and B, an alternating potential difference will be observed with the same frequency as the sound waves. The frequency of the alternating ultrasonic vibrational potential (UVP) corresponds to that of the sound field. A similar effect exits for colloidal particles caused by the distortion of the ionic atmosphere. It was first predicted by Rutgers [196] and has been treated theoretically by others [197,198].

Babchin et al [199] have reviewed the use of electroacoustical methods in the determination of electrokinetic properties. The main advantage of the electroacoustical methods is that it is perfectly capable of providing electrokinetic data in nontransparent and nonpolar media along with the ability to monitor coagulation/coalescence processes [200].

Enderby [198] obtained for the colloidal vibration potential

$$\Phi_v = \left(\frac{A\,V_u}{72kT\,\eta\,u_i}\right)\left(\frac{n_c\,W_c}{e}\right)\zeta\left\{\frac{B(\kappa a)}{[\kappa^4 + w(kT\,u_i)^{-2}]^{1/2}}\right\} \tag{34}$$

The function $B(\kappa a)$ varies from 96 to 144.

The colloidal vibrational potential was first measured by Yeager and co-workers [201,202] and by Rutgers and Vidts [203]. More recently, Beck et al. [204] and Babchin et al. [199] have developed new electroacoustical techniques that, usually, yield different ζ-potential values than other electrokinetic techniques. However, the cases studied by Babchin et al. were often in reasonable agreement.

The main disadvantage of the ultrasonic potential lies in the fact that it is a complex combination of the colloidal and the ionic vibrational potential. At low free salts concentration (less than 10^{-2} M), the ionic contribution can be neglected. Above this limit, the influence of the retention aid on the particle potential is no longer detectable.

The use of electroacoustical methods to obtain electrokinetic properties of polymer colloids is very recent [152,205–207].

Electroacoustics, when compared to microelectrophoresis and streaming potential, shows considerable advantages: (a) measurements on particle sizes up to 3 mm can be performed using low frequency (100 kHz) and a wide electrode distance (13 mm). (b) The concentration of the suspension may vary within wide ranges (>> 1% or more) depending on the electrolyte concentration. (c) The measurement is almost instantaneous (milliseconds range). (d) Continuous monitoring is in principle possible.

Shubin et al. [152] have performed an interesting comparative study on the electroacoustic and dielectric responses of carboxylated polystyrene beads. The ζ potentials are calculated from dynamic mobility using the measured surface conductances obtained from the complex conductivity of the polymer colloids. These ζ values are found to be smaller than those calculated from conductivity data. A triple layer model (TLM) is used to interpret measurements of electrophoretic mobilities at zero and

high (1 MHz) frequencies, and the complex conductivities over the frequency range from 1 to 20 MHz. In order to reconcile these two sets of data, these authors considered two alternative electrokinetic mechanisms in the TLM: (i) the ζ-potential is measured some distance (from 1 to 3 nm) from the Outer Helmholtz Plane (OHP) and the anomalous conductivity occurs in the diffuse layer or (ii) the ζ-potential is measured in the OHP and the anomalous conductivity occurs in the Stern layer. The second model gives a reasonable description of the ζ-potentials and surface conductance for the entire pH range. According to these authors the anomalous conductivity (the extra surface conductivity not accounted for in the standard theory) is always presented in the highly charged ($\sigma_0 > 10\mu C/cm^2$) polymer–water interface, which is not generally accepted by other authors [107,134,147].

5.1.7. Electroviscous effects

The presence of an e.d.l. exerts a pronounced influence on the flow behaviour of a fluid and leads to an increase in the suspension viscosity due to energy dissipation within the e.d.l. All such influences are grouped together under the name of electroviscous effects. These kind of effects appear both in concentrated colloidal dispersions (porous plugs or membranes) [208] and in dilute ones [209].There are three distinct effects, called respectively the primary, secondary, and tertiary electroviscous effect. The primary electroviscous effect is due to the increase of the viscous drag forces on the particles as their e.d.l. are distorted by the shear field. The resulting contribution to the viscosity is, in first order, proportional to the volume fraction of the suspended particles. The primary electroviscous effect is a useful tool to investigate e.d.l. at polymer–liquid interfaces. This effect can be interpreted on the basis of several theoretical treatments for spherical particles.The primary electroviscous effect occurs in a dispersion, in which the particles are electrically charged. The equation describing the particles, and the e.d.l. thickness in relation to the radius of the particles.

The primary electroviscous effect is due to increase of the viscous drag forces on the particles as their e.d.l's are distorted by the shear field. The resulting contribution to the viscosity is, in first order, proportional to the volume fraction of the suspended particles. Thus, this effect occurs in a suspension, in which the particles are electrically charged [159]. The first theory for the primary electroviscous effect was presented without proof for the limiting case of thin e.d.l. by Smoluchowski [210]. Later Krasny-Ergen [211] calculated the viscous dissipation in the same

limit to obtain a result similar to Smoluchowski's, only different by a numerical factor. Booth [156] performed a definitive analysis in the low shear limit for arbitrary e.d.l. thickness, obtaining a Newtonian viscosity with an $0(\phi)$ coefficient which increased with increasing surface charge and e.d.l. thickness.

The magnitude of the primary electroviscous effect is proportional to the first power of the particle concentration, and for a suspension of spherical particles it appears as a correction p to the Einstein equation

$$\frac{\eta}{\eta_0} = 1 + 2.5(1 + p)\,\phi \tag{35}$$

The predicted enhancement of the coefficient over the Einstein value of 2.5 is generally of the same magnitude as or smaller than 2.5 and hence difficult to measure accurately; nevertheless some experiments with polystyrene latexes show similar effects [157].

The calculation of p for any κa value can be carried out by a numerical analysis of the equation developed independently by Hinch and Sherwood [212] and Watterson and White [158]. The various equations describing the primary electroviscous effect of dilute monodisperse suspensions with spherical particles can all be put in the form

$$\frac{\eta}{\eta_0} = 1 + 2.5\phi\left[1 + \frac{3Q^2\, e^4\, N_A}{2\pi\eta_0 \varepsilon\, kT\, a^2}\, F(\kappa a)\, G(\lambda_i)\right] \tag{36}$$

where η is the viscosity of the suspension and η_0 that of the solvent, ϕ is the volume fraction, a the radius of the suspended particles, Q is the number of elementary charges on each particle, N_A is the Avogadro number, ε is the dielectric constant of the dispersion, λ_i are the conductivities of the various ionic species in the dispersion, $b = \kappa a$, and e, k, and T have their usual significance. The functions $F(\kappa a)$ and $G(\lambda_i)$ can be found in [214]. For simple electrolytes, the concentrations of the ionic species enter only through the function $F(\kappa a)$. According to the D–H approximation

$$Q_e = a\,\zeta\,\varepsilon\,(1 + \kappa a) \tag{37}$$

Hence, Eq. (37) can be utilized in low ζ-potential determinations.

For the primary electroviscous effect all approximate equations are based on the following assumptions:

(i) laminar flow, neglect of inertia terms, no slip at the surface of the particles

(ii) small volume fraction of particles, which are nonconducting and spherical

(iii) uniformity of ionic conductivities, dielectric constant, and solvent viscosity throughout the electrolyte solution

(iv) uniform immobile charge density on the surface of the particles

(v) no overlap of double layers of neighbouring particles

(vi) the electroviscous effect must be less than the Einstein coefficient (2.5 ϕ), i.e. low surface charge or low ζ-potential.

Honing et al. [213] have determined the dependence of the viscosity of silica (ludox) sols on the electrolyte concentration of various aqueous solutions. For volume fractions below 5% silica, the viscosity was found to be linearly dependent on the volume fraction of silica. The sols showed Newtonian behaviour at these low volume fractions. The electrolyte concentration had a marked effect on the viscosity. Very reasonable fits were obtained with the Booth equations by assuming the charge of the particles to be constant. Delgado et al. [161] could not fit their data to the Booth or the Watterson and White equations. The source of the discrepancy may be the fact that their particles (anionic polystyrene latex) were not smooth, whereas the theory assumes smooth particles with an uniform surface charge. In the same way, McDonogh and Hunter [159] indicated that the results obtained with polystyrene latices lead to conclude that either polystyrene latices prepared by emulsion polymerization and purified by dialysis or ion-exchange are good examples of smooth, spherical hydrophobic particles or they are not. If they are smooth spheres then there are serious experimental discrepancies between experimental results and the current theories of the primary electroviscous effect. This would be a matter of real concern because the mathematical model assumptions used for developing the theory are the same as those employed in the theoretical description of the electrophoretic mobility of a colloidal particle. If so this could jeopardize the use of the ζ-potential as the main characterizing parameter of the e.d.l.

In the opinion of McDonogh and Hunter [159], it would be more comfortable to believe that this discrepancy is caused by some peculiar feature of the polystyrene latex system and, certainly, there seems to be some evidence that this system when prepared by the usual procedures (with presence of emulsifiers) is not as well behaved as would be expected from its appearance in electron micrographs. The results

obtained by Honing et al. [213] with silica sols seem to support that second possibility, since silica sols are indeed smooth. Ali and Sengupta [160] have measured the primary electroviscous effect in two different series of polystyrene latices of increasing particle size, prepared without addition of surfactants. They found that whereas for the larger particle size latices the measured electrical contribution to the primary electroviscous effect

$$\left(\frac{\eta_{el}}{\eta_0\phi} = \frac{(\eta - \eta_0)}{\eta_0\phi - 2.5}\right)$$

decreases with increasing counterion concentration (quaternary ammonium of different ionic sizes) as required by the theory, it either remains (more or less) constant or increases slowly in the case of smaller latices.This might possibly be due to the simultaneous occurrence of a slow feeble agglomeration of latex particles in the presence of increasing counterion. Also, Yamanaka et al. [214] found a satisfactory agreement between experimental primary electroviscous effect and the Booth's theory for relatively high-salt concentrations. Furthermore, they used ionic polymer latices prepared without surfactants. Finally, Quadrat et al. [215] have demonstrated that the dissociation of carboxylic groups on the surface of polymer colloids induces changes in the effective hydrodynamic volume due to an increased electroviscous effect and swelling.

The secondary electroviscous effect results from the overlap of the e.d.l. of neighbouring particles, resulting in repulsion. This repulsive force leads to a larger effective volume of the particles and hence to an increase in viscosity. The leading contribution to the viscosity is proportional to the square of the volume fraction, because at least two particles are involved. Although, the secondary electroviscous effect depends on the square of particle concentration while the primary effect is only proportional, in most practical cases the secondary effect is much larger than the primary effect, even at low concentrations. Actually the primary effect is important only if the thickness of the e.d.l. is of the same order of magnitude as the size of the particles. This implies that the particles must be very small for the primary electroviscous effect to be dominant [213]. With regard to the secondary electroviscous effect, Stone-Masui and Watillon [157] have obtained results which indicate the treatment of Chan et al. [216], although it predicts to high values, represents a more realistic approach than Street's equation, which yields too low values for the viscosity.

5.2. Possible explanations for the electrokinetic behaviour of polymer colloids

Marlow and Rowell [97] have noted five possible explanations for electrokinetics behaviour of polymer colloids:

(1) shear plane expansion (the hairy layer model) [17,18,74,103, 108–110,141]
(2) preferential ion adsorption [32,52,71,143,146,147,179]
(3) osmotic swelling or core-shell redistribution [38]
(4) crossing of the mobility/ζ-potential minimum [190], and
(5) anomalous surface conductance [21,30,50,56,68,69,76,83,99, 112,132,162,178]

Numbers 1, 2 and 3 are qualitative explanations, whereas 4 and 5 try to explain quantitatively the electrokinetic behaviour of polymer colloids.

Two very different models have been proposed to account for the non-classical behaviour of polymer colloids. Recently, Seebergh and Berg [217] have published a most interesting paper where both models are extensively discussed.

The hairy layer model postulates the presence of a layer of flexible polymer chains, or hairs, at the surface [108]. Zimehl and Lagaly [218] have suggested that the hairy layer is just one of several types which may be formed during emulsion polymerization, as shown in Fig. 4. The hairs extend into the bulk solution, owing to electrostatic repulsion between the ionic groups terminating the hairs and the ionic groups anchored at the surface. The distance of hair extension (i.e. the thickness of hairy layer) will also be influenced by the extent of solvation of the polymer chains and the ionic end-groups, as elucidated by some authors [219]. At low ionic strength, the hairs are in an extended conformation, so that some fraction of the total fixed charge of the particle is now located in the Stern layer and/or the diffuse layer. The shear plane has shifted away from the surface, so the ζ-potential is less than it would be for a non-hairy particle with the same fixed charge. The shear plane shift may also allow for electrical conduction between the shear plane and the surface, further reducing the electrophoretic mobility or streaming potential. As the ionic strength increases, the hairs collapse back towards the surface owing to charge shielding. This the shear plane moves closer to the surface and the ζ-potential increases. At high ionic strength, the hairs have completely collapsed and the ζ-potential decrease with increasing electrolyte is due to the compression of the electrical double layer. This mechanism is shown in Fig. 5.

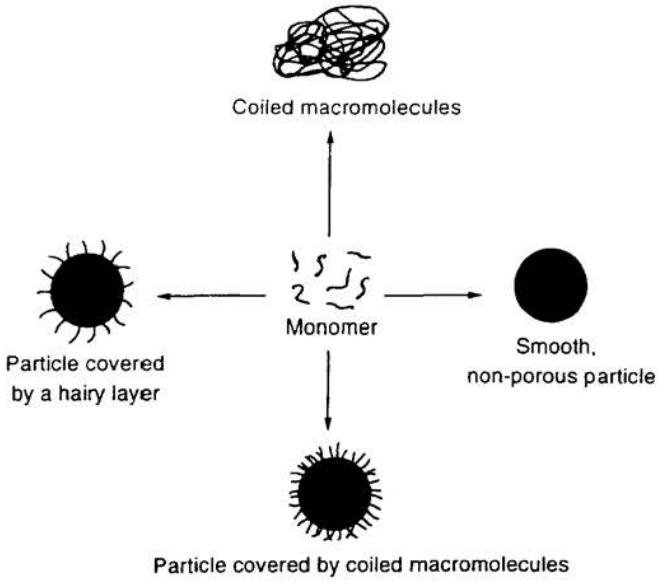

Fig. 4. Types of layer of flexible polymer chains formed during emulsion polymerization.

Very recently, Seebergh and Berg [217] have published a paper where they verify the presence of a hairy layer via simultaneous measurement of both the size and electrokinetic characteristics of a given latex over a range of conditions. The presence of a hairy layer was investigated by comparing size, mobility, critical coagulation concentration, and surface charge density measurements of three different surfactant-free latices before and after heat treatment. Most of the literature has focused on trying to explain the anomalous electrokinetic behaviour of polymer colloids. In fact, polymer colloids exhibit other behaviour which does not agree to the predictions of theory. Several studies have reported decreases in the hydrodynamic diameter as a function of increasing ionic strength, based on photon correlation spectroscopy measurements [219–222]. Any proposed model of the polymer colloid/fluid interface must account for these observations as well as for the electrokinetic behaviour. According to the hairy layer model, with increasing ionic strength, the hairs move gradually closer to the surface and the shear plane shifts inwards. The hydrodynamic diameter is thought to reflect the existence of bound surface layers, so a decrease in the hairy layer thickness should result in a decrease in the hydrodynamic diameter. The observed hydrodynamic diameter behaviour is therefore consistent with the hairy layer

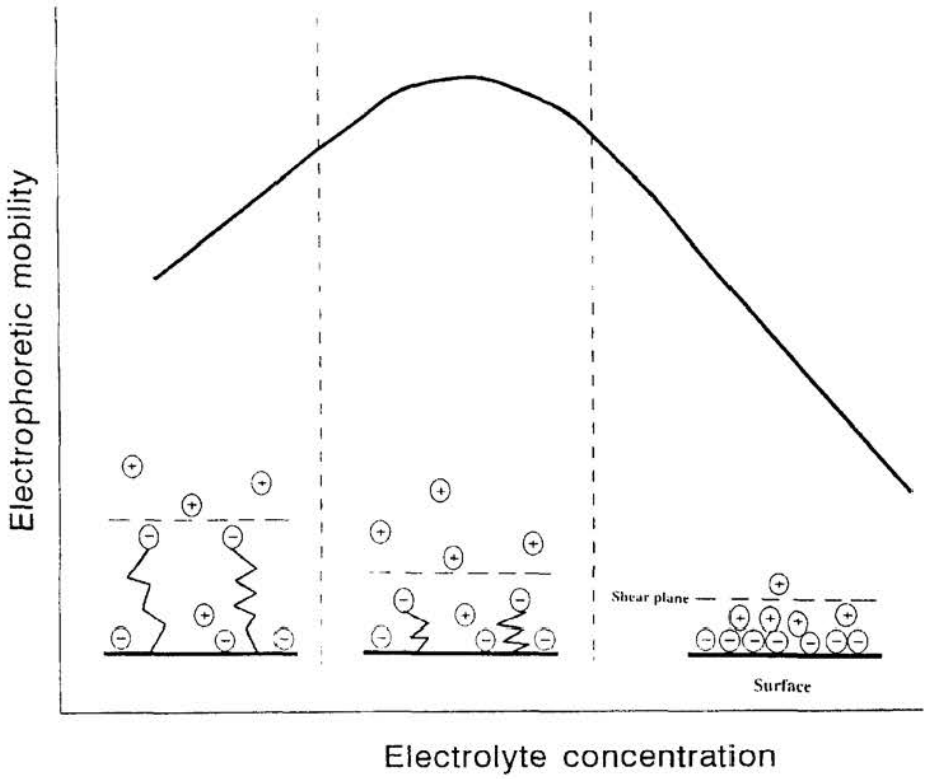

Fig. 5. Hairy layer mechanism.

model of the interface [223]. An alternative explanation of the size behaviour was offered by Saaki [221], who suggested that the reduction of the hydrodynamic radius with increasing electrolyte is due to the ion-initiated destruction of the rigid water layer at the polymer bead surface.

The hairy model has been criticized for several reasons. A number of studies have reported a secondary maximum in the mobility of anionic latex at very low electrolyte concentration which cannot readily be explained by the hairy layer mechanism [71,185,220]. Elimelech and O'Melia [71] reported that the addition of lanthanum ions (La^{3+}) to an ionic latex dispersion did not eliminate the minimum in mobility as a function of potassium chloride concentration, even though La^{3+} ions should strongly adsorb onto the negatively charged sites and collapse a hairy layer through charge shielding (see Fig. 6). Also, Midmore and Hunter [83] considered it unlikely, based on energetic considerations,

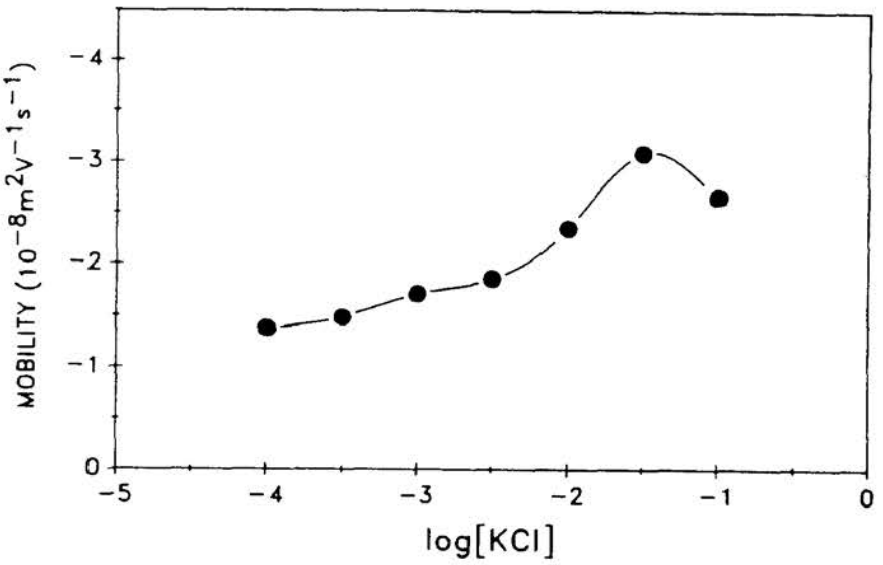

Fig. 6. Electrophoretic mobility of an anionic polystyrene latex (diameter 0.753 μm, surface charge density 56.4 mC m^{-2}) as a function of log molar concentration of KCl in the presence of 10^{-4} M $LaCl_3$ as a background electrolyte (pH 6.0) [71].

that hydrocarbon chains would extend into the aqueous medium. Owing to these apparent weaknesses, some investigators have invoked models based on ion adsorption to explain their results.

The second model is based on ion adsorption. This model postulates that the electrokinetic behaviour of the polymer colloids is a consequence of the extent of counter-ion and co-ion adsorption at the surface [32,52, 71,143,146,147,179]. At very low electrolyte concentrations, counter-ions adsorb, causing a decrease in the ζ-potential with increasing electrolyte concentration. At somewhat higher electrolyte concentrations, co-ion adsorption occurs as counter-ion sites become filled. This causes an increase in the ζ-potential with increasing electrolyte concentration. At relatively high electrolyte concentrations, there is no further ion adsorption, and the ζ-potential decreases as the electric double layer is compressed.

Very recently, a new qualitative explanation for the minimum in the mobility-ionic strength curves of anionic polymer colloids has been proposed [222]. According to it, three competing processes are involved in determining the shape of the mobility curve in the presence of electrolytes; for the case of anionic polystyrene particles, they are: (a) neutralization

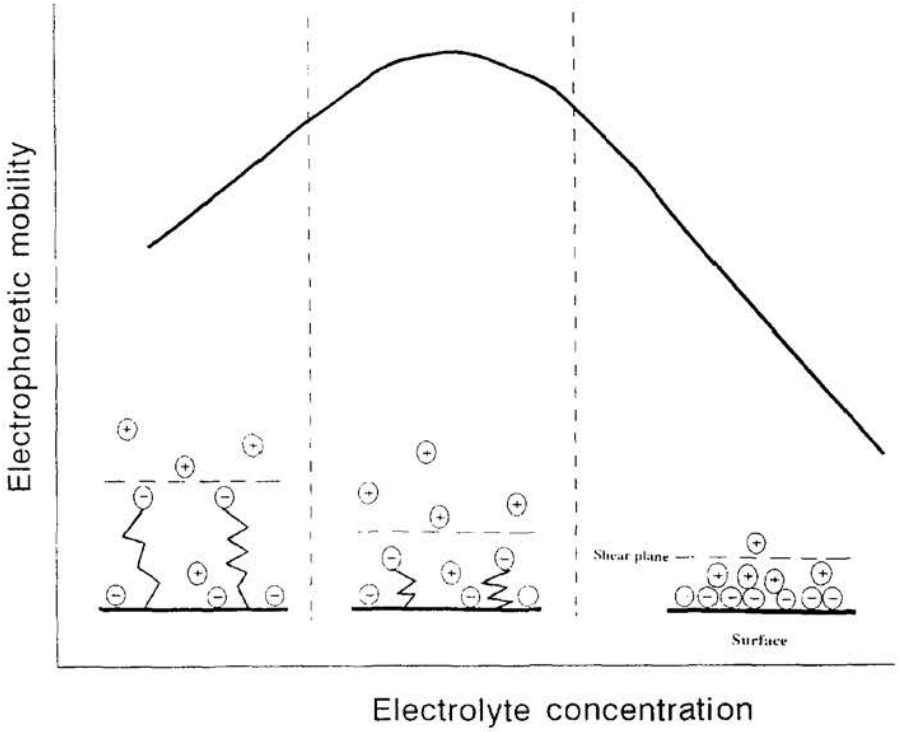

Fig. 7. Ion adsorption mechanism.

of negative charge on the surface by adsorption of counterions causing an increase in the electrokinetic potential (less negative); (b) approach of co-ions close to the hydrophobic surface of the particles, causing a decrease in the electrokinetic potential (more negative); (c) compression of the diffuse double layer due to high bulk concentration of electrolyte, causing an increase in electrokinetic potential (less negative). Thus, the effect of each process along the mobility curve determines the shape of the electrokinetic potential as a function of the electrolyte concentration. Figure 7 shows this process.

The issue of co-ion adsorption has recently gained greater significance because of the works of Zukoski–Saville [185,187] and Elimelech–O'Melia [71]. They interpret their electrokinetic data by invoking specific co-ion adsorption. This ion adsorption model postulates that the anomalous behaviour of polymer colloids is due to counter- and co-ion adsorption at the surface [71,182,185,187].

The ion adsorption model has also been criticized. In particular, the driving force for co-ion adsorption of simple, inert electrolytes onto

polymer colloids is not well understood [185,223]. Some authors have suggested that the driving force is hydrophobic in nature [147], where the co-ions have an affinity for the relatively hydrophobic surface of polymer colloids. This hypothesis is plausible for anionic polymer colloids, where the co-ions are relatively hydrophobic ions; however, it is difficult to accept in the case of cationic polymer colloids, where the co-ions are strongly hydrated cations. Several experimental studies have demonstrated that cationic polystyrene colloids exhibit a mobility maximum as a function of electrolyte concentration [50,78,103,112], which implies that co-ion adsorption is not hydrophobically driven. In any case, although some conductivity studies indicate that co-ions adsorb at the surface of the polymer colloids [185], there have been no direct measurements of such adsorption [223,83]. In fact, adsorption studies have shown that neither chloride nor sulfate ions adsorb at the surface of anionic polystyrene colloids dispersed in water [224].

Another criticism of the ion adsorption model is that it cannot account for the observed insensitivity of the mobility to the co-ion species. Midmore and Hunter [83] measured the mobility of an anionic polystyrene latex as a function of KF, KCl, KBr and KI concentration, and found that the mobility behaviour was virtually identical for each electrolyte. These results cast additional doubt on the mechanism of co-ion adsorption, as it seems likely that the adsorption affinity would differ according to the ionic species. Nevertheless, the hydrated size of these ions are quite similar, and this might explain the insensitivity of the mobility behaviour to these ions. A slightly different ion adsorption model has been proposed by Goff and Luner [52], "the ion exchange" model. In this model they assumed the original negative surface charge, i.e. in the absence of additional electrolyte, to be fully compensated by H^+ counterions. It is assumed that these protons are mainly inside the slipping plane and so do not contribute to the diffuse charge which is responsible for the zeta-potential. Thus, both the electrokinetic charge density and the ζ-potential are also less negative at low ionic strength. As electrolyte is added (e.g. NaCl), the H^+ ions are gradually replaced by Na^+ ions which takes place in the diffuse layer outside the slipping plane and thus act to decrease the zeta-potential (more negative), until compression of e.d.l. at still higher ionic strengths causes the latter to increase (less negative) again. The transition occurs with an electrolyte concentration of 10^{-3} to 10^{-2} M and this gives rise to a minimum for the ζ-potential in that region. This model is supported by observations made in connection with the conductometric titration of latices. However, Goff

and Luner [52] pointed out that their model is only valid for latices whose charge is due to strong acid, so a different explanation must be sought to cover the behaviour of latexes whose charge is due to weak acids. Also this "ion-exchange" model has been criticized by some authors. Van den Hoven and Bijsterbosch [109,110] obtained electrokinetic data where the particles were strictly in K^+ form only, so that any ion exchange was out of the question. Under these experimental conditions electrophoretic mobility as well as streaming potential techniques used on the same particles showed both the disputed minimum. Also, de las Nieves et al. [17] working with highly sulfonated polystyrene latex beads obtained no appreciable difference in the electrophoretic mobilities versus NaCl concentration where the sulfonated particles were in H^+ or Na^+ forms. Figure 8 shows the μ_e values for a sulfonated latex in Na^+ and H^+ forms. From these results the ion exchange theory does not seem to be the final answer to the controversial electrokinetic behaviour of polymer colloids. Also, Ma et al. [63] found that the minimum in mobility with increasing ionic strength was not due to the titratable

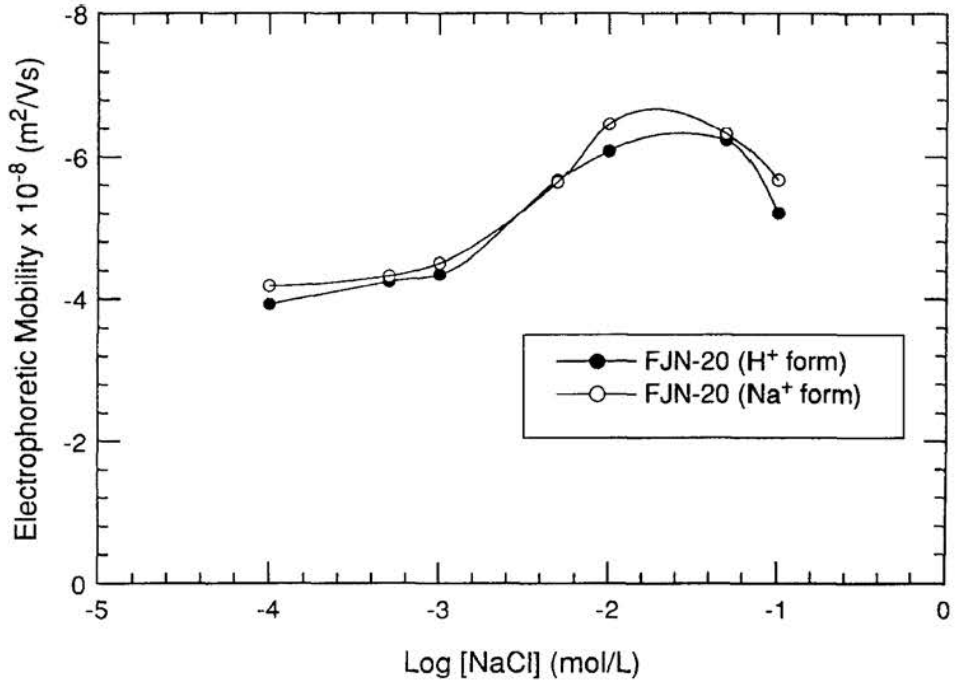

Fig. 8. Electrophoretic mobility of latex FJN20 (diameter 248 nm, surface charge density 139 mC m^{-2}) in sodium and hydrogen forms, vs. electrolyte (NaCl) concentration [17].

surface charge. In their experiments, the titratable surface charge was varied by hydrolysis of the sulfate surface groups such that the resulting latex had no measurable titrable surface charge. However, the electrophoretic properties of these hydrolysed latices were virtually identical to the original sample over a wide salt concentration range. These authors suggest that their results can be understood if the origin of the latex electrokinetic charge were primarily due to the adsorption of anions onto the hydrophobic parts of the latex surface.

Although the hairy layer model and the ion adsorption model are capable of explaining many of the observed phenomena, neither is able to account for all of them. Thus, some authors suggest that both mechanisms are operative [179,222]. The primary weakness of each model is a lack of direct experimental verification of the underlying mechanism [222]. Independent measurements of co-ion adsorption and clarification of the hydrophobic adsorption mechanism, for cations in particular, are necessary to validate the ion adsorption model. This is a very challenging experimental problem, since ion adsorption is usually inferred via ζ-potential determinations. Likewise, additional non-electrokinetic proof of hairs at the polymer surface is necessary to validate the hairy layer model.

The appearance of a minimum in ζ-potential is closely related to the theoretical treatment used to convert mobility into ζ-potential. ζ-potential values obtained from D–S equation agree reasonably with those theoretically expected. Hence, the most likely explanation for the mobility/concentration minimum seems to be a movement of the shear plane away from the surface with decreasing electrolyte concentration. This phenomenon results in two effects. First, it lowers the ζ-potential in the usual way and, secondly it lowers the mobility by a much greater percentage by introducing ionic conduction in the diffuse layer but inside the shear plane [83]. Henry's equation, with the surface conductance correction, and Dukhin–Semenikhin's equation seem to give ζ-potentials that agree remarkably well, and both remove the ζ-potential maximum. Also, this explanation agrees with the model proposed by Midmore and Hunter [83] for the electrolyte/polymer interface. According to this model the Stern layer is empty when the surface charge density is less than 6 $\mu C/cm^2$ and the Poisson–Boltzmann equation applies to all the solution side of the double layer. At high electrolyte concentration the surface is smooth and the shear plane corresponds with the outer Helmholtz plane. At lower electrolyte concentrations, however, the surface becomes either rough or hairy, causing the shear

plane to move some little distance (~1 nm, this is the diameter of a hydrated sulfate ion) away from the surface. This leads to some lowering of the zeta-potential in the normal way but to a much greater reduction in the electrophoretic mobility because of the surface conduction effect. The postulated shift in the shear plane has the effect of immobilizing a layer of water of 1 nm thickness but does not influence the mobility of the diffuse layer ions. Thus, these ions are able to conduct in this region and thereby reduce the mobility of the particle.

Surface conductance has been very useful to explain why the ζ-potentials obtained from electrophoretic mobility data are usually less negative than the ζ-potentials obtained from low-frequency dielectric dispersion [130,132,178]. Nevertheless, this explanation has also been cast doubt upon by Russell et al [107]. These authors claim that the theory of O'Brien and White [57] correctly predicts the electrokinetic potential without the need to invoke the surface conductance. They studied the high-frequency dielectric response of sulfonate latexes and the ζ-potentials obtained were compared to ζ-potentials from electrophoresis measurements. They found that the differences encountered between both techniques may not be related to theory or anomalous effects such a Stern layer conduction but merely experimental limitations. Thus, and according to Russell et al. only one technique is needed to characterize the electrokinetic properties of polymer colloids and it is highly unlikely that their latex sample is unique. The two-shot polymerization process employed to prepare these polymer colloids will lead to a highly charged "hairy" surface [17,18,69,76] with high concentrations of specifically adsorbed counterions. Extant hypothesis would make it a prime candidate for Stern layer conduction [55]. Despite this postulate, they did not found evidence of surface conduction and only one out of ten systems studied showed any dielectric response anomalies. They claimed, too, that the method of sample preparation may be of importance and that this could be the reason for the inconsistencies observed by Zukoski and Saville [185–188]. Dunstan and White [146] found reasonable agreement between static conductivities and electrophoretic mobilities with an amphoteric latex of 176 nm and 62 $\mu C/cm^2$ of surface charge density when dialysis was used to bring the samples to an equilibrium electrolyte concentration. Other methods of sample preparation, such as centrifugation and dilution were found to be totally unsuitable. They also showed that very small errors in the electrolyte concentration caused large discrepancies between the two measurement techniques. In a second paper, Dunstan and White [134] reported on the

dielectric response of amphoteric latices and suggested that surface conductance is not present in these systems or if present that the ions in the Stern layer have the same conductivity as those in the bulk. However, they claimed that the latices used in their study did not display a maximum in the mobility versus KCl concentration.

An alternative approach to the explanation of the electrokinetic behaviour of negatively charged polymer colloids is the possible crossing of the mobility/ζ-potential minimum (or maximum for cationic polymer colloids). The phenomenon of the mobility/ζ-potential minimum is caused by the distortion of the double layer at high ζ-potentials resulting in a reduction of the mobility, μ, compared with that expected from Smoluchowskis equation which predicts a linear relation between ζ and μ. If ζ is high enough, the mobility begins to drop with increasing ζ giving rise to a minimum. There exist, therefore, two possible ζ-potentials as solution to any given mobility, one low and the other high. It is thus possible that an apparent drop in ζ with a decrease in concentration is caused by taking the wrong solution for a given mobility. Until now, no reference has appeared in literature of a system in which this problem has been shown to occur. However, Gittings and Saville [190] have just published a paper where they measured the dielectric response and electrophoretic mobility to test the classical theory of electrokinetics. Good agreement between the ζ-potentials derived from the two complementary measurements was found using the standard model of electrokinetics and the ζ-potential from the upper branch of the mobility–ζ-potential relation.

5.3. Effect of heat treatment on the electrokinetic behaviour of polymer colloids

A curious hypothesis on the latex particle surface has been introduced by Chow and Takamura [70]. According to these authors, the ζ-potential maximum may be attributed to surface roughness, which results in a more distant location of the shear plane, and thus in a smaller value for the ζ-potential. In order to check this hypothesis, they modified the surface roughness of the latex by heating it above its glass transition temperature. Under these conditions, the polymer chains will acquire mobility and will be or leave or collapse onto the surface of the particles. Such alterations in the structure of the interfacial region should be revealed in the surface properties and electrokinetic behav-

iour. Their experimental results showed a decrease in the particle radius and an increase in the measured mobilities (and therefore, ζ-potential) of the heat-treated latex for various electrolytes below 10^{-4} M. They suggested that surface roughness is one of the most important factors in the determining zeta potentials from electrophoresis and the O'Brien and White's computer solution [57] overestimates the electrokinetic relaxation effect when $\kappa a < 100$.

Other works have been published recently that use the heat treatment to verify if a "hairy layer" exists on the surface of the polymer beads. Bijsterbosch and van der Linde [162], using a negatively charged latex, obtained an apparent decrease of the ζ-potential calculated with the O'Brien–White theory, upon prolonged exposure at high temperature, whereas the maximum disappeared. The two effects were accompanied by a notorious decrease in the experimentally obtained (surface) conductivity. The particle diameter remained unchanged, contrary to the observation of Chow and Takamura. But in none of these papers surface charge densities for the heat treated latices were presented. In a first paper Rosen and Saville [143] compared results obtained for an amphoteric and anionic latices before and after heat treatment by making low-frequency dielectric measurements. Their results indicated that the mean particle diameter and uniformity were essentially unaffected by the heat treatment procedure. For the amphoteric latex, the dielectric constant and conductivity decreased with heat-treatment time, and the characteristic relaxation frequency increased. They suggested that the heat treatment smooths the surface, creating particles which more closely conform to the assumptions of the classical theory. Experiments with the anionic latex suggested the presence of surface structure, but discrepancies between experiment and theory persisted. They concluded that factors other than hairiness contribute to these discrepancies. In a second paper [179], they used low-frequency dielectric spectroscopy and electrophoretic light scattering to test the applicability of the classical electrokinetic theory to latex particles with and without surface grafted water-soluble polymer. They employed two surfactant-free anionic latices: a bare poly(methyl methacrylate)/acrolein particle, and a hairy particle, prepared by chemically grafting a layer of water-soluble poly(acylamide) onto the bare particle surface. Their results showed that the mean particle diameter and uniformity were not significantly altered by heat treatment, but that the surface charge densities had increased after the heat treatment. Dielectric spectroscopy response of the heat treated bare latex agreed with theo-

retical predictions based on the ζ-potential measured electrophoretically. For the heat treated hairy latex, the agreement between theory and experiment improved. They concluded that the "beneficial" effects of heat treatment are attributed to smoothing of the molecular surface structure.

Seebergh and Berg have published a paper [217] in which they confirmed the presence of a hairy layer on the surface of some polymer colloids via simultaneous measurement of both size and electrokinetic characteristics of a given latex for a range of conditions. The presence of a hairy layer was investigated by comparing size, mobility, critical coagulation concentration, and surface charge density measurements on three different surfactant-free latexes before and after heat treatment. Light scattering measurements of size as a function of electrolyte concentration indicated that the thickness of the layer may be greater than 7 nm. The results showed that pronounced mobility and ζ-potential minima were no longer observed after heat treatment. But these parameters were smaller than the original ones (contrary to predictions of hairy layer model). This result was attributed to a loss of surface charge density after heat treatment. The high c.c.c. values of untreated latices were consistent with the presence of a hairy layer, which would provide an additional steric barrier to coagulation. After the heat treatment there was a decrease in c.c.c. values and a better agreement was found between theoretical DLVO predictions and experimental c.c.c. results. They conclude that their results strongly support the hypothesis that latex particles are covered with a layer of polymer hairs. Although they note that the new results do not rule out ion adsorption as co-mechanism.

Dunstan [147] presented experimental data from electrophoretic mobility, conductivity and dielectric response measurements on polystyrene latices and colloidal alkane particles. Measurements had been made on both normal (raw) and heat-treated latices. Figure 9 shows the measured electrophoretic mobility values for the raw sulfate latex, the heat-treated sulfate latex and the docosane particles as a function of KCl concentration. Two significant features are apparent, the mobility minima are present both before and after heat treatment and the colloidal alkane shows the mobility minimum. From these results they concluded that the mobility minima are not due to surface hairiness. The docosane particles do not have polymeric hairs protruding into the solution. The reduced mobility for the heat-treated particles compared with the raw particles arises from the hydrolysis of some sulfate groups

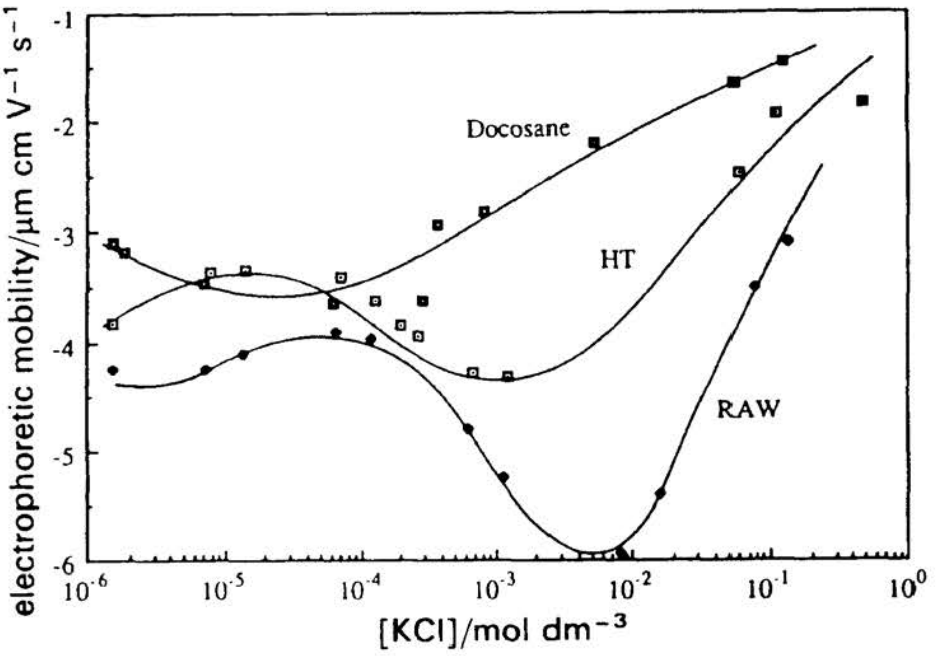

Fig. 9. Electrophoretic mobility of 0.30 μm diameter sulfate latices vs. KCl concentration. The two data sets are for the heat treated (□) and raw (♦) latices. Also shown are the data for 1.0 μm diameter docosane particles (■). Measurements were performed at 25°C at an ambient pH of 5.8 [147].

on the surface of the latices. The data of the concentration of excluded electrolyte as a function of the electrolyte concentration at which the particle were exposed showed that no specific co-ion adsorption occurs on the surface of the particle. From the results obtained with dielectric and conductivity measurements they suggested that the hydrophobic surface disturbs the water structure causing preferential solvation of the ions of one charge in the interfacial region, combined with overall exclusion of those ions from interfacial region. As conclusion they claim that the interpretation of electrokinetic data from different measurements do not yield the same values for the ζ-potentials for the same suspension. The perturbation in the ion distribution due to the hydrophobic surface of the latices is postulated as the reason for the inadequacy of the theory. As such polystyrene latices are not ideal classical electrokinetic model colloids. To describe these systems electrokinetically, a spatially varying electrostatic and chemical potential should be used in the Poisson–Boltzmann description of the interface. The spatially

varying chemical potential term arises from the fact that the interfacial water is entropically different from the bulk water.

Bastos et al. studied the effect of heat treatment on four surfactant free polystyrene latices with different functional groups on their surface (sulfate, sulfonate, aldehyde, and carboxyl). The latex with and without heat treatment were analyzed by PCS, IR spectroscopy, conductometric and potentiometric titrations, adsorption of non ionic surfactant and by measuring their electrophoretic mobilities as a function of pH and electrolyte concentration. It was observed that the mean particle diameter of four latices did not change after heat treatment. This result is similar to those obtained by Rosen and Saville and van der Linde and Bijsterbosch but contrary to that obtained by Chow and Takamura and Seebergh and Beerg. In relation to the surfaces charge densities it was found that the strong acid charge was converted into weak acid and that there was an increase in the total surface charge density of the heat treated sulfate and aldehyde latexes. They justified these changes by taking into account that sulfate groups oxidised in carboxyl groups and that part of the surface groups were hydroxyls, products of Kolthoff reaction, and therefore impossible to detect through titrations. As result of heat treatment these groups could be oxidized in carboxyl groups and become measurable with titration. Similar results were observed by Rosen and Saville when they used potassium persulfate as initiator in the synthesis of their latices. The sulfonate and carboxyl latices did not alter their charge after heat treatment. The electrophoretic mobility versus NaCl (and KBr) concentrations on sulfonate and aldehyde latexes showed an attenuation and displacement of the maximum to lower concentrations for the heat treated samples. The sulfonate and carboxyl latices showed similar electrokinetic behaviour before and after heat treatment. They concluded that heat treatment could affect latices with sulfate groups on the surface due to the hydrolysis of these groups but that the changes observed could not be attributed to the presence of a hairy layer.

In short, we can conclude that the effect of heat treatment on the electrokinetic behaviour of polymer colloids is another controversial aspect of these colloidal systems. However, there appears to be a consensus that the heat-treated polymer colloids are closer to the "ideal colloid" as predicted by standard electrokinetics theories.

6. Colloidal stability of polymer colloids in 3-D

Interactions between particles determine the stability, rheology, and many other properties of polymer colloids–liquid dispersions. The stability control of suspensions warrants detailed attention, since the development of different applications of these systems to biophysics, medicine and modern technologies are dependent to a large extent on a better understanding and manipulation of the colloidal interactions. For most of these applications colloidal particles have to remain dispersed within a relative large range of electrolyte concentration. For these reasons and in addition to the proper importance of the study of this system as colloidal models, a large number of papers has been written about the mechanisms which can induce aggregation or stabilization.

Preparation of stable polymer colloids in aqueous media needs a well balanced composition of the polymerization mixture. The dispersions in initial growing states can be stabilized by different mechanisms [225]:

(i) Creation of electrostatic repulsion forces between the polymer beads by adding an initiator, which adds charged groups to the growing macromolecular chains (emulsifier-free emulsion polymerization of hydrophobic monomers).

(ii) Addition of emulsifying agents (classical emulsion polymerization).

(iii) Copolymerization of a hydrophobic monomer and readily polymerizable emulsifying agents or hydrophilic derivatives of the hydrophobic monomer (*in situ* polymerization of surface active agents or *in situ* grafting).

(iv) Polymerization in the presence of preformed polymers (template polymerization or *in situ* grafting polymerization).

In cases ii–iv, an additional repulsive force can be operative, which arises from thin emulsifier layers (case ii) or from oligomers and macromolecules at particle surface (cases iii and iv).

These different stabilization mechanisms during particle growth sensitively influence the properties of the final polymer colloidal dispersion, such as particle shape, size and size distribution, particle structure (core/shell structure), aggregation behaviour, shear stability, thermal stability, and stability against salts.

During particle growth, the influence of electrostatic and steric or electrosteric stabilization can change, so that the degree of steric or electrosteric stabilization in the final dispersion not only depends on the composition of the starting emulsion, but also on the way the particles

form during synthesis. A further important point is that purification process can strongly change the chemical composition of the particles and, as a consequence, particle structure and stabilization mechanisms.

6.1. Classical stability theory: DLVO

The stability factor W, is used extensively in the literature to characterize the stability of hydrophobic colloids. W is the ratio of the rate constants for rapid and slow coagulation, respectively. Alternatively, in slow coagulation only a fraction 1/W of the collisions leads to coagulation. Rapid coagulation is a limit situation where there is no energy barrier between the particles, and therefore, the coagulation rate is determined by diffusion. This process was described by von Smoluchowski [226]. This theory assumes that there is no interactive forces (hydrodynamic or colloidal) present between the spheres and that once touching, particles do not subsequently separate. When an energy barrier is present, the rate of coagulation is retarded and $W > 1$. The relation between the resultant potential energy V(s) and the stability factor, considering slow coagulation was obtained by Fuchs [227]

$$W = 2\int_{2}^{\infty} \frac{\exp\left(\frac{V(s)}{kT}\right)}{s^2} ds \tag{38}$$

where $s = (H + 2a)/a$ for two spherical particles of equal radii a, and H is the distance between two spheres.

According to the theory elaborated by Derjaguin and Landau [228] and, independently, by Verwey and Overbeek [229,230], that is, DLVO theory, the stability of hydrophobic colloids, could be calculated as a balance between attractive (van der Waals) interactions (V_A) and electrical double layer repulsion (V_R). It is clear that the free energy of repulsion must depend on the charge (or electrical potential) of the particles. If we describe the e.d.l. as a pure Gouy–Chapman double layer, the electrostatic repulsion is related to the surface potential ψ_0. Furthermore any realistic model for the e.d.l. has to include the ion size [231] with the electrostatic repulsion being determined by the Stern potential ψ_δ or ζ-potential [232].

By considering the presence of a Stern layer another modification is necessary since in the original DLVO the reference planes for attractive

and repulsive energy coincide. Vincent et al. [233] refined this picture by shifting the reference plane for the repulsive energy outwardly over a distance corresponding with the thickness (Δ) of the Stern layer. Considering these corrections the electrical double layer repulsion between two equal spheres of radius a, is given by:

$$V_R = \frac{64nkT}{\kappa}(a + \Delta)\,tgh^2\left(\frac{zF\varphi_D}{4kT}\right)e^{-\kappa(H-2\Delta)} \tag{39}$$

The attraction energy of the Gouy–Chapman–Stern double layer model, as a function of the distance H, is given by [234]:

$$V_A = -\frac{A}{6}\left(\frac{2a^2}{H(4a+H)} + \frac{2a^2}{(2a+H)^2} + \ln\frac{H(4a+H)}{(2a+H)^2}\right) \tag{40}$$

To calculate the attractive interactions, only dispersion forces are considered. Equation (40) should only be used where the interaction occurs over large distances, since at small distances orientation and induction forces become important.

The van der Waals force decays as an inverse power of particle distance, whereas the electrostatic repulsion decays exponentially as $\exp(-\kappa H)$. This total interaction energy between two particles, with the addition of a short range Born repulsion energy, presents a maximum at certain distance; if through thermal agitation these particles have enough energy to overcome this barrier they will approach one another up to very close distances and the system will coagulate. But if the maximum is high enough the system will remain stable as the particles cannot overcome the barrier. Increasing the concentration of an indifferent electrolyte the e.d.l. compresses and, reduces the electrostatic repulsion between the particles. Thus, W decreases with the increasing of electrolyte concentration. The electrolyte concentration at which the energy barrier disappears, i.e. $V = 0$ and $dV/dH = 0$, is known as critical coagulation concentration (CCC). The CCC is also defined as the minimum concentration of added electrolyte to bring about diffusion-controlled rapid coagulation [235].

Reerink and Overbeek have shown [236], through several approximations, that a linear relationship exists between log W and log C_e

$$\text{Log } W = -k' \log C_e + \log k'' \tag{41}$$

where k′ and k″ are constants and C_e is the electrolyte concentration.

The stability factor is, in general, obtained by studying the change of the optical properties of suspension (using turbidity [237] or light scattering [238]) versus time is function of the electrolyte concentration.

The diffuse potential and the Hamaker constant can be estimated from the coagulation kinetics as described by Reerink and Overbeek. They related the slope of the stability curve, $-d \log W/d \log C_e$, to the radius particle, a, the diffuse potential, ψ_d, and the electrolyte valence, z. This relation is given by

$$-d \log W/d \log C_e = 2.15\times10^7 a\gamma^2/z^2 \quad (42)$$

where $\gamma = \tanh \psi_d/2$.

The Hamaker constant, which characterizes the attraction between two particles, can be obtained experimentally from the slope of the stability curve and the CCC value of the latex. For a symmetrical electrolyte the Hamaker constant, A, is given by the equation

$$A = (1.73\times10^{-36} (d \log W/d \log C_e)^2/a^2 z^2 CCC)^{1/2} \quad (43)$$

where a is in units of cm and CCC is in mmol/l. The theoretical value of the Hamaker constant for the polystyrene–water–polystyrene interface was 5.5×10^{-21} J as obtained by Gregory in 1969 making use of the approach of Lifshitz [239]. Nevertheless, Prieve and Russel [240] obtained the non retarded theoretical value 1.37×10^{-20} J, using the Lifshitz theory. In addition they showed that "A" is not really constant but that its value decays with increasing distance between the surfaces of the particles, being equal to 9×10^{-21} J at 1 nm. However, experimental values obtained by several authors are often much lower than the theoretical, i.e., (in 10^{-20} J): 0.1–1.1 [238], 0.1–0.5 [241], 0.2–1.1 [242], 0.1–0.6 [243], 1.3 [244], 0.3–0.8 [245], 0.4 [246], 0.9 [247], 0.1–0.4 [101].

Calculation of the Hamaker constant using Eqs. 38 and 39 at the CCC and with $\Delta = 3.6$ Å [248], yields values that are in better agreement with theory.

In addition to the colloidal forces between the particles the coagulation rate can be diminished through hydrodynamic interaction. Spielman [250] incorporated the viscous interaction between two spheres to coagulation process and one year later Honig et al. [251] carried out a profound study, establishing analytic approximate solutions for the effect of the hydrodynamic interaction.

According to Spielman the modified stability factor W can be written as

$$W_{visc} = 2\int_{2}^{\infty}\left(\frac{D_{12}^{\infty}}{D_{12}}\right)\exp\left(\frac{V(s)}{kT}\right)\frac{ds}{s^2} \tag{44}$$

where the Brownian diffusivity for relative motion $D_{12} = kT/f$ and f is the hydrodynamic resistance coefficient for relative motion. The relative Brownian diffusion coefficient D_{12} depends on viscosity, particle dimensions, and the relative separation between particle centres. Numerical evaluation of D_{12} has been performed using formulas presented in the Appendix of Spielman's paper [249]. The effect of particle separation on the dimensionless relative diffusion coefficient for a monodisperse colloidal suspension is shown in Fig. 10. As can be seen, the diffusion coefficient D_{12} undergoes a marked decrease when the particle separation is smaller than the particle radius. Thus, ignoring viscous interactions in the absence of repulsion could lead to large error in the values of Hamaker constants obtained from stability experiments. This could be an explanation for the disagreement between experimental and theoretical Hamaker constant values obtained by different authors for the same colloidal system [101].

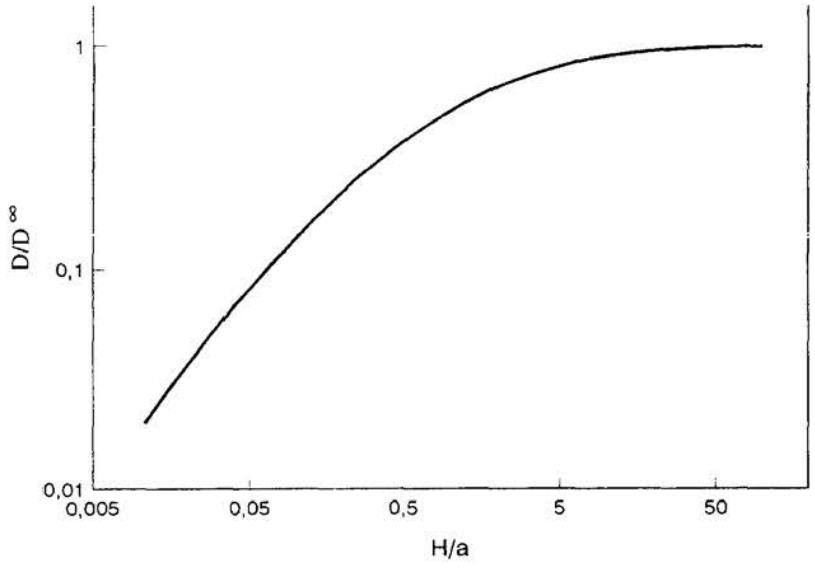

Fig. 10. Effect of particle separation on the dimensionless relative diffusion coefficient.

To verify this theory [249] the Hamaker constants of anionic and cationic latices were estimated using the modified stability factor W_{visc} [91] and found good agreement between theory and experiment ($A = 1.1\times10^{-20}$J for the positively charged polystyrene latex, and $A = 1.0\times10^{-20}$ J for the anionic sample). This supports Spielman's prediction that Hamaker constants estimated from measured coagulation rates under low repulsion can be greatly in error if viscous interactions are ignored. These viscous (hydrodynamics) interactions, essentially resisting the approach of Brownian particles, tend to increase the stability of the dispersion. The small discrepancies still existing between theoretical and experimental values could be due to the retarded effect on the estimation of the Hamaker constant from Lifshitz theory. The retarded Hamaker constant at κa equal to coagulation conditions for the latices was $(0.9–1.0)\times10^{-20}$ J, a value very close to the experimental Hamaker value obtained from the colloidal coagulation rate.

Another reason for the discrepancy between theoretical and experimental values could be the existence of features on the surface of the particles. Geometric surface features can have substantial influence on the electrostatic and van der Waals interactions. Herman and Papadopoulos [251] have quantified the significance of shape factors to the interparticle forces. They used a mode for conical and spherical asperities in parallel flat and found that surface features influence much more the electric double layer repulsion than the van der Waals attraction. This would cause an increase in the suspension stability. Therefore, the Hamaker constant obtained without taking this fact into account should be lower than the theoretical value.

In the same way Lenhoff [252] applied a perturbation method in order to determine the effect of surface roughness on the potential distribution within and around a rough quasispherical, colloidal particle carrying an internal point charge at the centre. Kostoglou and Karabelas [253] employed a model to represent roughness of colloidal surfaces based on a periodic variation of each surface. This allows the estimation of the tangential forces by taking into account the interaction of the "rough" colloidal surfaces. Again, their results showed that the energy of repulsion is always larger for rough than for smooth surfaces.

Two more aspects of the DLVO theory have been refined:

(a) Classical DLVO theory used the Derjaguin's approximation for deriving the repulsive energy of the two identical spheres at small surface potential. This approximation can be used when the thickness of the double layer is small compared with the radius of the sphere.

Although calculations using more advanced theoretical e.d.l. models yield different values at short surface separations, the decay of the double layer force still has an exponential form for large enough separations. This was shown in a recent article in this journal [254].

(b) Ohshima [255] studied the electrostatic interaction between two interacting charged ion-penetrable spheres, namely soft spheres. He showed how the linearized spherical Poisson–Boltzmann equation can be solved exactly without recourse to Derjaguin's approximation or numerical methods.

6.2. Extended DLVO theory

In addition to the electrostatic and van der Waals forces there is another category of physical interactions which have to be considered in order to get a complete theory of colloidal stability. Stabilization of colloidal dispersions may also be influenced by steric stabilization and structural forces. These mechanisms become important when there are hydrophilic macromolecules adsorbed or bounded to the particle surface. Several reviews on the effect of polymers on the dispersion stability are available [256–258].

6.2.1. Steric stabilization

This stabilization can be caused by two different mechanisms [259]:

– When two particles covered with long chains molecules come at close distance, the layers of containing adsorbed or bound molecules overlap. This overlap is equivalent to a local increase in the concentration of these molecules and, therefore, an increase in free energy. If the solvent is a good solvent, its molecules have a tendency to enter this overlap zone and separate the particles. This effect has been called the osmotic effect.

– Another effect that can occur, is due to the possible contact between polymeric chains of molecules adsorbed on the surfaces of the particles. At very close distance, these molecules lose some of their conformational possibilities, which again causes an increase in free energy. This effect is known as the volume restriction effect.

Present day understanding of these mechanisms is well covered in the literature [260–263].

Vincent et al. [264] made a quantitative consideration of steric stabilization. According to them, two particles with an external covering of polymeric chains of thickness d are influenced by the osmotic effect

when they are nearer to one another than 2d. The osmotic potential of repulsion (V_{osm}) is then given by

$$V_{osm} = \frac{4\pi a}{v_1} (\phi_2)^2 (1/2 - \chi) (\delta - H/2)^2 \tag{45}$$

with v_1 the molecular volume of the solvent, ϕ_2 the effective volume fraction of segments in the steric layer and χ the interaction parameter of Flory–Huggins.

If both particles are closer than d, the effect of the volume of restriction appears. This can be expressed by a new potential of repulsion (V_{vr}), so that at this distance the expression of the osmotic potential must be modified to

$$V_{osm} + \frac{4\pi a}{v_1} (\phi_2)^2 (1/2 - \chi) \delta^2 \left[\left(\frac{H}{2\delta}\right) - \frac{1}{4} - \ln\left(\frac{H}{\delta}\right)\right] \tag{46}$$

$$V_{vr} = \left(\frac{2\pi a}{MW} \phi_2 \delta^2 \rho_2\right)\left(\frac{H}{\delta} \ln\left[\frac{h}{\delta}\left(\frac{3 - H/\delta}{2}\right)^2\right] - 6\ln\left[\frac{3 - H/\delta}{2}\right] + 3(1 + H/\delta)\right) \tag{47}$$

where ρ_2 and MW are the density and molecular weight of the adsorbed polymer, respectively.

If we consider that the total energy is equal to the sum of all the attractive and repulsive potentials as additive

$$V = V_R + V_A + V_{osm} + V_{vr} \tag{48}$$

Figure 11 shows the different interaction energies as a function of the interparticle distance.

Recent studies have quantified the contribution of steric stabilization to the stability of a system with nonionic surfactants adsorption [265, 266]. Einarson and Berg [266] have found a reasonable agreement between the theoretically and experimentally determined values of stability ratios. To obtain the stability factor they used a kinetic model developed by Marmur [267] and modified by Wang [268].

Electrostatically stabilized dispersions are very sensitive to the presence of electrolytes, while sterically stabilized dispersions are thermodynamically stable and as such much less influenced by electrolyte

concentration. However, there are systems stabilized by polyelectrolytes, such as proteins, where it is difficult to distinguish the dominant mechanisms. In these cases the stabilization has been called electrosteric [266,269].

A weak point in the above interpretations appears if the steric and electrostatic stabilization are not independent. Thus, polymer adsorption and conformation are affected by the e.d.l. and the charge and potentials distributions around particles may be affected by the presence of an adsorbed polymer layer. Then a description of the possible interdependence of steric and electric double layer interactions is necessary.

On the other hand, improving the stabilization of a latex by a steric mechanism, one has to take the possibility into account that in addition to this stabilization a destabilization might also be present due to the dispersion of the polymers. Two ideas have been proposed. One is the bridging effect and the other is based on the charge neutralization of the particles by adsorption of opposed charged polyelectrolytes.

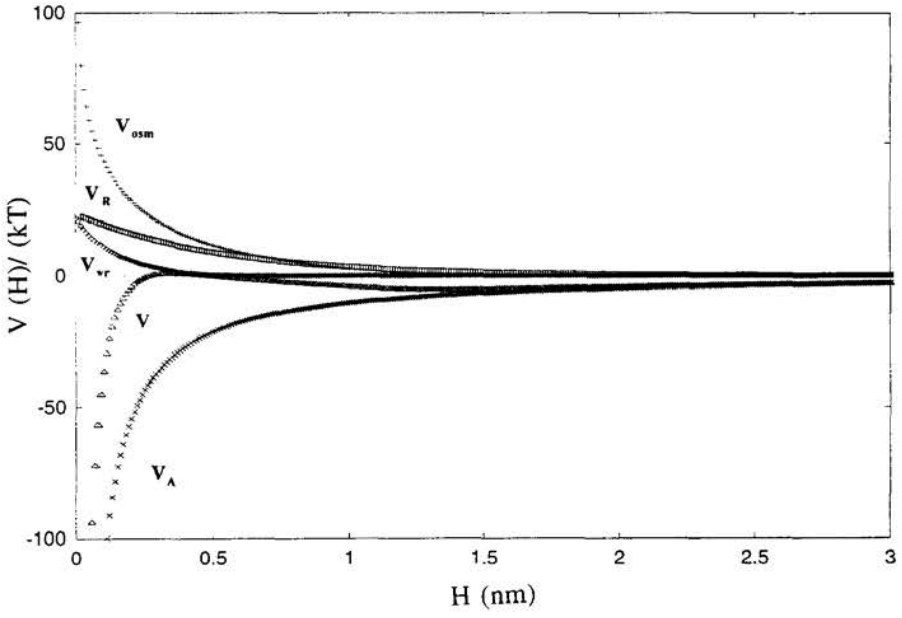

Fig. 11. Interaction energy (V, V_R, V_A, V_{osm} and V_{vr}) as a function of interparticle distance. ψ_d = 15 mV, A = 5.5 10^{-21} J, δ = 7.5 Å, ϕ_2 = 0.10 y, χ = 0.40.

6.2.2. Structural forces

Another stabilizing effect due to adsorbed hydrophilic macromolecules on the surface of the particles may be attributed to the effect of the structural forces. When two particles become close the polar interactions should be considered. These polar interactions are largely based on electron acceptor–electron donor [270]. This mechanism of stabilization is due to the changes of the water structure in the overlapping zone of the interacting particles [271], and is of special importance for the stabilization of hydrophobic sols containing water-soluble polymers or non-ionic surfactants. Structural interaction energy contributions have to be taken into consideration when two surfaces interact through a water layer. An exponential function has been adopted as the best fit to describe the distance dependence of this polar interaction. There still is an uncertainty about the actual exponent [272].

In addition to the above mechanisms of stabilization it is possible to produce stabilization or coagulation of a colloidal system through the addition of "free" or "non-adsorbing" polymers. This effect is called depletion stabilization or flocculation. In this case the loss of conformational entropy for the polymers, close to the surface is not compensated by the adsorption energy and a depletion zone develops that is void of polymer. The thickness of the depletion zone depends on the solution concentration, that is, flocculation or stabilization occur over a certain range of bulk polymer volume fraction [273]. A general approach towards the interaction of spheres in the presence of non-adsorbing polymer was introduced by Fleer et al. [274]. Their approach belongs to the groups of theories commonly referred to as "scaling". Scaling methods are adequate for weakly overlapping, long flexible chains in good solvents [275] and a good agreement has been obtained between theoretical and experimental results [276].

In a recent paper Seebergh and Berg [277] have applied the depletion mechanism to the interaction of two particles by giving each particle its own depletion layer. The model is successful in predicting the salient features of the stability behaviour, including the effects of salt due to solvency and the existence of stability plateaus at low free polymer concentration. In some cases, they obtained good quantitative agreement between their theory and experimental values of W and the critical depletion flocculation concentration. However, the model is not able to account for observations under all conditions.

6.3. Heterocoagulation with polymer colloids

In the study of colloidal dispersions, stability is mainly dependent on the interactions between the colloidal particles. When a system contains more than one type of particle, these interparticle interactions will differ from the situation where only one type of particle is present. The aggregation of particles with different characteristics (as size, surface charge, composition, etc.) plays an important role in mineral separations, corrosion and the processing of advanced ceramic materials. Although homocoagulation is the more widely studied field, it is nevertheless inadequate in explaining the mixed systems due to the complexities which result from mixing different particles [278,279]. The term heterocoagulation is generally used to describe permanent contact between particles and hence irreversibility [280]. This field has been investigated from both theoretical and experimental points of view, and recent reviews have appeared about heterocoagulation theories [281], and on heteroaggregation in colloidal dispersion including experimental investigations and applications [282].

The experimental studies of heterocoagulation usually focus on particles of very different characteristics and sizes, as clay particles on fibres [5], hematite particles (33 nm) and glass beads (55 μm) [283]. Some authors reported the adsorption of small particles onto larger particles observed by direct electron microscopy studies [284].

In order to study heterocoagulation from a kinetic point of view and to estimate the rate constant, several authors have used colloidal particles of opposite charge and different sizes and compositions [285–290]. Kitano et al. [285] studied the association processes between oppositely charged polystyrene particles, with different sizes and surface charges, by using an ultramicroscope and a spectrophotometer. The experimental heterocoagulation rate constant was found to be different to the theoretical ones, although of the same order of magnitude. Matijevic et al. [286,287] have used polystyrene (65.5 to 260 nm in particle radius), silica (210 nm) and cerium oxide (110 nm) particles and more recently anionic (167 nm) and cationic (97 nm) polystyrene latices [288]. They used a static light scattering technique to measure the stability factor and calculate the heterocoagulation rate constant of different particles mixtures. The discrepancies between the theoretical and experimental values of the heterocoagulation rate constant were explained by the discrete nature of surface ionic charges.

Dumont et al. [289] studied the formation and structure of the

resulting heteroparticles when mixing cationic and anionic polystyrene particles or some inorganic hydrosols, with very different particle size (52 to 2100 nm). Using a counting technique they concluded that the size ratio and the relative number of the interacting units are the only parameters which govern the structure of the resulting particles. These authors did not estimate the rate constant. Lichtenfeld et al. [290] studied the time evolution of singlets, doublets and triplets using a single-particle light scattering technique. They used anionic polymer colloids of the same size but a different nature (hard polystyrene spheres and soft poly-vinyl acetate spheres) and found that the coagulation constant was independent of the initial particle number.

Other authors have used the heterocoagulation process of polymer colloids to produce anomalous polymer beads having uneven surfaces [291,292] or to model the processes occurring during the growth of colloidally stable particles by aggregation with smaller particles [293].

Matijevic et al. [287] also studied the effect of the ratio of particle number concentrations on the stability factor. The effect of the ratio of large to small particles on the kinetic of the process and on the dispersion structure of binary mixtures has been studied by Rodriguez and Kaler [294] and Maroto and de las Nieves [278]. In reference [294] latex particles with two different radii, 141 and 84 nm, were studied using a static light scattering technique and the interactions between both type of particles were investigated. Maroto and de las Nieves [278,279] studied the heterocoagulation process of two polystyrene latices of similar but opposite charge and different particles size (177 and 297 nm) and followed the process by detecting changes in the optical absorbance with a spectrophotometer.

In heterocoagulation experiments with latex particles of different size the initial proportion of cationic to anionic particles can influence the final result. This proportion can affect significantly the estimation of the heterocoagulation rate constants owing to the different scattering section of both types of particles [278,279].

The aggregation of a colloidal system is expressed in terms of the stability factor W. For a system containing two particle types there are three types of interactions which may occur: 1÷1, 2÷2 and 1÷2 interactions. An expression of the total stability ratio, W_T, has been developed by Hogg et al. [295]

$$\frac{1}{W_T} = \frac{n^2}{W_{11}} + \frac{(1-n^2)}{W_{22}} + \frac{2n(1-n)}{W_{12}} \tag{49}$$

where W_{ij} is the stability factor for the formation of 1:1, 2:2 and 1:2 doublets; $n = N_1/(N_1+N_2)$ and N_i denotes the number of particles of type i.

An experimental method used to obtain the stability factor of heterocoagulation, W_H, is finding the rate of change in turbidity against the change in time, $(d\tau/dt)$, for both homo and heterocoagulation experiments

$$W_H = \frac{\left(\frac{d\tau}{dt}\right)_{0,HOMO,F}}{\left(\frac{d\tau}{dt}\right)_{0,HET}} \tag{50}$$

where $(d\tau/dt)_0$ is the initial slope, and HOMO,F signifies fast homocoagulation.

The changes in the turbidity at zero time $[(d\tau/dt)_0]$ can be related to the rate constant of doublets (K_D) by the expression

$$(d\tau/dt)_0 = (C_D/2 - C_S)\, K_D\, N_0^2 \tag{51}$$

where N_0 is the initial particle number, and C_S and C_D are the scattering section of singlet and doublet, respectively. This equation can be generalized to the heterocoagulation process of the species 1 and 2 by the relationship [278]:

$$\left(\frac{d\tau}{dt}\right)_{0,HET} = K_{D1}N_1^2\left(\frac{1}{2}C_{D1} - C_{S1}\right) + K_{D2}N_2^2\left(\frac{1}{2}C_{D2} - C_{S2}\right) + \\ + 2K_{D12}N_1N_2\left(\frac{1}{2}C_{D12} - \frac{1}{2}C_{S1} - \frac{1}{2}C_{S2}\right) \tag{52}$$

where, C_{S1}, C_{S2}, C_{D1} and C_{D2} are the scattering section of a singlet and a doublet of species 1 and 2, and C_{D12} is the scattering section of a doublet 1:2. K_{D1}, K_{D2} and K_{D12} are the slow rate constants for the formation of 1:1, 2:2 and 1:2 doublets, respectively. The scattering sections are different for the several doublets that can be formed and the optical factors cannot be cancelled. Therefore, the stability factor for heterocoagulation of particles of different sizes cannot be estimated from the comparison of homo and heterocoagulation experimental results [278]

as in Eq. (50). However, this equation would be valid for heterocoagulation of particles of the same size. Under this condition, the only useful equation to estimate the heterocoagulation rate constant is Eq. (52). Maroto and de las Nieves [278] proposed to simplify Eq. (52) by using specific experimental conditions in which the cationic and anionic particles are stables (for example, low ionic strength and intermediate pH), and K_{D1} and K_{D2} are negligible

$$\left(\frac{d\tau}{dt}\right)_{0,HET} = K_{D12}N_1N_2\,(C_{D12} - C_{S1} - C_{S2}) \tag{53}$$

In this equation the difficulty is to estimate the scattering section of the doublet 1:2, when both particles have different size. With the relationship existing between N_1, N_2, the total particle number (N_0) and n, Eq. (53) can be written as:

$$\left(\frac{d\tau}{dt}\right)_{0,HET} = K_{D12}N_0^2n(1 - n)\,(C_{D12} - C_{S1} - C_{S2}) \tag{54}$$

The initial slope $(d\tau/dt)_{0,HET}$ presents a maximum against n when n = 0.5, i.e, when the initial number of cationic and anionic particles are the same. Thus, the most favourable condition for the heterocoagulation process is when n = 0.5. Utilizing this, Maroto and de las Nieves [278] have also introduced another stability factor, W_{HET}, to connect a standard heterocoagulation experiment (when n = 0.5) to other heterocoagulation experiments

$$W_{HET} = \frac{\left(\frac{d\tau}{dt}\right)_{0,HET,0.5}}{\left(\frac{d\tau}{dt}\right)_{0,HET}} \tag{55}$$

This parameter is different to the usual heterocoagulation stability factor defined in Eq. (50), which connects homocoagulation and heterocoagulation experiments. W_{HET} connects different experiments, but both heterocoagulation experiments. By using Eq. (54) for each specific experiment, and given the same total particle number (N_0), Eq. (55) can be written in the form

$$W_{HET} = \frac{0.25\, K^*_{D12}}{n(1-n)K_{D12}} \tag{56}$$

where K^*_{D12} is the rate constant when n = 0.5, and K_{D12} was considered different for experiments with different n. In principle, W_{HET} should be a function of the proportion of cationic to anionic particles (n) and the heterocoagulation rate constants ($K_{D,12}$) of each experiment.

In order to test Eqs. (55) and (56), Maroto and de las Nieves [278,279] determined the initial slopes of the turbidity versus time curves under different conditions by varying: the proportion of cationic–anionic particle number, N_1/N_2; the total particle number ($N_0 = N_1 + N_2$) into the cell; and the wavelength. The heterocoagulation experiments were performed under low ionic strength (0.001 M) in order to eliminate the homocoagulation of cationic or anionic particles for various particle ratios, N_1/N_2 (represented as [NJA3]/[NRP]), and pH.

Figure 12 shows the logarithm of the heterocoagulation stability factor, W_{HET}, versus the pH of the dispersion, for various proportions of cationic to anionic particles, [NJA3]/[NRP], between 1 to 10 ($N_0 = 6.5\ 10^{16}$ part./m^3 and $\lambda = 770$ nm). At pH between 4 to 10, when both latices maintain the opposite charge, W_{HET} was constant for each series of

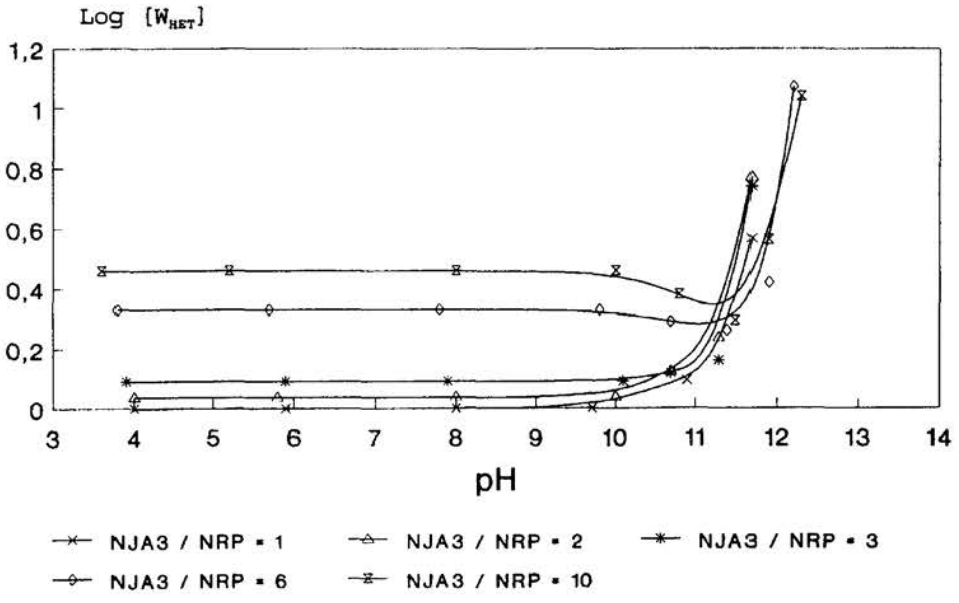

Fig. 12. W_{HET} factor versus the pH for different N_1/N_2 ratios, when the number of smaller particles, [NJA3], is the majority: [NJA3]/[NRP] = 1 (×); [NJA3]/[NRP] = 2 (Δ); [NJA3]/[NRP] = 3 (*); [NJA3]/[NRP] = 6 (◊); [NJA3]/[NRP] =10 (⧖) [280].

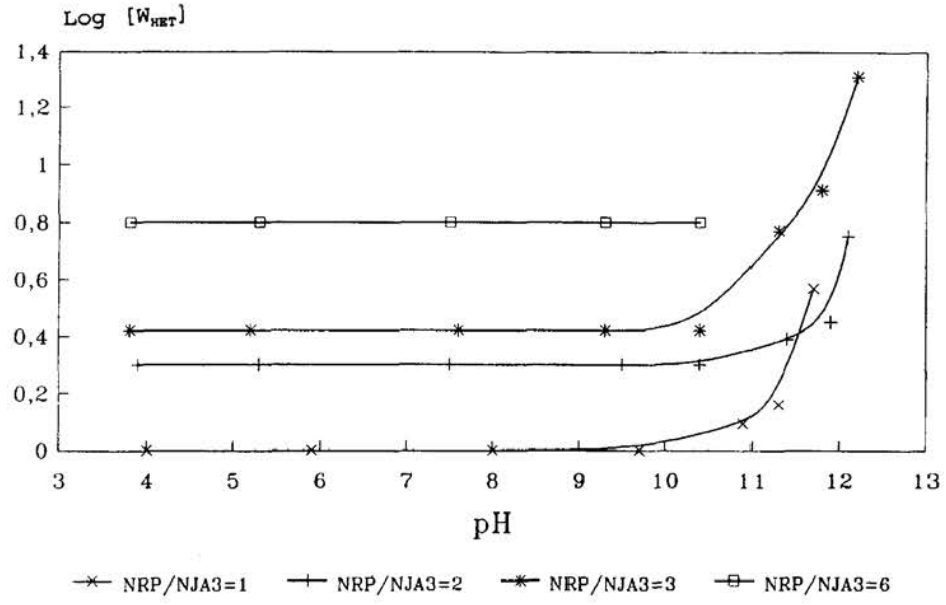

Fig. 13. W_{HET} factor versus the pH for different N_1/N_2 ratios, when the number of larger particles, [NRP], is the majority: [NRP]/[NJA3] = 1 (×); [NRP]/[NJA3] = 2 (+); [NRP]/[NJA3] = 3 (*); [NRP]/[NJA3] = 6 (–) [280].

experiments and it was concluded that the change in the surface charge of the cationic latex does not affect the rate of the heterocoagulation process, once the proportion of cationic to anionic particles is fixed. This negative influence of the particle surface charge was also found by Dumont et al. [289]. However, at pH around 11, the cationic latex was uncharged and its homocoagulation appeared, provoking a decrease in W_{HET} [280]. At pH higher than 11, the heterocoagulation rate decreased and the ratio W_{HET} increased (see Fig. 12), because the cationic latex was negatively charged and there is no homo or heterocoagulation (both latexes were negatively charged). When the ratio [NJA3]/[NRP] was 6 or 10, the homocoagulation of the cationic particles was significant at pH around 11 and W_{HET} decreased [278,279].

With the majority of particles anionic, these authors [278,279] found (see Fig. 13) that W_{HET} displayed a similar behaviour. However the decrease of W_{HET} at around pH 11 did not appear at any [NRP]/[NJA3] ratio, because the change in turbidity owing to the homocoagulation of the latex JA3 did not seem to be significant in comparison due to the presence of a majority of stable (and larger) anionic particles [278].

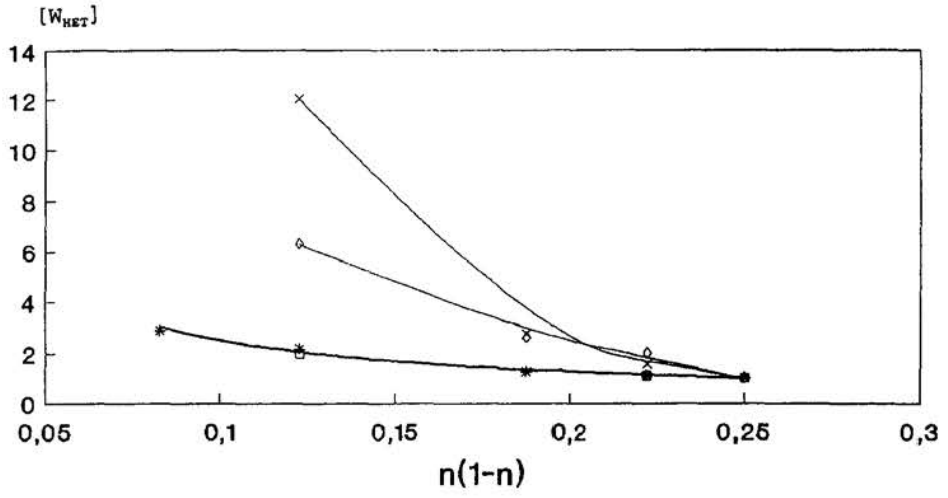

Fig. 14. Theoretical (thicker line) and experimental W_{HET} values versus n(n – 1), for several conditions. First run, λ = 770 nm and N = 6.5 10^{16} part./m^3: *, smaller particles (JA3) in the majority; ×, larger particles (RP) in the majority. Second run, λ = 600 nm and N = 4 10^{16} part./m^3: ◊, JA3 particles in the majority; ×, RP particles in the majority [280].

Maroto and de las Nieves also checked the validity of the experimental factor W_{HET} from Eq. (56), by comparing experimental and theoretical values (see Fig. 14). They calculated W_{HET} taking into consideration the fact that the rate constants K_{D12} and K^*_{D12} were independent of n, i.e. independent of the ratio N_1/N_2. Therefore, Eq. (56) was simplified as [278]

$$W_{HET} = 0.25/n(1 - n) \tag{57}$$

The W_{HET} values so estimated and those obtained from experimental data by using Eq. (55) were compared with the cationic or anionic latex in the majority [278]. The values obtained in the experiments with a majority of smaller (cationic) particles were in very good agreement with the theory. The experiments involving a majority of smaller particles showed a heterocoagulation rate constant, K_{D12}, independent of the ratio N_1/N_2. However, when the larger (anionic) particles were in the majority, the disagreement between the experimental and theoretical W_{HET} values increased with the ratio [NRP]/[NJA3].

To calculate the heterocoagulation rate constant, K_{D12}, by Eq. (53) or (54), these authors used the coalescence hypothesis to estimate C_{D12}. In

TABLE 1

Heterocoagulation rate constant (K_{D12}) values vs. different ratios [NJA3]/[NRP], for N_0 = 6.5 10^{16} particles/m^3 and λ = 770 nm

[NJA3]/[NRP]	10^{-18} K_{D12} (particles m^3/s)
10	2.08
6	2.24
3	2.14
2	2.04
1	1.97
1/2	1.10
1/3	0.98
1/6	0.58

Table 1 are the heterocoagulation rate constant, K_{D12}, calculated from Eq. (54). With the smaller latex (cationic) in the majority, a constant K_{D12} value was found, similar to the one obtained under the standard conditions (when $N_1 = N_2$ (n = 0.5)). However with the larger anionic latex in the majority, K_{D12} decreased with increasing proportion of anionic particles. Maroto and de las Nieves [278,279] explained these results as being a consequence of the increase in the amount of solid in the cell which could imply the loss of sensitivity in the spectrophotometer.

In order to confirm the conclusions about the influence of the increase of the solid content in the measurement cell, the influence of the total number of particles, N_0, on the heterocoagulation rate constant, K_{D12}, was studied [278,279]. In Fig. 15 can be seen that K_{D12} increases as N_0 decreases. For a fixed proportion of anionic to cationic particles ([NRP]/[NJA3] = 2 and 3), when the particle number was 2.5 or 3.10^{16} particles/m^3, K_{D12} showed a plateau with a similar value to that found when $N_1 = N_2$ (n = 0.5). They concluded that with an increasing proportion of larger particles, the total number of particles had to be diminished in order to obtain a reliable value for the heterocoagulation rate constant. With homocoagulation experiments using two different latices, Lichtenfeld et al. [290] showed that the homocoagulation constant was independent of the initial particle number, while other authors showed an increase of the rate constants when the initial particle number increased [296,297]. Ryde and Matijevic [288] varied the number of smaller and larger particles in a series of different experiments, but they did not

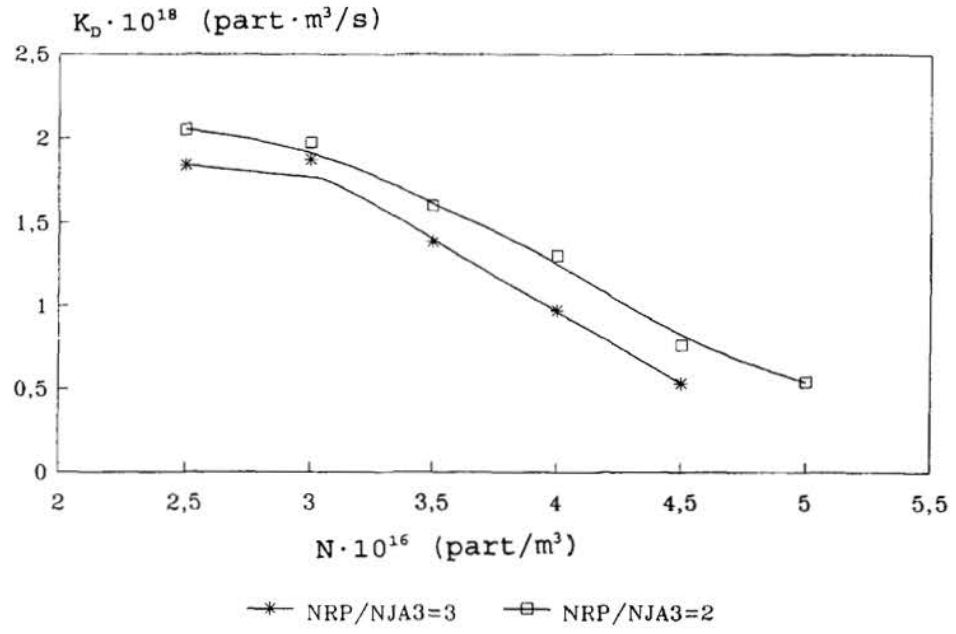

Fig. 15. Heterocoagulation rate constant (K_{D12}) values versus the total particle number (N_0), for the ratios: *, [NRP]/[NJA3] = 3; □, [NRP]/[NJA3] = 2 [280].

maintain a constant total particle number. The influence of the total number of particles and its relation to the ratio of larger to smaller particles needs still to be studied. More experiments and different techniques are necessary to get a clearer understanding of this process. These experimental studies should be supported by an adequate theoretical development in order to get more insight in heterocoagulation processes of particles of different characteristics. The possibility to use model systems with controlled particle sizes and surface charge densities, make polymer colloids a good candidate when studying heterocoagulation processes.

7. Aggregation kinetics of polymer colloids in 3-D

The last decade has seen the development of models describing the structure which results from the union of subunits. The aggregation of colloidal particles is a good model for describing this phenomenon,

central to many physical [298], chemical [299] and biological [300] processes. Determining the detailed cluster-size distribution is important since many of the properties of colloids depend on that distribution, and by now, the number of theoretical predictions and computer simulations on the form and time dependence of cluster-size distribution far exceed the number of experimental results. When the aggregation of clusters is diffusion limited (DLCA) or reaction limited (RLCA) [5,301–307] both theory and experiments shown an universal behaviour, independent of the colloid. DLCA occurs when every collision between diffusing clusters results in the formation of a bond. With this regime, the rate of aggregation is limited by the time the clusters need to diffuse towards one another. RLCA occurs when only a small fraction of collisions between clusters results in the formation of a bond and thus bigger clusters. In this case, the rate of aggregation depends not only on the diffusion, but also on probability of forming a bond. The two most prominent features of this universal behaviour are the reaction kinetics and the cluster morphology. The former is described using Smoluchowski's coagulation equation [308] and the latter by considering clusters to have a fractal structure [309,310].

The aggregation mechanism depends on the interaction between clusters. The latter may be modified by adding salt to a stable colloid dispersion. This reduces the electrostatic interaction at large distances, while keeping a the short range residual interaction large. To ensure DLCA conditions, hydrochloric acid (HCl) is usually added to a system of negatively charged particles to eliminate their surface charge density [306]. Under these conditions, an irreversible fast process takes place, primarily due to the Brownian motion of the colloidal particles. When the electrostatic interaction between the particles is not completely removed, the rate of aggregation is slower and the aggregation is not only due to the Brownian motion of the particles. Then, the intensity of the interactions define the aggregation mechanism. When the interaction is very strong the mechanism will be RLCA.

7.1. Smoluchowski's theory

The Smoluchowski rate equation provides a useful mean field approach to the kinetics of aggregation and a framework to classify the wide variety of growth processes. This classification helps to distinguish between DLCA and RLCA and to clarify the difference between aggregation and gelation processes, frequently observed in colloidal systems.

In general, a colloidal aggregation process may be described by the following reaction scheme

$$(\text{i–mer}) + (\text{j–mer}) \xrightarrow{k_{ij}} (\text{i+j})\text{–mer} \tag{58}$$

where i-mer denotes a cluster of i subunits and $k_{ij} = k_{ji} \geq 0$ is the concentration-independent coefficient or kernel of the irreversible reaction. This kernel parameterizes the rate of such reaction, giving the probability of an i-mer reacting with a j-mer. Kernels contain the physical information on the aggregation process and, in general, only depend on the size of the reacting clusters. A kernel is a configurational and orientational average of the reaction rate between two colliding clusters. For dilute suspensions, only collisions between two clusters need be considered, since the probability of three-cluster collisions is negligible. Furthermore, this equation assumes that clusters are uniformly distributed in the solution.

For certain irreversible aggregation processes, a cascading growth may occur in which an infinite-size cluster grows within a finite time. This big cluster is usually called gel phase and the finite-size clusters coexisting with the gel phase are referred to as the sol phase. From a certain time called time of gelation, t_{gel}, mass flows from the sol phase to the gel phase which is growing fast.

Smoluchowski's equation [308] expresses the time evolution of the size distribution of the clusters, $N_n(t)$, in terms of the reactions kernels k_{ij}

$$\frac{dN_n}{dt} = \frac{1}{2} \sum_{i+j=n} k_{ij} N_i N_j - N_n \sum_{i=1}^{\infty} k_{in} N_i \tag{59}$$

This equation takes into account all pairs of collisions which may generate or deplete a given cluster-size. The first term accounts for the creation of n-mers through binary collisions of i-mers and (n–i)-mers. The second one represents the depletion of n-mers due to binary collisions with other clusters.

The structure of this equation is simple, although it is difficult to know the form of the reaction kernel for a given system. Smoluchowski's equation is analytically solvable only for a few kernels; for example, constant kernel ($k_{ij} = k_{11}$), sum kernel ($k_{ij} \sim i+j$), product kernel ($k_{ij} \sim ij$), and linear combinations thereof.

Constant kernel

The simplest form is when k_{ij} is independent of the cluster size, i and j, namely, k_{ij} = constant. Physically this means that the rate of reaction between all pairs of clusters i and j is identical. Though this choice is a mathematical idealization, there are aggregation processes for which this kernel is appropriate. For example, diffusion-limited aggregation of an initially monodisperse suspension is well modeled by a constant kernel during the early stages of the reaction. For monomeric initial conditions and constant kernel, the solution is given by [311–312]

$$N_n(E) = N_0 \frac{E^{n-1}}{(1+E)^{n+1}} \tag{60}$$

where N_0 is the initial monomer concentration and $E \equiv t/t_{agg} \equiv t\, N_0\, k_{11}/2$. For this solution the number of monomer, N_1, decays steadily, reflecting the depletion of monomers as larger clusters are formed. For larger aggregates, N_i ($i \geq 2$) grows to a maximum and then decreases. The time at which each N_n peaks is given by $E_{peak} = \frac{1}{2}(n-1)$. This growth and decay is reflected by the opposite signs of the gain term and loss term in the coagulation equation. For monomers, the gain term does not exist and thus N_1 decreases monotonically.

The zero moment of the cluster-size distribution, $M_0 = \sum N_n$ is a measurement of the total number of clusters present in the colloidal solution. For constant kernel, $M_0 = (1+E)^{-1}$. Only half the initial number of clusters are present at $t = t_{agg}$ and thus for a constant kernel, t_{agg} is a sort of half-life time. It should be noted that the N_0 dependence of t_{agg} implies that the larger the initial concentration of initial particles, the faster the aggregation proceeds. The first moment, $M_1 = \sum n\, N_n$ coincides with the initial particle concentration and indicates the mass conservation in the sol phase. For this kernel, M_1 remains constant which implies that a constant kernel does not lead to gelation.

Sum kernel

The solution to Smoluchowski's equation for a sum kernel, $k_{ij} \sim i+j$ and monomeric initial conditions is [311]

$$N_n(E) = N_0 \frac{(1-\Lambda)\,(n\Lambda)^{n-1}\exp(-n\lambda)}{n!} \tag{61}$$

$$\Lambda \equiv 1 - \exp(-E)$$

This solution is qualitatively similar to the solution for a constant kernel, but the rate of aggregation is higher. This may be seen by calculating the time at which N_n peaks, $E_{peak} = \frac{1}{2} \ln n$. This faster growth rate was to be expected since the sum kernel increases with increasing cluster size.

For sum kernels, the zero moment of the cluster-size distribution, is $M_0 = \exp(-E)$, which represents a faster decrease than M_0 for constant kernels. M_1 is constant which implies that this kernel does not lead to gelation.

Product kernel

When the rate of aggregation depends on the product of the cluster size, $k_{ij} \sim ij$, the rate becomes so fast that gelation occurs. The solution to Smoluchowski's equation for a product kernel and monomeric initial conditions is [311]

$$N_n(E) = N_0 \frac{(2nE)^{n-1} \exp(-2nE)}{n\, n!} \qquad E \leq E_{gel} \equiv \tfrac{1}{2} \tag{62}$$

The curve $N_n(E)$ peaks at $E_{peak} = \frac{1}{2}(1-1/n)$ and thus, in the limit of big clusters ($n \to \infty$), reaches its maximum at $E = E_{gel} \equiv \frac{1}{2}$. It is interesting to note that for constant and sum kernels, $E_{peak} \to \infty$ with $n \to \infty$, implying that infinite-size clusters only appear after an infinite time. The zero moment of the cluster-size distribution, $M_0 = 1 - E$ and the first moment, $M_1 = 1$, imply that gelation does not occur. At $E = E_{gel}$, we have that $dM_1/dE = -2$, implying a mass flux from the sol phase to the gel phase.

The time evolution of the cluster-size distribution for $E > E_{gel}$ depends on the interaction between the sol phase and the gel phase. The simplest model for this time evolution is the Stockmayer model which assumes that there are no sol–gel interactions. This model does not require the coagulation equation to be modified. This model leads to

$$N_n(E) = \frac{E^{-1}}{2} N_n(E_{gel}) \tag{63}$$

Both the zero moment of the cluster-size distribution, $M_0 = E^{-1}/4$ and the first moment, $M_1 = E^{-1}/2$. M_1 proportionally decrease E^{-1} revealing mass flux from the sol to the gel phase.

A model that includes sol–gel interactions is the Flory model. This model adds new terms to the coagulation equation [313].

7.2. Dynamic scaling in aggregation phenomena: homogeneous kernels

Most coagulation kernels used in the literature are homogeneous functions of i and j, at least for large i and j [314–316]. Van Dongen and Ernst [317] introduced a classification scheme for homogeneous kernels, based on the relative probabilities of large clusters sticking to large clusters, and small clusters sticking to large clusters. If small–large interactions dominate, then large variations in cluster mass are discouraged, and the size distribution will tend to be tightly bunched, like a bell-shaped curve. If large–large interactions dominate, the small clusters tend to be left behind in the scramble and the result is a monotonically decreasing size distribution. In this theory it is assumed that, in the scaling limit (i.e., long times and large clusters) the cluster-size distribution has the form [317–319]:

$$N_n(t) \sim s^{-\theta}\, \Phi(n/s) \tag{64}$$

where θ is a kinetic exponent, s(t) is related to the average cluster size and $\Phi(x)$ is the time-independent scaling function. A direct consequence of mass conservation is $\theta = 2$.

Dependence of homogeneous kernels on i and j at large i and/or j, may be characterized by two exponents defined as follows

$$k_{ai,aj} \sim a^{\lambda}\, k_{ij} \qquad (\lambda \leq 2) \tag{65}$$

$$k_{ij} \sim i^{\mu}\, j^{\nu} \qquad (\nu \leq 1) \qquad i << j \qquad \lambda = \mu + \nu \tag{66}$$

Kernels with either, $\lambda > 2$ or $\nu > 1$ are unphysical, since the reactivity cannot increase faster than the cluster mass. No restrictions are imposed on μ.

The homogeneity parameter λ expresses the tendency of a big cluster to join up with another big cluster. For $\lambda > 1$ the rate of aggregation becomes so fast that an infinite-size cluster forms within finite time, i.e. gelation occurs. Kernels with $\lambda \leq 1$ give non-gelling behaviour, i.e., an infinite cluster only forms after an infinite time. Thus, the magnitude of λ allows to distinguish between gelling and non-gelling systems. λ takes the value 0 in DLCA, and 1 in the case of RLCA [320].

The exponent μ establishes the rate at which big clusters bind to small clusters and its sign determines the shape of the size distribution. For $\mu < 0$ big–small cluster unions are favoured and large clusters gobble up small ones resulting in a bell-shaped size distribution. Kernels with negative μ appears to be a good description for DLCA. When $\mu > 0$ large–large interactions dominate and size distributions to be polydisperse since small clusters may still exist even in the presence of large ones. Thus, distribution decays monotonously with increasing n. For the exactly solvable kernels the exponents are shown in Table 2.

TABLE 2

Values of λ and μ-parameters for different kernel combinations

Kernel	λ	μ
$k_{ij} \sim k_{11}$	0	0
$k_{ij} \sim i+j$	1	0
$k_{ij} \sim ij$	2	1

A product kernel has the homogeneity parameter $\lambda > 1$ and only this kernel leads to gelation. All the exact kernels have $\mu \geq 0$ indicating that reactions between small and large clusters do not play any special role in the cluster-size distribution for long time periods. For those distributions small clusters may still be present even in the presence of large clusters an i.e., the cluster-size distribution tends to be polydisperse.

Both s(t) and $\Phi(x)$ in (7) contain the exponents λ and μ of the kernels [8,317].

For the function s(t):

$$s(t) \sim \begin{cases} t^{\frac{1}{1-\lambda}} & \lambda < 1 \\ \exp(\alpha t) & \lambda = 1 \end{cases} \tag{67}$$

where α is a constant. This function is related to some ratios of moments of the cluster-size distribution. It is directly proportional to the weight-average mean cluster size $\langle n_W \rangle \equiv M_2/M_1$, where $M_i = \sum n^i N_n$. s(t) is also related to the number-average mean cluster size $\langle n_n \rangle \equiv M_1/M_0$. The relationship between s(t) and $\langle n_n \rangle$ depends on the sign of μ. For kernels with $\lambda < 1$ [8,321]

$$s(t) \sim \begin{cases} \langle n_n \rangle & & \mu < 0 \\ \langle n_n \rangle^{\frac{1}{2-\tau}} & \tau < 1+\lambda & \mu = 0 \\ \langle n_n \rangle^{\frac{1}{(1-\lambda)}} & & \mu > 0 \end{cases} \tag{68}$$

The analytical form of $\Phi(x)$ is known for large and small x [8,317]:

$$\Phi(x >> 1) \sim x^{-\lambda} \exp(-\beta x) \tag{69}$$

$$\Phi(x << 1) \sim \begin{cases} \exp(-x^{-|\mu|}) & & \mu < 0 \\ x^{-\tau} & \tau < \lambda + 1 & \mu = 0 \\ x^{-(1+\lambda)} & & \mu > 0 \end{cases} \tag{70}$$

For large x, $\Phi(x)$ decreases and is related only to the exponent λ, where β is a fitting parameter. For small x, $\Phi(x)$ depends on the sign of μ. Therefore, when $\mu < 0$, $\Phi(x << 1)$ increases with x, whilst for $\mu \geq 0$, $\Phi(x << 1)$ decays monotonically. Thus, the shape of the function $\Phi(x)$ depends critically on the sign of μ. For kernels with $\mu < 0$, $\Phi(x)$ is a bell-shaped function, whilst for $\mu \geq 0$, a monotonically decreasing one. If $|\mu| \to 0$, an intermediate x range exists, $x_0 << x << 1$, where kernels with $\mu > 0$ and $\mu < 0$ show typical $\mu = 0$ behaviour, with crossover to respectively $\mu > 0$ and $\mu < 0$ behaviour at $x \sim x_0$. x_0 depends on μ as $x_0 = \exp(-1/|\mu|)$ [317].

The above formulae (69) (70) imply the following predictions for the long time behaviour of the cluster-size distribution $N_n(t)$ (7). Thus, when $\lambda < 1$

$$\begin{cases} \dfrac{N_n(t)}{N_1(t)} & \to \infty & \mu < 0 \\ N_n(t) \sim t^{-w} n^{-\tau} & w > 1 \quad \tau < 1+\lambda & \mu = 0 \\ N_n(t) \sim t^{-1} n^{-(1+\lambda)} & & \mu > 0 \end{cases} \tag{71}$$

7.3. Monitoring aggregation processes

Knowledge about the cluster-size distribution is essential for the characterization of the kinetics and mechanisms controlling cluster growth. Powerful techniques have been successfully applied to deter-

mine cluster-size distributions. They may be classified into two groups: multiparticle and single particle detection techniques. Multiparticle techniques do not alter the aggregating system, however, they only provide average information on size distribution [302,322–330]. Single particle detection allows detailed cluster-size distributions to be measured directly by counting the number of different clusters during aggregation [331–338]. Nevertheless, the forces involved in cluster separation can break up the aggregates under certain experimental conditions and thus, modify the cluster-size distribution. Due to the difficulties in detecting and classifying single clusters, accurate measurements are rare and by now, the number of theoretical predictions and computer simulations far exceeds the number of experimental results.

Multiparticle techniques.

There exist three classical multiparticle techniques: sedimentation, filtering and measuring of the dielectric constant. In the first, the sedimentation volume is measured to estimate the aggregation stage. Aggregation processes may be monitored by measuring the time evolution of the sedimentation gradient [339–341]. The main difficulty with this technique that the data interpretation requires the application of Stoke's equations. It is also possible to obtain information about the aggregation process by filtering the aggregating samples. This method selects and classifies clusters [342]. In general, the results are very criticizable due to the forces acting on the clusters during the filtering process which may modify the cluster-size distribution. The electrical conductivity and the dielectric constant also offer information about the aggregation stage but they are not often used in studies [343].

Turbidimetry is a very extended technique usually employed to study aggregation. This technique offers information on the cluster-size distribution by solving an inverse problem of light scattering [344,345]. The instrumental set-up consists of an spectrophotometer and a personal computer for collecting the data as a function of time. The turbidimetry is based on the measurement of the optical transmittance of a colloidal sample, $T_{opt} = I/I_0$ (I is the transmitted intensity and I_0 is the incident intensity).

The turbidity, τ, is defined for monochromatic light as follows

$$T_{opt} = \exp(-NC_{ext}l) \equiv \exp(-\tau l) \tag{72}$$

where N is the particle concentration, C_{ext} is the extinction section for the particles and l is the optical path.

Monitoring the turbidity of an aggregating system, it is possible to determine the Smoluchowski rate constant, k_{11}, for the initial stages [346]. Both, the temporal evolution of the turbidity and an optical factor offered by the Rayleigh–Gans–Debye approximation (RGD) must be known. This technique is useful but sometimes the interpretation of the results becomes difficult. An interesting modification of the classical turbidimetry is the analysis of the turbidity fluctuations with dynamic light scattering.

Static light scattering is another powerful technique, measuring the mean scattered intensity. The results are usually interpreted by using a light scattering theory: the Mie theory for the most general case or the approximation of Rayleigh–Gans–Debye (RGD) for small particles [347, 348]. The information is obtained through measuring the angular and temporal dependence of the scattered intensity. The Smoluchowski rate constant can be calculated using the following equation

$$\left(\frac{1}{I(q,0)}\frac{dI(q,t)}{dt}\right)_{t\to 0} = k_{11}N_0\frac{\sin(2qa)}{qa} \tag{73}$$

where $q = |\mathbf{K_s} - \mathbf{K_i}|$ is the modulus of the scattering vector, $\mathbf{K_s}$ and $\mathbf{K_i}$ are the scattered and incident wave vectors respectively and a is the diameter of a monomer. The RGD approximation was used to deduce equation (73).

Dynamic light scattering is another technique used for particle size determination. This technique analyzes the fluctuation of the light scattered by the particles. With this technique the autocorrelation function $g(\tau) = \langle I(q,t)\ I(q,t+\tau)\rangle$ is measured. The logarithm of the autocorrelation function is expressed as a power series [348–350]

$$\ln(g(\tau)) = -\mu_1\tau + \mu_2\left(\frac{\tau^2}{2}\right) + \mu_3\left(\frac{\tau^3}{3}!\right) + \ldots \tag{74}$$

The first cumulant, μ_1, is related to the average diffusion coefficient, $\langle D\rangle$, by $\mu_1 = q^2\langle D\rangle$. The ratio $Q = \mu_2/\mu_1^2$ is a measure for the polydispersity of the system.

Single particle detection

Another group of techniques to determine the size distribution is based on single particle detection. With optical microscopy size distri-

butions for particles bigger than 1 μm can be measured. The electron microscopy is a very general and useful technique which requires the introduction of size patrons. In the last decade electron microscopy was employed in some interesting works on colloidal aggregation; for example the work referred to in Ref. [351]. The basic problem of this technique is the modification of the aggregation stage in the sample preparation and measurement.

The coulter counter is an instrument based on the change of electrolyte conductivity when a particle crosses a hole placed between two electrodes. The colloidal particles are injected through a capillary and focused hydrodynamically into a hole of about 30 μm diameter [352]. A particle crossing the hole interrupts the ionic conduction and this pulse in the conductivity is observed. This set-up allows the measurement of cluster size distributions for particle concentration of the order of 10^6 or 10^7 cm^{-3} and particle size bigger than 0.5 μm or 1 μm. The main problems with this technique are electrical noise and electrolyte contamination. Another important problem appears for polydisperse systems. When big and small particles are detected almost simultaneously, the big pulses overlaps to the smaller pulses causing an apparent depletion of the smaller particles. Information about some very improved instruments may be found in [353–355].

Single particle optical detection is probably the most advanced technique developed in the last years to measure particle size distributions and to monitor aggregation processes. Now, we will briefly describe a single particle optical sizer built in our laboratory [356,357] based on the Pelssers et al. device [331,332]. In this instrument of a colloidal dispersion, single clusters, insulated by hydrodynamic focusing, are forced to flow through a focused laser beam. Measurements of the cluster-size distribution are obtained by analyzing the light intensity scattered by single clusters at low angle, where intensity is monotonically related to the square cluster's volume: $I_n(\theta)/I_1(\theta) = n^2 \sim V^2$. At this angle, the scattered light intensity is high enough to detect particles accurately and the strong dependence of the scattered light intensity on particle's volume, makes it possible for a high resolution to be achieved. For larger angles the intensity is lower and data interpretation become difficult due to intensity oscillations caused by particle size changes [344].

Figure 16 shows a block diagram of the instrument. Basically, it is a flow ultramicroscope in which pulses of light from single particles are detected. Light from a laser goes through the input optical system which

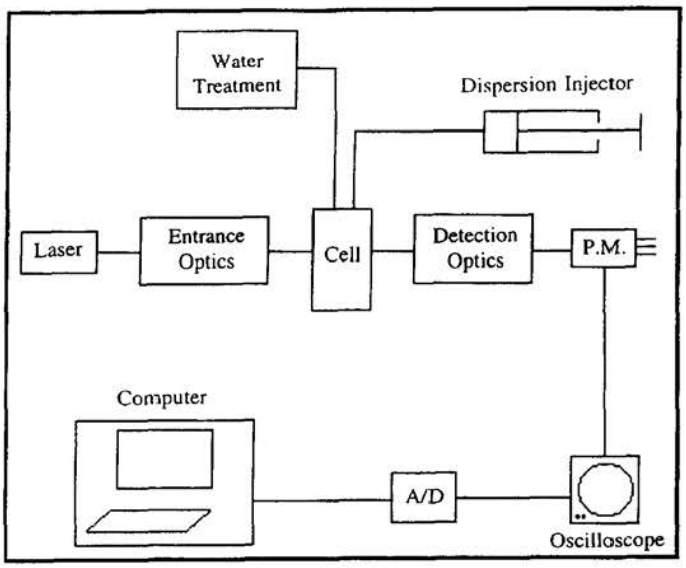

Fig. 16. Block diagram of the experimental set-up.

creates a homogeneously illuminated zone at the centre of the flow cell, where the cluster separation are separated. In the focusing cell, a colloidal dispersion is injected into a fast flowing water stream thereby obtaining a narrow particle stream. Single particles cross this illuminated zone, creating pulses of light scattered. Detection optics selects only light scattered at low angle which is detected by a photomultiplier which supplies the pulses to a computer. This computer recognizes, classifies and counts the pulses by running an algorithm on-line.

Size distribution is obtained by representing counts versus pulse intensity. Figure 17 shows a frequency histogram of an aggregating latex dispersion. Peaks correspond to different cluster-sizes, from singlets to hexamers. Bigger clusters may be detected but it is difficult to distinguish between them. This instrument allows the detailed cluster-size distribution to be measured for n up to 6 or 7, without applying numerical peak separation methods. The relationship $I \sim V^{(1.85\pm0.04)}$, between scattered light intensity and the volume of the clusters was found, which is close to Rayleigh's prediction, $I \sim V^2$. The cluster-size distribution is determined by integrating the peaks appearing in the histograms, and the time evolution is obtained by analyzing a consecutive series of the latter. The statistical counting error $N_n^{1/2}$ was considered, being a criterion to set the time of measurement. The zero moment of

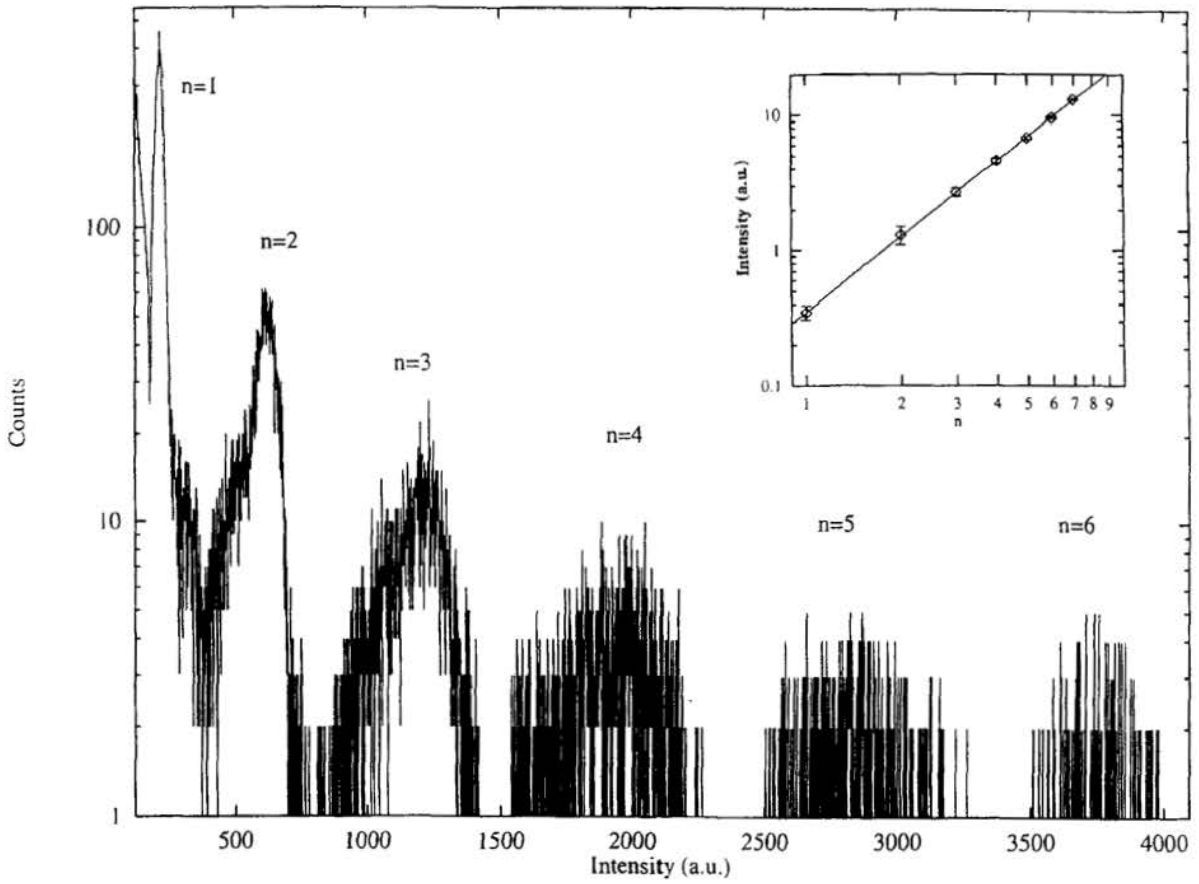

Fig. 17. Cluster-size distribution of an aggregated sample. Clusters from monomers up to hexamers are shown. Dependence of the scattered light intensity on the cluster size, n, is plotted in the top right hand corner. The best fit leads to $I \sim V^{(1.85\pm0.04)}$ [357].

the cluster-size distribution, $M_0 = \sum N_n$, is measured by adding the total number of counts in a histogram, including off-scale pulses. In this calculation every cluster must be counted, though they need not be separated according to their size. This allows the number-average mean cluster size $\langle n_n \rangle = N_0/M_0(t)$ to be calculated. This is related to s(t) and is needed together with the distribution $N_n(t)$, to determine the scaling function $\Phi(x)$.

Hydrodynamic forces acting on aggregates could break them up them under certain conditions. These forces are related to the stream velocity in the longitudinal and transversal directions with respect to particle movement. Extensional and shear forces appear, respectively. These forces are also proportional to the extensional and shear rates, respectively [331,358,359]. Size distributions were measured for different focusing fluxes to check the cluster break-up. Control measurement demonstrated that cluster break-up does not affect our experiments since they were carried out using smaller monomers [357].

7.4. Experimental results on aggregation of polymer colloids

In this section, some experimental results on Brownian and reaction-controlled aggregation are described. Furthermore, the effect of the surface charge density and particle size will be discussed.

Cluster-size distribution and rate constant in Brownian aggregation

The time evolution of monomers up to heptamers is shown in Fig. 18. Measurements were performed with the single particle instrument described in Section 7.3. Monomers decrease monotonically; for dimers and larger clusters, peaks appear to shift over to longer times the larger the cluster. Data were analyzed in the framework of Smoluchowski's coagulation equation. The best fit leads to an experimental rate constant, $k_{11} = (5.6 \pm 0.6) \times 10^{-12}$ cm^{-3} s^{-1}. This value falls within the range of values commonly reported for fast aggregation [332,346,356–368]. The equation was computed under the condition $N_{j>3} = 0$ using k_{ij} as fitting parameters. The large errors found for k_{ij} render this method useless for its determination.

The experimental value for k_{11} is now compared with the theoretical Smoluchowski rate constant, $k_{11} = 8/3\ k_B T/\eta$. For our experimental conditions, the theoretical rate constant is 11.0×10^{-12} cm^{-3} s^{-1} which is about twice the experimental value. In order to explain the difference, viscous interaction between the particles was considered and the value

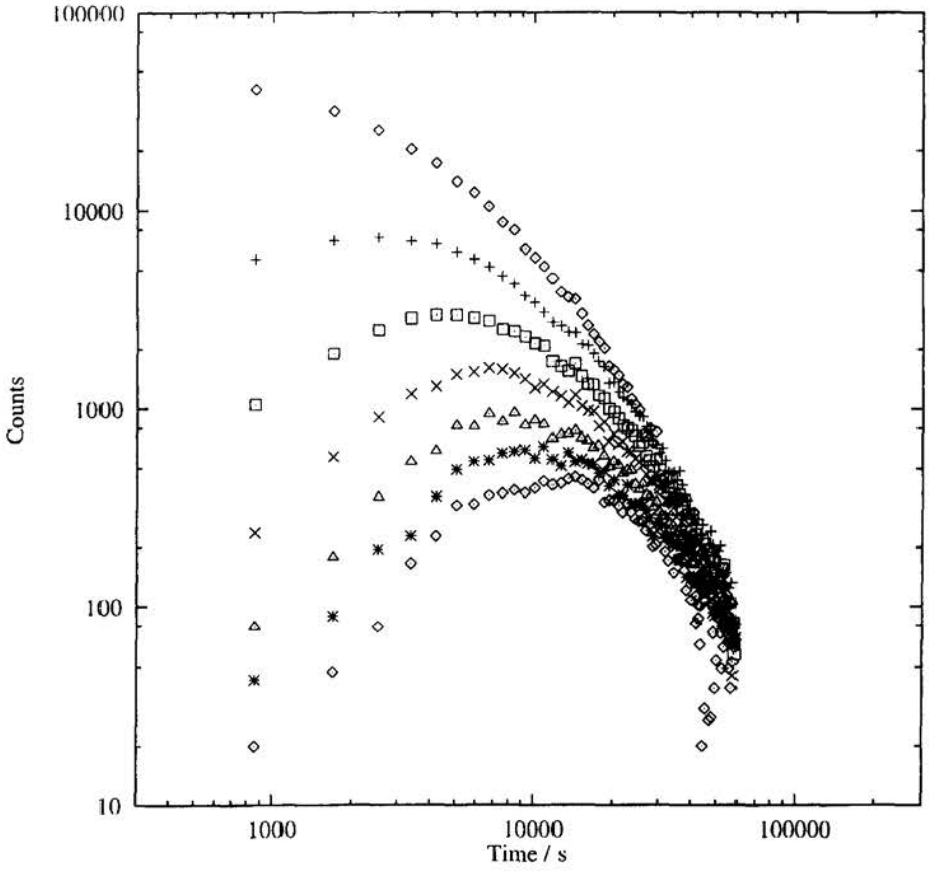

Fig. 18. Time evolution of the cluster-size distribution: monomers (◊), dimers (+), trimers (□), tetramers (×), pentamers (Δ), hexamers (*), heptamers (◊) [357].

of the modified rate constant, k_{11}^{vis}, was calculated. W_{vis} was obtained by numerical evaluation of Eq. (33) and using Spielman's formulae [352]. $W_{vis} = 1.97$ was found and, therefore, $k_{11}^{vis} = 8/3(k_BT)/(\eta W_{vis}) = 5.5 \times 10^{-12}$ cm^{-3} s^{-1}, which coincides perfectly with the experimental rate constant.

Dynamic scaling

The aggregation data were analyzed using the dynamic scaling formalism. The main questions are whether the cluster-size distribution scales, if so when scaling becomes apparent and what information about the aggregation mechanisms can be obtained. For this purpose, the zero moment of the size distribution, $M_0 = \Sigma N_n$ is measured by adding the

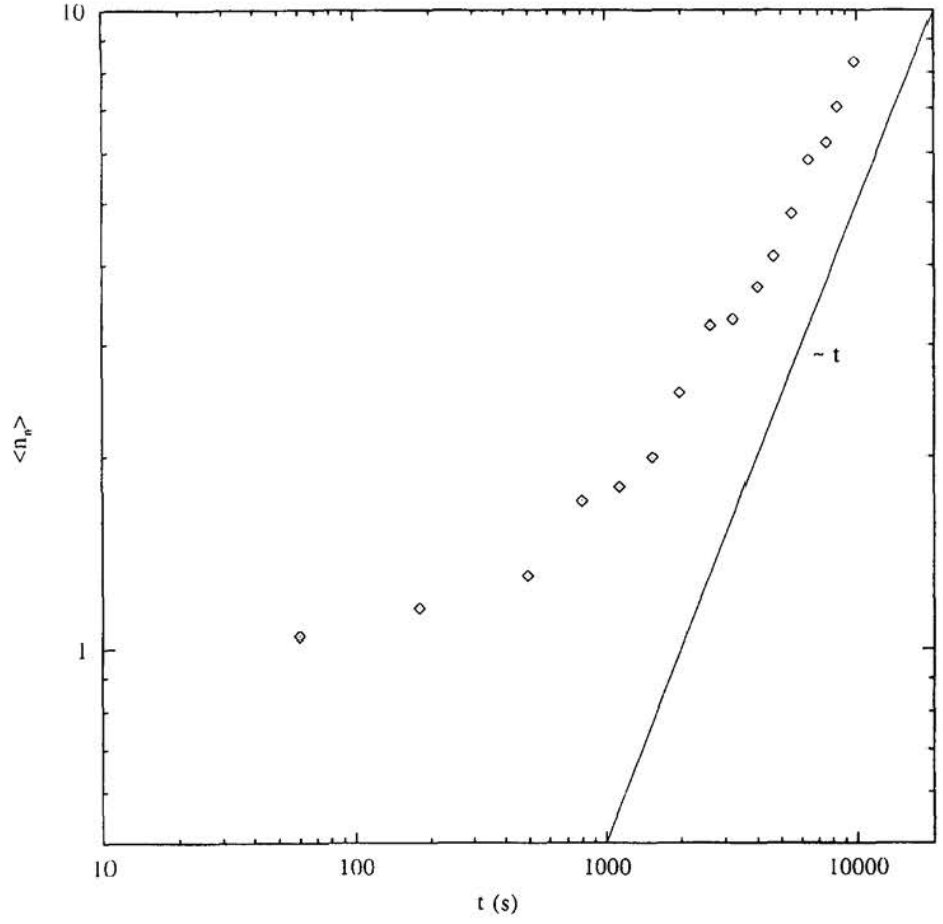

Fig. 19. Plot showing the time evolution of the number-mean cluster size. The solid line corresponds to a kernel with $\lambda = 0$ [357].

total number of counts in a histogram, including off-scale pulses. In this calculation, the clusters need not be separated according to their size. With the aid of M_0, the number-average mean cluster size $\langle n_n \rangle = N_0/M_0(t)$ is calculated. This average is related to s(t) and together with the distribution $N_n(t)$ allow the scaling function, $\Phi(x)$, to be determined. A typical result is presented and discussed below.

Figure 19 shows the time evolution of $\langle n_n \rangle$. For longer times, this function exhibits an asymptotic behaviour and grows linear in time for mean cluster sizes as low as 3. In order to obtain the function s(t), the sign of μ must be known, since the relationship between $\langle n_n \rangle$ and the

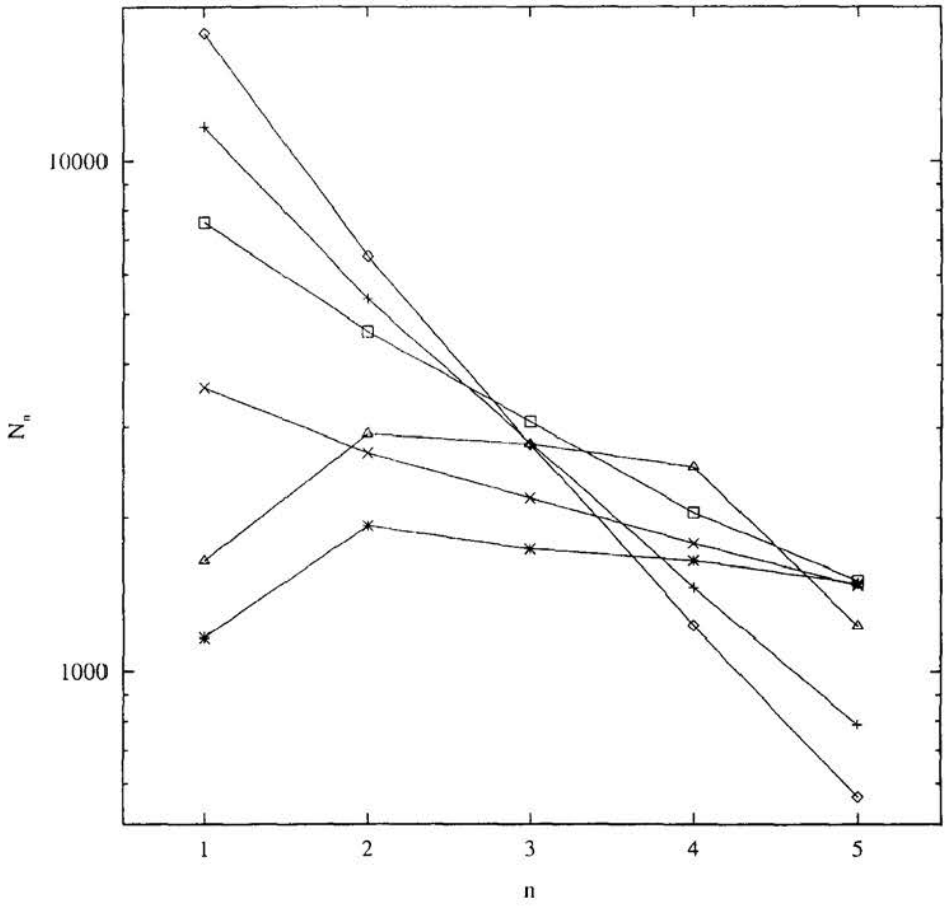

Fig. 20. Plots of $N_n(t)$ versus n for different aggregation times. Curves correspond to the following dimensionless time t/t_{agg}: ◊ (0.9 ± 0.1), + (1.7 ± 0.1), □ (2.9 ± 0.2), × (6.2 ± 0.3), Δ (7.2 ± 0.3), * (11.0 ± 0.6) [357].

scaling function, s(t), depends critically on its sign, Eq. (68). For this purpose, N_n is plotted as a function of n (Fig. 20). The cluster-size distribution is bell-shaped for aggregation times longer than 7.2 t_{agg}. As was stated at the end of the theoretical part of this article, cluster-size distributions exhibiting this behaviour have $\mu < 0$, Eq. (71). This allowed the number-average mean cluster size $\langle n_n \rangle$ to be used as the scaling function, s(t), Eq. (68). At this stage, $\Phi(x)$ may be determined by plotting $s^2(t)N_n(t)/N_0$ versus $x \equiv n/s(t)$ at different times, where $s(t) = \langle n_n \rangle$. Figure 21 shows $\Phi(x)$ corresponding to aggregation times from $t \approx t_{agg}$

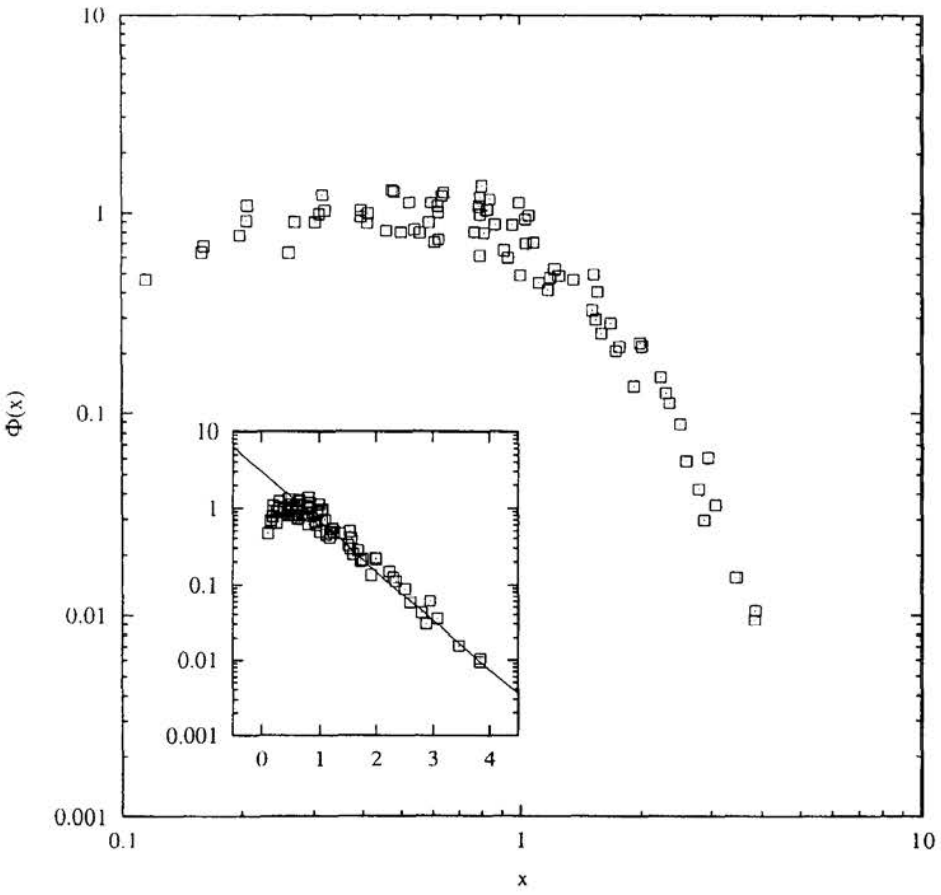

Fig. 21. Experimental time-independent scaling distribution $\Phi(x)$ corresponding to aggregation times from $t \approx t_{agg}$ up to $t \approx 11\ t_{agg}$ for clusters from monomers to pentamers. The semilog plot shows the behaviour of $\Phi(x)$ for $x > 1$ [357].

up to $t \approx 11\ t_{agg}$. The data collapses on a single time-independent master curve.

The fact that s(t) exhibits an asymptotic linear behaviour in time and that the data collapses on a single time-independent master curve proves dynamic scaling for the measured cluster-size distributions. It should be noted that this behaviour is observed for short aggregation times and small clusters. This is somewhat surprising since the scaling behaviour is strictly valid only for the limit of large clusters and long aggregation times. Recently, Thorn et al. [369] used a stochastic simu-

lation to recover the scaling behaviour of microsphere colloids. This simulation was carried out for a Brownian kernel and monodisperse initial conditions. They also observed that the final scaling limit is reached during early aggregation stages. This peculiar feature may also be seen for kernels as simple as the constant kernel. In order to illustrate this, we use the well known analytical solution of the Smoluchowski equation for constructing the corresponding scaling function, $\Phi(x)$. The data, represented in Fig. 22, correspond to our experimental conditions, i.e., clusters from monomers to pentamers and aggregation time from t_{agg} to 11 t_{agg}. One can clearly see that the data points define a time-independent master curve even for early aggregation stages. A slight difference may be observed for mono-

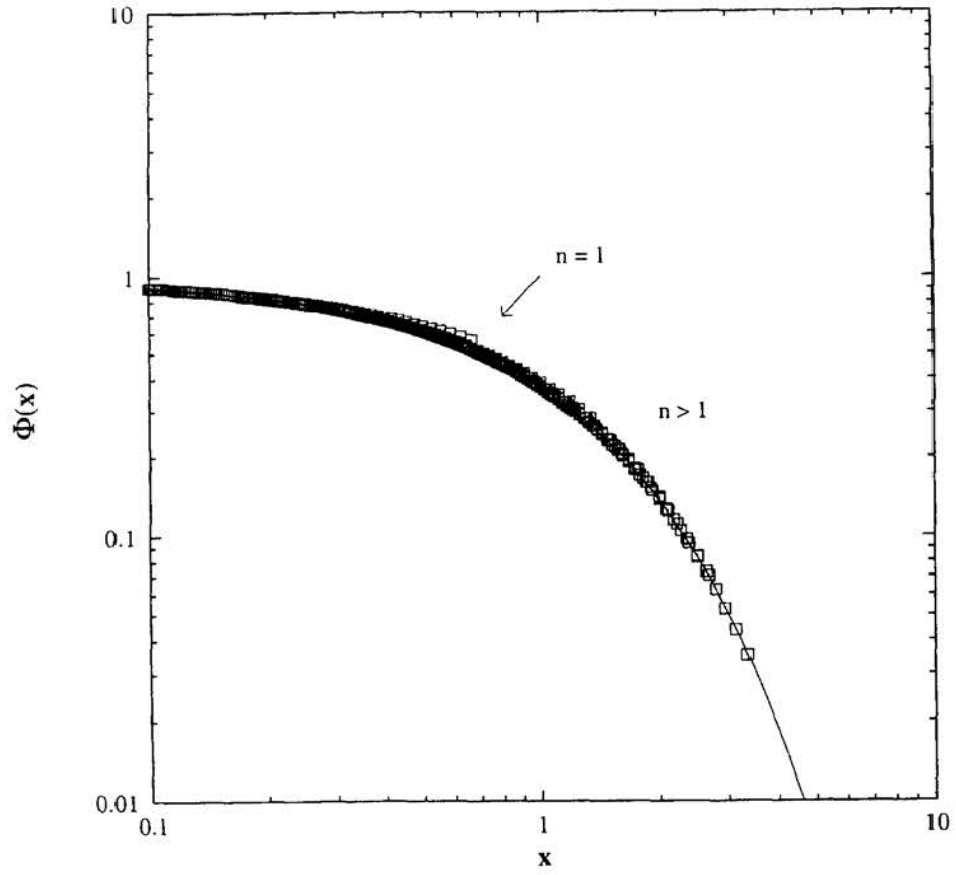

Fig. 22. Dynamic scaling form for the constant kernel. The data points correspond to clusters from monomers to pentamers and aggregation times from t_{agg} to 11 t_{agg}. The solid line is the theoretical scaling curve.

mers only, though it disappears over a period of time. Bigger clusters show perfect theoretical scaling (solid line). Here, as for the experimental data presented and the simulations mentioned above, the final scaling behaviour is observed for short times and small clusters. This makes it possible for the scaling formalism to be used to describe almost the entire aggregation process.

Knowledge about the scaling functions s(t) and $\Phi(x)$ reveals information about the aggregation mechanisms, since both contain the exponents λ and μ. Equation (67) predicts that the scaling function s(t) will grow as a power of time, $s(t) \sim t^{1/(1-\lambda)}$, where the exponent depends on the parameter λ. The linear asymptotic behaviour of $\langle n_n \rangle$, which is proportional to s(t), leads to $\lambda \approx 0$ (see Fig. 19). This value is confirmed by the decreasing exponential behaviour of $\Phi(x)$ for $x > 1$ (Fig. 21, bottom left corner). Several values of λ were tried for when fitting to the theoretical prediction Eq. (69). The best fit resulted in $\lambda \approx 0$, which is in line with other DLA experiments [5,304,370,371]. Unfortunately, the experimental uncertainty in $\Phi(x)$ does not allow the value of λ to be found accurately.

The parameter μ has already been observed to be negative due to the depletion of smaller clusters appearing for the curves N_n vs. n at longer aggregation times (Fig. 20). This indicates that small clusters bind preferentially to big clusters. A constant kernel is not suitable for describing this process since it predicts $\mu = 0$, leading to a size distribution always decreasing with n. The characteristic depletion of small clusters under diffusion-limited conditions has also been observed in computer simulations [372], as well as in experiments on the aggregation of gold particles [351] and polystyrene microspheres [8]. The latter authors found that the size distributions reach peaks for times longer than 8.3 t_{agg} which is consistent with our experimental result 7.2 t_{agg}. Information on parameter μ is also contained in the $x < 1$ region of the scaling function $\Phi(x)$. The non-decreasing behaviour of this function once again confirms the negative sign of μ, Eq.(70).

The experimental results are now compared with theoretical models in order to give them a physical, meaningful interpretation. The first kernel developed to describe diffusion-controlled aggregation processes was proposed by Smoluchowski [308]. He obtained the reaction rate as a collision cross section due to the diffusion of spheres of radius R. His result

$$k_{ij} = 4\pi(R_i + R_j)(D_i + D_j) \sim (i^{1/3} + j^{1/3})(i^{-1/3} + j^{-1/3}) \tag{75}$$

is a kernel with $\lambda = 0$ and $\mu = -1/3$, where $D = k_B T/6\pi\eta R$.

A more realistic description may be made when clusters are considered to be fractal in structure. Using $R_i = R_0\, i^{1/df}$ and $D_i = (k_B T/6\pi\eta R_0)\, i^{-1/dh}$ for the particle radius and diffusion

$$k_{ij} = \frac{2k_B T}{3\eta}\left(i^{\frac{1}{d_f}} + j^{\frac{1}{d_f}}\right)\left(i^{-\frac{1}{d_h}} + j^{-\frac{1}{d_h}}\right) \tag{76}$$

where d_f and d_h are the fractal dimension and hydrodynamic fractal dimension, respectively [373]. For this kernel, the aggregation exponents are $\lambda = 1/d_f - 1/d_h$ and $\mu = -1/d_h$. In the experiments described above, $\lambda \approx 0$ was found and therefore $d_f \approx d_h$, which is confirmed by direct measurements of d_f and d_h [374]. This kernel also predicts a negative value for μ, agreeing with our experimental results. A computer simulation, carried out by Thorn et al. [368] using precisely this kernel with the widely accepted value $d_f = 1.75$ and $d_f \approx d_h$ reproduced a bell-shaped curve for the scaling function $\Phi(x)$ which agrees perfectly with experimental results.

Cluster-size distribution and rate constant in reaction and intermediate aggregation

The time evolution of the clusters slows down substantially when decreasing the salt concentration in the suspensions. Broide et al. [8] found the rate of aggregation to be $k_{11} = (2.63 \pm 0.02) \times 10^{-14}\ cm^{-3}\ s^{-1}$. They calculate the value $W = 418 \pm 4$ for the stability factor. Their measurements were carried out by a single particle detection instrument.

The cluster distribution dependence of the cluster size is shown in Fig. 23 for different aggregation stages with $T = t/t_{agg}$. As T increases the distribution for slow aggregation develops a power-law decay in n given by $N_n \sim n^{-\tau}$, with $\tau \approx 1.5$. This power-law behaviour suggests that the kernel has $\mu \geq 0$ which is distinctly different from the values observed for fast aggregation. The time dependence of the cluster-size distribution for the late stages of slow aggregation is given by $N_n \sim T^{-1}$. For kernels with $\mu > 0$ Eq. (71) predicts that $N_n \sim T^{-1}\, n^{-(1+\lambda)}$. Thus, the experimental form for the cluster-size distribution suggests that $\lambda \approx 0.5$.

Dynamic scaling

For size distributions exhibiting a power-law decay the scaling function is $s(t) \sim \langle n_n \rangle^{1/(2-\tau)}$. Assuming $\tau \approx 1.5$ the relationship $s(t) \sim \langle n_n \rangle^2$ is deduced for slow aggregation. $\Phi(x)$ is determined by plotting $s^2(t)N_n(t)/N_0$ versus $x \equiv n/s(t)$ for different times, where $s(t) = \langle n_n \rangle^2$. Figure 24 shows

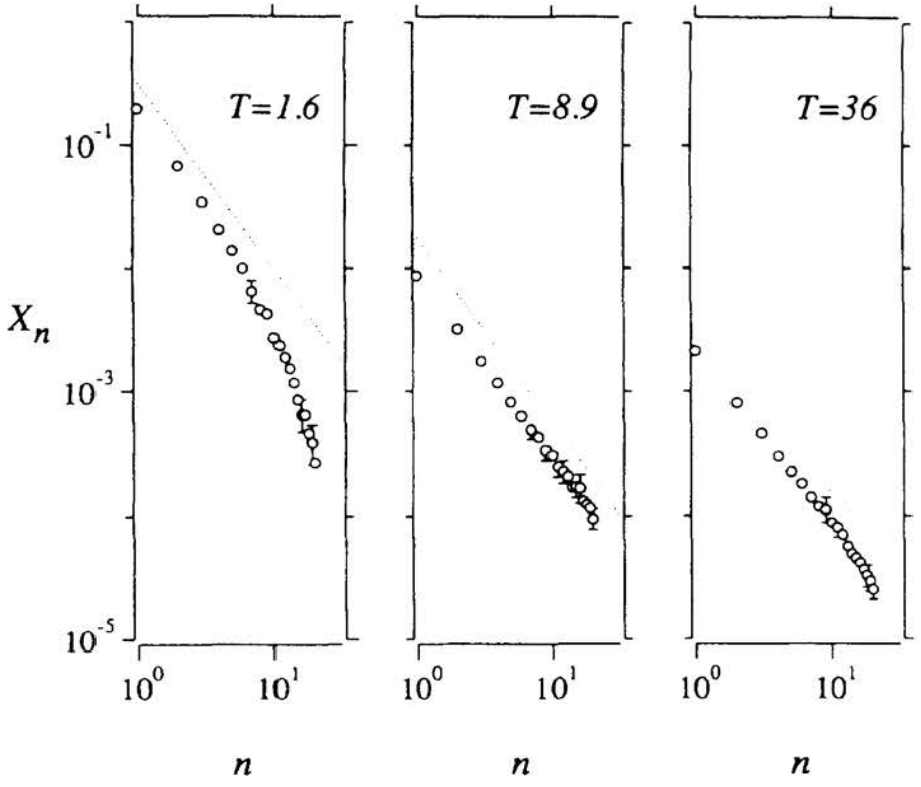

Fig. 23. Cluster distribution dependence on the cluster size for different aggregation stages [8].

$\Phi(x)$ corresponding to aggregation times from $t \approx t_{agg}$ up to $t \approx 39\ t_{agg}$. The data collapses on a single time-independent master curve. The theoretical prediction for the large-x behaviour of $\Phi(x)$, Eq. (69), also supports the hypothesis that $\lambda \approx 0.5$. The function $\Phi(x) \sim x^{-0.5} \exp(-1.33\ x)$ results in a satisfactory fit to the data for $\Phi(x > 1)$. The small-x behaviour of $\Phi(x)$, $\Phi(x << 1) \sim x^{-\tau}$, demonstrates that the kernel for slow aggregation has $\mu \geq 0$ (Eq. (70)) and the finding that $N_n \sim T^{-1}$ suggests that $\mu > 0$. Equation (71) predicts $\tau = 1 + \lambda$ and experimentally $\tau = 1.5$ is found from the slope of the data in Fig. 24, which implies $\lambda = 0.5$.

Direct [300,370,375,376] and indirect [303] measurements of size distributions for slow aggregation have shown that $\tau = 1.5$. In other studies [377] higher values of τ have been found, 1.8–2.0. Also, dynamic light-scattering studies of slow aggregation have shown that the hydrodynamic radius grows exponential in time [3,4,302,303,371,377,378],

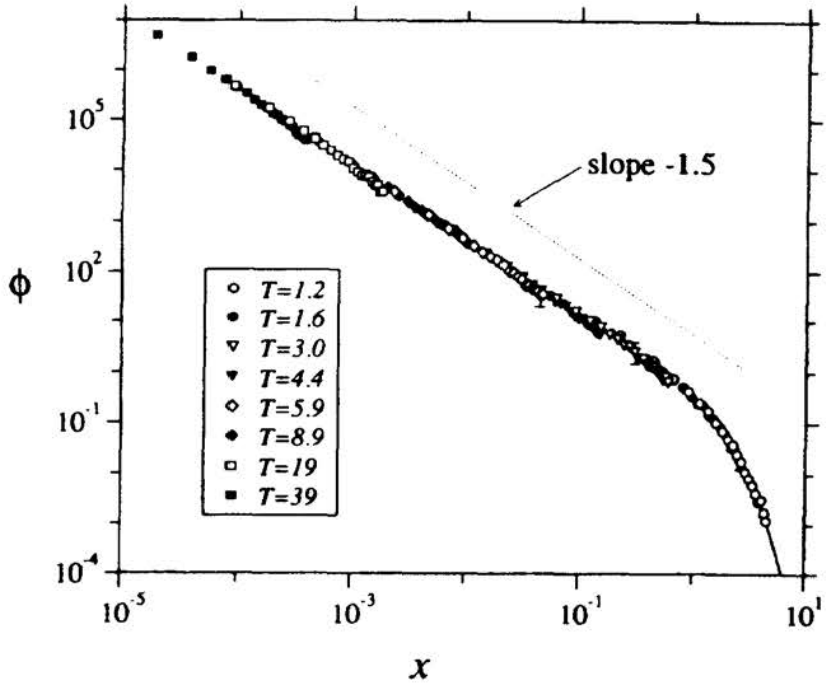

Fig. 24. Φ(x) corresponding to aggregation times from $t \approx t_{agg}$ up to $t \approx 39\ t_{agg}$ [304].

which implies $\lambda = 1$. The results of these studies are consistent with those expected for RLCA. However, there are several experiments which do not observe exponential growth for slow aggregation [4–6,370,376, 379,380]. Other experiments [5,379,380] show $\lambda \approx 0.5$ with no observed exponential growth. Lin et al. found deviations from exponential growth for slow aggregation of polystyrene microspheres and deviation absent in experiments involving silica and gold particles. Pefferkorn et al. also observed an increasing power-law for the number-average mean cluster size, $\langle n_n \rangle$ and their results suggest that $\tau = 1.5$ is a universal characteristic of slow aggregation. These authors did not see exponential growth in any of the experiments. It has been shown [381] that the values of τ and λ depend on the details of the rate-limiting step. If the probability for two clusters to combine depends only on the time they spend in contact with each other, the values $\lambda = 1$ and $\tau = 1.75$ are found (exponential growth). When the probability depends only on the number of times that they collide with each other, then $\lambda \approx 0.5$–0.6 and $\tau = 1.5$ are found. It is possible that the different types of aggregation kinetics depend on the differences in the colliding mechanism.

When the experimental conditions lie between DLCA and RLCA, λ changes continuously from 0 to 0.5 as the aggregation conditions change from fast to slow aggregation [5,6]. Differences between authors exist; for example, Zhou and Chu [378] show that λ changes from 0 to 1.

7.5. *Effect of the particle surface charge density*

In this section we address the following question: how does the particle surface charge density affect the aggregation kinetics in processes induced at high salt concentration? In other words, how does the aggregation mechanism depend on the residual interaction between the particles? The detailed cluster-size distribution of aggregating colloids of polystyrene microspheres, was measured by single particle light scattering. We carried out a series of measurements for different surface charge densities at high salt concentration [382].

The experimental system was a conventional polystyrene latex with negative surface charge due to sulphate groups. The radius of the spherical microspheres, 292 ± 19 nm, was determined by T.E.M. The electrophoretic mobility of the particles, μ_e, was measured to control the modification in charge produced by pH. μ_e was determined as a function of pH at 0.015 M of ionic concentration. For every case it was found that $\mu_e < 0$, which confirmed the negative sign of the surface charge. Mobility was converted into ζ-potential using Smoluchowski's theory [48,91]. The electrokinetic surface charge, σ_{ek}, was calculated using the Gouy–Chapman model for the e.d.l. [48]. Table 3 shows the three experimental cases studied. In case I, the system is practically at its isoelectric point and therefore $\sigma_{ek} \approx 0$. In case II, the electrokinetic charge is larger by an order of magnitude than in the previous case, and in case III the charge is larger by a further factor of 2. Table 3 also shows the critical KCl concentration of the suspensions at different pH and the stability factor, $W = k_s^{brow}/k_s^{exp}$, for the different experimental cases. For cases I and II, DLCA conditions are satisfied. For case III, the stability factor is higher than in the previous cases. This is due to repulsive forces appearing when the surface charge of the particles increases. Thus, in case III, DLCA conditions are not completely achieved.

In all cases, we found that distributions exhibit dynamic scaling for times longer than t_{agg}. For particles with low surface charge density, the scaled size-distribution is bell-shaped (Fig. 25), with a shift appearing at the maximum position when the charge increases. In this case, the kernel is characterized by the parameters $\lambda \approx 0$ and $\mu < 0$ [382], which

TABLE 3

Electrophoretic mobility, electrokinetic charge density and stability of the colloidal particles for the three experimental cases

Experimental case	pH	$-\mu_e/10^{-8}$ ($m^2\ V^{-1}\ s^{-1}$)	$-\sigma_{ek}/10^{-2}$ (C/m^2)	c.c.c. (M)	W
I	2.3 ± 0.1	0.2 ± 0.1	0.1 ± 0.1	≈ 0.00	1.9 ± 0.2
II	4.2 ± 0.1	2.1 ± 0.2	0.8 ± 0.2	≈ 0.10	1.9 ± 0.2
III	9.3 ± 0.1	3.7 ± 0.2	1.5 ± 0.2	≈ 0.35	3.2 ± 0.4

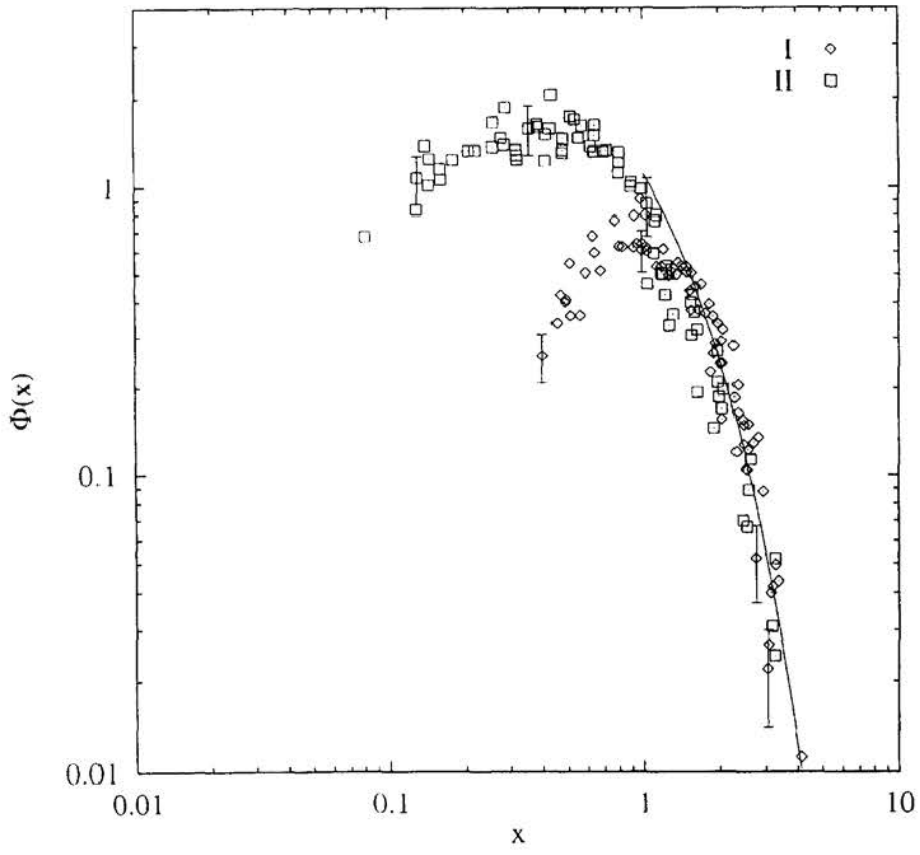

Fig. 25. Experimental Φ(x) distributions. The distributions are aligned for different times, showing dynamic scaling. For cases I (◊) and II (□), bell-shaped curves confirm the negative sign of μ. A shift in the maximum position is observed when the surface charge rises [382].

agrees with the value of the exponents for the Brownian kernel and with results obtained by simulation using this kernel [369]. Thus, for low surface charge densities, our results are in agreement with DLCA. Big clusters bind preferentially to small clusters. The shift in the position of the maximum might be due to a change in the value of the parameter μ towards zero [382]. Moreover, for low surface charge densities, the same value for W does not guarantee the same scaled distribution.

When the particle surface charge density increases even more, the distribution exhibits a power-law decay (Fig. 26), which demonstrates that the aggregation mechanism changes. In this case we found $\lambda \approx 0$ and $\mu > 0$. Thus, for the highest particle's surface charge density, the

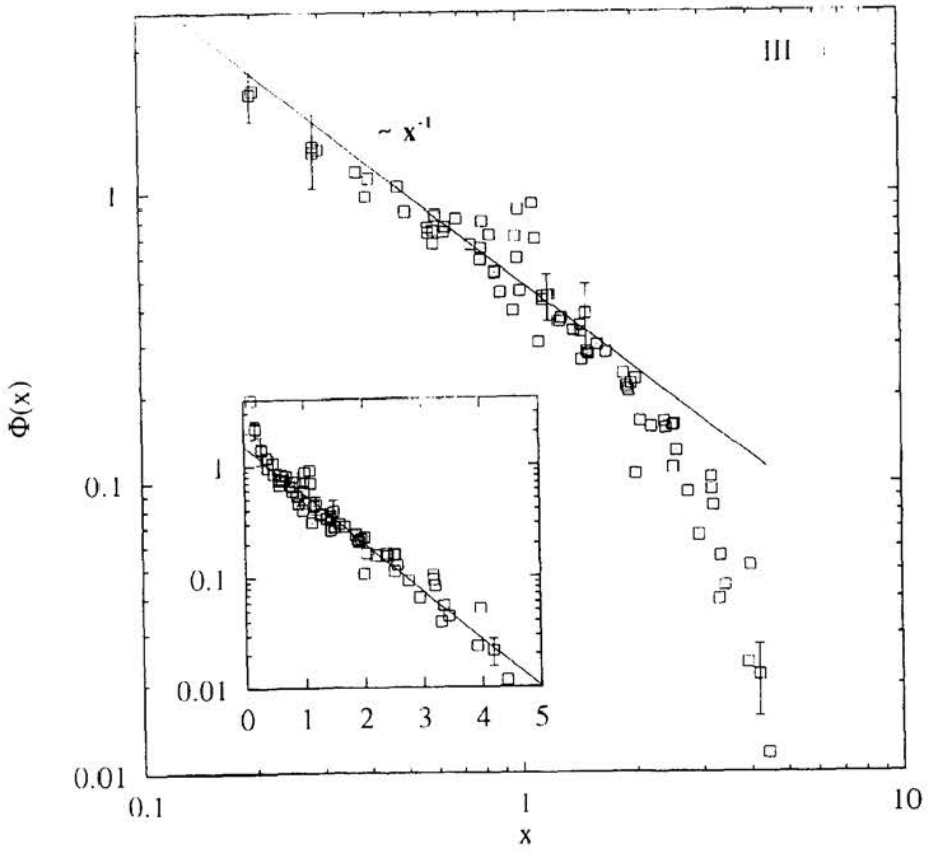

Fig. 26. For case III $\Phi(x)$ decays monotonically, demonstrating that the sign of μ has changed to $\mu \geq 0$. For $x > 1$, a decreasing exponential behaviour is shown in every case (solid lines), which suggests $\lambda \approx 0$ [382].

residual interaction controls the aggregation, and when this interaction increases, big clusters bind preferentially to big clusters. This result suggests that the residual electrostatic interaction could control the reactivity between big and small clusters.

8. Aggregation of polymer colloids in 2-D

Two-dimensional aggregation is a widely observed phenomenon in industrial applications. Most notable is the manufacture of emulsion polymers in stirred-tank reactors [383]. Colloidal particles are used in separation processes such as froth and solvent extraction. Then the emulsifying action [384] of colloidal particles at the bubble interfaces which plays a key role is dependent on the degree of surface aggregation [385].

For the description of two dimensional aggregation we can not use the mean field approximation used for the three dimensional case [386]. This is because in two dimensions, the fractal dimension [387] of the Brownian path is not less than the spatial dimension. Also, there is no equivalent for the Smoluchowski equation.

The theoretical studies of two dimensional aggregation processes can be classified into two groups: stability and aggregation studies.

8.1. Stability

The DLVO [388] theory can help us to study the aggregation in bulk but not in an interface. New expressions for the van der Waals, electrostatic and structural forces must be deduced. There are new elements like capillary attraction, intrinsic to interfacial phenomena with no analog in bulk aggregation. These capillary forces are due to the meniscus produced around a partly immersed particle. The calculation of the pair potential energy is dependent on the model used to describe wetting of the interfacial particle. The counter-ion cloud has lost its symmetry with respect to the plane of the interface, resulting in dipole–dipole repulsion between particles the strength of which can be reduced by increasing the subphase electrolyte concentration. If this reduction is large enough then the van der Waals attraction could be expected to dominate. Because of the different electric permittivities, the interaction between colloidal particles is different in the half upper than in the lower space.

Electrostatic interaction

An analog to the Poisson–Boltzmann equation has been developed by Lyne [389]. He has solved the Poisson–Boltzmann equation in the aqueous phase simultaneously with the Laplace equation in the dielectric phase. The Derjaguin [390] approximation can be used to estimate the electrostatic interaction under the condition that the range of the interaction is small compared with the particle's radius of curvature. If the particle part in the dielectric phase is considered to have no charge the strength of interaction between increases with increasing immersion.

van der Waals interaction

For partially immersed particles in the air–water interface, the van der Waals interaction is enhanced due to the particle exposure to the air phase. The Hamaker [391] development allows us to estimate the van der Waals interaction. The geometric mixing rule assumption for the dispersion interaction gives a simple expression for the Hamaker constant which is a function of the fraction of immersion, f, of the spherical particles [392]

$$A_{1,23,1} = A_{131} + f(A_{121} + A_{131}) \tag{77}$$

One needs to know the Hamaker constants for the interaction between particles fully immersed in both of the phases, A_{131} and A_{121}.

The retardation effect for the dispersion interaction was analyzed by Clayfield [393] and Gregory [394] for moderate and closer separations between two spheres, respectively.

Hydrophobic interaction

The hydrophobic properties of the particle's surface will determine the degree of wetting and thus the strength of hydrophobic forces. Partially wetted particles will experience a less interaction than fully wetted ones. Surface roughness affects the hydrophobic properties of the particles [395].

Christenson [396] has shown that the hydrophobic interaction decays exponentially for planar surfaces. Thus the Derjaguin approximation is useful to estimate the hydrophobic interaction between two partially immersed particles.

Capillary attraction

Capillarity has no equivalent in bulk aggregation. The depressed or elevated meniscus formed around a floating particle is the result of the equilibrium between the gravity, Archimedes pressure and surface tension. When two particles approach the curved meniscus generates a

pressure which enhances the aggregation process. To estimate the forces due to capillarity we need to solve the Laplace equation [397]. This equation has been solved for the simplest cases with axisymmetric geometries [398] and in the limit of small Bond number [399] (Bond No. = $\Delta\rho gr^2/\sigma_{23}$) when the Laplace equation can be linearized. Chan et al. [399] have found that the capillary attraction for particles smaller than 3.0 μm is negligible compared with thermal energy (kT). Thus the assumption of a flat meniscus is justified for the initial stages of the two dimensional aggregation of colloidal particles. For large aggregates however, the hydrophobic effect must be taken into account.

Total pair energy

To calculate the total pair energy we must add all the different contributions together: van der Waals, electrostatic, structural and capillary interactions.

The combination of the electrostatic and van der Waals interactions gives an equation similar to the DLVO theory. The assumption of a dry particle part without charge leads to a decreased stability for particles in the interface. This is due both to an increased van der Waals attraction and the diminished electrostatic repulsion. This DLVO-like equation has been studied in function of the electrolyte concentration and degree of particle immersion. This analysis shows a similarity with bulk aggregation. Higher electrolyte concentration reduces the electrostatic repulsion and as such destabilize the interfacial system. Moreover this destabilization might be due to a reversible flocculation into a secondary minimum at low concentration and to the disappearance of the potential barrier as the concentration increases [392]. The particle immersion effect onto the aggregation shows a decreasing stability for decreasing immersion. This loss of stability occurs due to the initial increase of the secondary minimum depth at immersion between 100% and 50% and the disappearance of the primary maximum at higher degrees of immersion [392].

The introduction of the hydrophobic attraction is quite difficult [400]. This difficulty is augmented since it has been shown that the Derjaguin approximation has been can not be applied for hydrophobic interaction where the curved surface plays a key role [401]. Hydrophobicity reduces stability. Contrary to the van der Waals attraction, the hydrophobic force increases in function of the particle wetting degree. When hydrophobic forces are considered the total potential loses its secondary minimum.

8.2. Aggregation kinetics

The theoretical studies of two dimensional aggregation have mainly focused on the analysis of the form and structure of the aggregates and the kinetics of the process. The structure irregularities described as fractal and their anisotropy has been analyzed. The initial stages of the aggregation kinetics can be described with a simple population balance which is structurally similar to the equation of Smoluchowski. Most studies of two dimensional colloidal aggregation use computer simulations.

Smoluchowski-like aggregation kinetic

The population balance applied to the two dimensional case gives the following equation

$$\frac{dc_k}{dt} = \frac{1}{2} \sum_{\substack{i=1 \\ i+j=k}}^{i=k-1} k_{ij}\, c_i\, c_j - \sum_{i=1}^{\infty} k_{ik}\, c_i\, c_k \tag{78}$$

which is equivalent to the Smoluchowski equation. c_j is the surface density of aggregates of size i and k_{ij} are the aggregation rate "constants" between particles of size i and j.

The evaluation of the rate constants for noninteracting particles is dependent on the analog construction of the Smoluchowski analysis of bulk aggregation. Thus the radial component of the Fick's law, in cylindrical coordinates, can be used to describe the Brownian motion of primary particles. This results in a rate constant for doublets that is not constant, but decreasing with time.

The comparison between particle collision frequencies for bulk and surface aggregation depends on particle size, liquid surface to volume ratio, time and particle density number. A comparison was made by Williams and Berg [402]. They showed that the frequency of collision in bulk is 50 times greater than at the surface for their experimental system. As the aggregation proceeds bigger aggregates are generated. These bigger aggregates have lower mobility and higher radius. This two factors are enough counterbalanced that the k_{ij} constants can be considered practically independent with i and j [392].

Computer simulations

Computer simulations [403] give information about the behaviour of the modeled system. These models are easily generalized to study

system at different spaces dimensionalities [404]. Computer simulations allow one to introduce the particle's interactions without any approximation or linearization [405].

Diffusion Limited Aggregation (DLA) model models the aggregation of colloidal particles as the sticking on contact of a Brownian particle to a growing seed [406]. This model was modified by Kolb et al. [407] and by Meakin [408] to include the movement of all aggregates. The moving aggregates can stick at the first contact (DLCA, Diffusion Limited Clusters Aggregation) or with a probability less than 1 (RLCA, Reaction Limited Clusters Aggregation) [409,410]. Hierarchical [409] and polydisperse [410] models have been introduced to describe RLCA.

The generated clusters have a fractal structure [411] and their size distributions show scaling [412].

Fractal structure

The fractal dimension shows the static scaling and compactness of the aggregates. The most important used fractal dimension is that obtained from the relationship that exists between the clusters mass and their radius of gyration ($M \propto R_g^D$). There are other forms to obtain the fractal dimension: the nested squares and two pair density correlation function.

The anisotropy is due to the loss of the spherical symmetry of growing clusters. This loss is intrinsic to the cluster–cluster aggregation process. The anisotropy is defined [413] as the ratio between the bigger and smaller self-values of the inertia tensor for the clusters. The anisotropy value can be calculated by averaging the anisotropy values of each cluster (A) or by calculating the ratio between the averaged bigger and smaller self-values (A′). The different obtained [414] values for two dimensional cluster–cluster aggregation through simulation are summarized in Table 4.

TABLE 4

Dimension fractal and anisotropy ratios for two-dimensional cluster–cluster aggregation

	DLCA	RLCA
D	1.44 ± 0.04	1.55 ± 0.03
A	4.4 ± 0.2	3.6 ± 0.2
A′	5.7 ± 0.2	4.7 ± 0.2

The larger fractal dimension value for RLCA shows the greater compactness of the RLCA clusters due to slower binding process. The need for multiple contacts allows the smaller clusters to approach nearer to the centre of the bigger ones. This closer approach produces a lower anisotropy for RLCA than for DLCA.When the effect of electrostatic polarization of the clusters is introduced a lower fractal dimension value is obtained. For the two dimensional case this value is 1.26 ± 0.06 [415].

Dynamical scaling behaviour

The scaling behaviour was studied by Vicsek and Family [416] for the two dimensional DCLA. They studied the cluster size distribution as a function of cluster size and time. The proposed dynamic scaling function

$$n_s(t) \sim t^{-w} s^{-\tau} f(s/t^z) \tag{79}$$

supported their simulation results. Vicsek and Family showed that the scaling function leads to the relationship $w = (2 - \tau) z$ between the dynamic exponents w and z and the static exponent τ.

The cutoff function $f(x) \simeq 1$ for $x << 1$ and $f(x) << 1$ for $x >> 1$. The scaling function is expected to be valid in the limit of low densities and large s and t.

Later Kolb [417] developed a scaling theory for aggregation by means of kinetic of clustering clusters. Kolb demonstrated by introducing the kernel dependence $k(i,j) = i^w j^w$ into the Smoluchowski equation one obtains $2w = \alpha + (d - 2)/D$ for the relation between the fractal dimension D of cluster formed in a space with dimension d. Here α is the exponent that gives the velocity of a diffusing cluster as a function of its mass m: $vt(m) = m^{\alpha}$. For $\alpha = 0$ and $d = 2$ values w must be 0 and the scaling function

$$p\left(\frac{m}{\overline{m}(t)}\right) = N(m,t)\ \frac{\overline{m}(t)}{N(t)} \tag{80}$$

decay exponentially.

Botet and Jullien [418] derived an analytic expression for the size distribution and generalized the expression given by Kolb [417] for the relation between the scaling exponents $2w = \alpha + (d - d_w)/D$ where d_w stands for the dimension of the trajectory that is followed by the

clusters(d_w = 2 in DLCA). Meakin et al. [419] studied the scaling behaviour as a function of the cluster diffusivity. The diffusion constant of a cluster of size s is assumed to be proportional to s^{γ}. They found that the results were consistent with the scaling theory, and the exponents in $n_s(t)$ depended continuously on γ. There is a value γ_c for which the cluster size distribution crosses from a monotonically decreasing function to a well shaped curve which can be described by the scaling form $n_s(t) = s^{-2}f(s/t^z)$ but with different scaling functions f and f'. A similar crossover has been described by Family et al. [420] for RLCA. They simulated the reaction limited aggregation process by using a sticking probability proportional to $(ij)^{\sigma}$, a power of the sizes' product. The system's behaviour depends on γ and σ values in a similar form. So for a fixed γ value there exists a σ_c that if $\sigma > \sigma_c$ the system behaves like DLCA and if $\sigma > \sigma_c$ the system behaviour is similar to standards RLCA. As the sticking probability is proportional to $(ij)^{\sigma}$ there is a crossover from RLCA\ to DLCA for large aggregation times.

Experimental results

The theoretical difficulties for studying two dimensional aggregation are counterbalanced by the number of experimental advantages. The visualization of the structure is direct and has not the problem of projection. Sedimentation of large aggregates does not represent a problem. Cluster size distribution is directly accessible. The high density limit and large time of aggregation can be studied too. In two dimensional aggregation there is no mechanical instability induced by bending or hydrodynamics stress.

Though two dimensional experiments has numerous advantages versus three dimensional until now the number of three dimension aggregation experiments greatly exceeds the number of two dimension experiments. The special properties of the interaction between interfacial particles was studied by Pieranski [421]. He observed the formation of two dimensional interfacial colloidal crystals. Polystyrene microspheres are trapped at water air interface. The asymmetry of charge distribution produces electrical dipoles associated with each interfacial particle. The dipole–dipole repulsive interaction organizes the polystyrene particles into a two dimensional lattice with triangular symmetry. This dipole–dipole interaction produces aggregates which repulsive interactions are anisotropic. This anisotropy account for the low dimensionality observed by Hurd and Schaefer [422] in the aggregation of silica microspheres at the air–water interface.

There are recent works that analyze the stability [402,423] and the crossover from RLCA to DLCA regimes [424–427].

Most important difference between the studies is related to the different described behaviours. Williams and Berg [402] have described the interfacial particles as having a special tendency to aggregate. This result is opposed to that of Robinson and Earnshaw [423] who suggest that the special stability of the particles must not directly related with the wetted area of the particle and not affected by electrolyte concentration of the subphase. Robinson and Earnshaw suggest that the incomplete wetting of the polystyrene particles may give rise to long-range electrostatic repulsions. The universality of RLCA and DLCA limits was studied by Robinson and Earnshaw [424–426] and by Stankiewicz et al. [427]. The transition from one regime to another was induced by adding salt to the subphase. This reduces the electrostatic repulsions and allows that the van der Waals force to dominate the aggregation process. Stankiewicz et al. has shown that the fractal dimension evolves from an initial value corresponding to DLCA towards a RLCA value. This evolution must be due to the restructuring of the particles that form part of the biggest aggregates. Their results were in good agreement with the dynamic scaling law $n_s(t) \sim s^{-2} f(s/t^z)$ for $z = 1$ and dilute latex dispersions. Robinson and Earnshaw have shown that the change occurs over a rather narrow range of electrolyte concentration [425]. This result is opposed to simulation results that predict a continuous change [420]. While the structure reflects two different behaviours, the kinetics results [425] exhibited a crossover from slow to rapid growth, as expected for reaction limited cluster–cluster aggregation. This implies that the probability of irreversible sticking was always very small. These results can be explained using the structural dynamics [425] concepts. The large clusters formed late in the aggregation process showed evidence of internal reorganization: the fractal dimension of the cores being significantly larger than that for the global cluster structure. Within error, the results [424] are in accord with the scaling relationship $w = (2 - \tau) z$.

Further investigations

Recent simulation studies have analyzed the reaction limited colloid aggregation using a different approach, i.e. by analyzing the sticking probability [428] and concentration [429] effects. For the lower sticking probabilities a crossover from slow to fast aggregation was demonstrated [429] and the scaling behaviour is verified [430].

Reversible aggregation was recently studied by Sintes et al. [431, 432], their results support the dynamical scaling behaviour except at very early times.

High density DLCA studies have been made [433]. These studies demonstrate that the dynamical structure factor, S(k,t), scales with the linear size of the aggregates, $R_g(t)$, according to $S(k,t) = R_g^{Df}F(k R_g(t))$, where D_f is the fractal dimension of the clusters and F is a universal scaling function.

Cluster–cluster gelation has been studied by Haw et al. [434]. Their simulation work demonstrates that the gel structure formed when given strong enough bonding is markedly different from the case where bonding is irreversible. Under the simulation limitation they have found a scaling for intermediate times [435].

To study two dimensional particle motion recent experimental studies have been using colloidal particles in thin aqueous suspensions layers [436]. For a layer thickness more than twice the particle size the experimental results agree well with experimental and theoretical three dimensional results. They also agree with Brownian dynamics simulations performed in two dimensions.

A numerical analysis of the influence of surface viscosity on the brownian motion of interfacial large particles [437] has revealed that for all contact angles the surface diffusivity strongly decrease with decreasing viscosity.

Capillary forces between colloidal particles appear to be strong enough to induce two-dimensional particle aggregation and ordering [438,439].

Long-range order [440] and topological correlation [441] has been reported for two dimensional aggregation. The structure factor scales for the DLCA regime and not for RLCA [440]. For moderately high fraction and for the diffusion limited regime the system exhibits ordering beyond the scale of fractal aggregates [442]. This ordering which persists into the gelled state arises from an effective inter-cluster repulsion due to mutually exclusive depletion zones surrounding each cluster. The ordering has been found to be stationary.

9. Conclusions

To derive a general explanation of the electrokinetic behaviour and colloidal stability of polymer colloids (even of those prepared by emulsifier-free emulsion polymerization) is impossible. This is because, the

structure of water near surfaces depends on a great number of hydrodynamic and physicochemical factors: surface charge density, type of charge group, oligomeric materials on polymer surface, cleaning procedure, surface structure and topography, hydration water of ions, superficial roughness, hydrophobicity of the polymer–solution interface, chemical composition of the polymer, etc. The interpretation of the electrokinetic properties of polymer colloids in the last two decades has gone through the following stages: (1) 1970s. The emulsifier-free polymer colloids are considered to be the "model" system to test electrokinetic theoretical approaches. (2) At the end of the 1970s. The mobility and ζ-potential present a minimum (or maximum) at intermediate concentrations of some indifferent electrolytes which is interpreted to be in contradiction with the theoretical predictions of Gouy–Chapman model. The ideality of polymer colloids is brought in question and the "hairy" layer model appears on the scene. (3) At the beginning of the 1980s. The dynamic Stern layer model is proposed as an alternative to explain the "anomalous" electrokinetic behaviour of polymer colloids since the diffuse layer model seems to be a failure. The co-ions adsorption mechanism is suggested as an explanation of the non-lineal dependence of ζ-potential with the electrolyte concentration. (4) At the middle of 1980s. According to several authors the different ζ-potential values obtained with two or more electrokinetic techniques (electrophoretic mobility and conductivity measurements, for instance) are due to "anomalous" surface conductance. (5) At the beginning of the 1990s. At first sight, the polymer colloids retrieve their character of "ideal" colloidal systems. The story is to be continued.

Acknowledgements

In the last few years a great number of colleagues have been helpful in discussing the electrokinetic properties, colloidal stability and aggregation kinetics of polymer colloids. We particularly want to thank Professor Bert Bijsterbosch, Mr. Ab van der Linde, Professor Marzio Giglio, Dr. Jacqueline Forcada, Dr. Martien Cohen-Stuart, Dr. Victor Shubin, and Professor Mohammed El-Aasser. This work is supported by the "Comisión Interministerial de Ciencia y Tecnología (CICYT)", project MAT 94-0560 and by "Junta de Andalucia (Grupo de Investigación 1218)".

References

[1] J. Lyklema, Colloids Surfaces A: Physicochem. Eng. Aspects, 92 (1994) 41.
[2] J. Ugelstad , P.C. Mørk, K.H. Kaggerud, T. Ellingsen and A. Berge, Adv. Colloid Interface Sci., 13 (1980) 101.
[3] M.Y. Lin, H.M. Lindsay, D.A. Weitz, R.C. Ball, R. Klein and P. Meakin, Nature, 339 (1989) 360.
[4] C. Cametti, P. Codastefano and P. Tartaglia, J. Colloid Interface Sci., 131 (1989) 409.
[5] D. Asnaghi, M. Carpineti, M. Giglio and M. Sozzi, Phys. Rev. A, 45 (1992) 1018.
[6] B.J. Olivier and C.M. Sorensen, Phys. Rev. A, 41 (1990) 2093.
[7] P.W. Zhu and D.H. Napper, Colloids Surfaces A: Physicochem. Eng. Aspects, 98 (1995) 93.
[8] M.L. Broide and R.J. Cohen, J. Colloid Interface Sci., 153 (1992) 493.
[9] H.J. Van den Hul and J.W. Vanderhoff, Brit. Polym. Sci., 2 (1970) 121.
[10] J.W. Vanderhoff, H.J. Van den Hul, R.J.M. Tausk and J.Th.G. Overbeek, in: G. Goldfinger (Ed.), Clean Surfaces: Their Preparation and Characterization for Interfacial Studies. p. 15. Marcel Dekker, New York, 1970.
[11] J.W. Goodwin, J. Hearn, C.C. Ho and R.H. Ottewill, Br. Polym. J., 5 (1973) 347.
[12] D.E. Yates, R.H. Ottewill and J.W. Goodwin, J. Colloid Interface Sci., 62 (1977) 356.
[13] K.-H. Lerche and G. Kretzschmar, Materials Sci. Forum, 25–26 (1988) 355.
[14] S.M. Ahmed, M.S. El-Aasser, G.H. Pauli, G.W. Poehlein and J.W. Vanderhoff, J. Colloid Interface Sci., 73 (1980) 388.
[15] Y. Chonde and I.M. Krieger, J. Colloid Interface Sci., 77 (1980) 138.
[16] T. Palberg, W. Härtl, U. Witting, H. Versmold, M. Würth and E. Simnacher, J. Phys. Chem., 96 (1992) 8180.
[17] F.J. de las Nieves, E.S. Daniels and M.S. El-Aasser, Colloids Surfaces, 60 (1991) 107.
[18] H. Tamai, K. Niino and T. Suzawa, J. Colloid Interface Sci., 131 (1989) 1.
[19] W.C. Wu, M.S. El-Aasser, F.J. Micale and J.W. Vanderhoff, in: P. Becher and M.W. Judenfreund (Eds.), Emulsions, Latices and Dispersions. Marcel Dekker, New York, 1978, p. 71.
[20] S.F. Schulz, T. Gisler, M. Borkovec and H. Sticher, J. Colloid Interface Sci., 164 (1994) 88.
[21] D. Bastos, J.L. Ortega, F.J. de las Nieves and R. Hidalgo-Álvarez, J. Colloid Interface Sci., 176 (1995) 232.
[22] A.A. Kamel, M.S. El-Aasser and J.W. Vanderhoff, J. Dispersion Sci. Technol., 2 (1981) 183.
[23] W.T. McCarvill and R.M. Fitch, J. Colloid Interface Sci., 64 (1978) 403.
[24] T.W. Healy and L.R. White, Adv. Colloid Interface Sci., 9 (1978) 303.
[25] M. Okubo, A. Yamada, and T. Matsumoto, J. Polym. Sci: Polym. Chem. Ed., 16 (1980) 3219.
[26] S.I. Alí, J.C. Steach and R.L. Zollars, Colloids Surfaces, 26 (1987) 1.
[27] B.R. Vijayendran, T. Bone and C. Gajiria, J. Appl. Polym. Sci., 26 (1981) 1351.
[28] W.M. Brouwer, Colloids Surfaces, 40 (1989) 235.

[29] J.A. Holgado, A. Martín, F. Martínez and M.A. Cabrerizo, Solid/Fluid Interfaces: Capillarity and Wetting: Dynamical Phenomena, Arnhem, The Netherlands, 1992.
[30] A. Martín, M.A. Cabrerizo and R. Hidalgo-Álvarez, Colloids Surfaces, A: Physicochem. Eng. Aspects (1996).
[31] D.H. Everett, M.E. Gültepe and M.C. Wilkinson, J. Colloid Interface Sci., 71 (1979) 336.
[32] M.E. Labib and A.A. Robertson, J. Colloid Interface Sci., 77 (1980) 151.
[33] W.T. McCarvill and R.M. Fitch, J. Colloid Interface Sci., 67 (1978) 204.
[34] J. Hen, J. Colloid Interface Sci., 49 (1974) 425.
[35] R. Rymdén, J. Colloid Interface Sci., 124 (1988) 396.
[36] K. Sakota and T. Okaya, J. Appl. Polym. Sci., 21 (1977) 1009.
[37] M. Hlavacek, P. Chenevière, M. Sardin and J. Dodds, Colloids Surfaces, A: Physicochem. Eng. Aspects, 95 (1995) 101.
[38] T. Gilány, Progr. Colloid Polym. Sci., 93 (1993) 45.
[39] F. Dobler, S. Affrossman and Y. Holl, Colloids Surfaces, A: Physicochem. Eng. Aspects, 89 (1994) 23.
[40] W. Grygiel and M. Starzak, J. Luminescence, 63 (1995) 47.
[41] D.A. Saville, Ann. Rev. Fluid Mech., 9 (1977) 321.
[42] B.H. Bijsterbosch and J. Lyklema, Adv. Colloid Interface Sci., 9 (1978) 147.
[43] S.S. Dukhin and V.N. Shilov, Adv. Colloid Interface Sci., 13 (1980) 153.
[44] M. Fixman, J. Chem. Phys., 72 (1980) 5177.
[45] R.H. Hunter, in R.H. Ottewill and R.L. Rowell (Eds), Zeta Potential in Colloid Science. Academic Press, 1981.
[46] D.C. Prieve, Adv. Colloid Interface Sci., 16 (1982) 321.
[47] A. Voigt, E. Donath and G. Kretzschmar, Colloids Surfaces, 47 (1990) 23.
[48] R. Hidalgo-Álvarez, Adv. Colloid Interface Sci., 34 (1991) 217.
[49] S.S. Dukhin, Adv. Colloid Interface Sci., 61 (1995) 17.
[50] J.A. Moleón, F.J. Rubio, F.J. de las Nieves and R. Hidalgo-Álvarez, J. Non-Equilib. Thermodyn., 16 (1991) 187.
[51] A. Delgado, F. González-Caballero and G. Pardo, J. Non-Equilib. Thermodyn., 10 (1985) 251.
[52] J.R. Goff and P. Luner, J. Colloid Interface Sci., 99 (1984) 468.
[53] R.W. O'Brien, J. Colloid Interface Sci., 171 (1995) 495.
[54] S. Levine and G.H. Neale, J. Colloid Interface Sci., 47 (1974) 520.
[55] C.S. Mangelsdorf and L.R. White, J. Chem. Soc. Faraday Trans., 86 (1990) 2859.
[56] C.S. Mangelsdorf and L.R. White, J. Chem. Soc. Faraday Trans., 88 (1992) 3567.
[57] R.W. O'Brien and L.R. White, J. Chem. Soc. Faraday Trans. II, 74 (1978) 1607.
[58] H. Ohshima, M. Nakamura and T. Kondo Colloid Polym. Sci., 270 (1992) 873.
[60] J.Th.G. Overbeek and B.H. Bijsterbosch, in: P.G. Righetti, C.J. van Oss and J.W. Vanderhoff (Eds.), Electrokinetic Separation Methods. Elsevier, Amsterdam, 1979.
[61] N.M. Semenikhin and S.S. Dukhin, Kolloidnyi Z., 37 (1975) 1123.
[62] M. Fixman, J. Chem Phys., 78 (1983) 1483.
[63] C.M. Ma, F.J. Micale, M.S. El-Aasser and J.W. Vanderhoff, in: D.R. Bassett and A.E. Hamielec (Eds.), Emulsion Polym. and Emulsion Polymerizat., ACS Symposium Washington D.C., Series 165, 1981, 251 pp.

[64] P. Stenius and B. Kronberg, in: G.W. Poehlein, R.H. Ottewill and J.W. Goodwin (Eds.), Science and Technology of Polymer Colloids II, Martinus Nijhoff, Boston, 1983.
[65] R. Xu, Langmuir, 9 (1993) 2955.
[66] R.H. Ottewill and J.N Shaw, J. Electroanal. Chem., 37 (1972) 133.
[67] R.H. Ottewill and J.N. Shaw, J. Colloid Interface Sci., 26 (1968) 110.
[68] A.A. Baran, L.M. Dudkina, N.M. Soboleva and O.S. Chechik, Kolloidn. Zh., 43 (1981) 211.
[69] D. Bastos and F.J. de las Nieves, Colloid Polym. Sci., 271 (1993) 860.
[70] R.S. Chow and K. Takamura, J. Colloid Interface Sci., 125 (1988) 226.
[71] M. Elimelech and C. R. O'Melia, Colloids Surfaces, 44 (1990) 165.
[72] R. Hidalgo-Álvarez, F.J. de las Nieves, A.J. van der Linde and B.H. Bijsterbosch, Colloid Polym. Sci., 267 (1989) 853.
[73] A.A. Kamel, C.M. Ma, M.S. El-Aasser, F.J. Micale and J.W. Vanderhoff, J. Disp. Sci. Technol., 2 (1981) 315.
[74] J.J. Spitzer, C.A. Midgley, H.S.G. Slooten and K.P. Lok, Colloids Surfaces, 39 (1989) 273.
[75] T. Okubo, Ber. Bunsenges. Phys. Chem., 91 (1987) 1064.
[76] D. Bastos and F.J. de las Nieves, Prog. Colloid Polym Sci., 93 (1993) 37.
[77] E. Donath, P. Kuzmin, A. Krabi and A. Voigt, Colloid Polym. Sci., 271 (1993) 930.
[78] F. Galisteo, F.J. de las Nieves, M. Cabrerizo and R. Hidalgo-Álvarez, Progr. Colloid Polym. Sci., 82 (1990) 313.
[79] A. Fernández, R. Martínez, M.A. Cabrerizo and R. Hidalgo-Álvarez, Colloids Surfaces, A: Physicochem. Eng. Aspects, 92 (1994) 121.
[80] W.M. Brouwer and R.L.J. Zsom, Colloids Surfaces, 24 (1987) 195.
[81] A. Delgado, F. González-Caballero and J. Salcedo, Acta Polymerica, 37 (1986) 361.
[82] K. Higashitani, H. Iseri, K. Okuhara, A. Kage and S. Hatade, J. Colloid Interface Sci., 172 (1995) 383.
[83] B.R. Midmore and R.J. Hunter, J. Colloid Interface Sci., 122 (1988) 521.
[84] H. Tamai, H. Hasegawa and T. Suzawa, J. Appl. Polym. Sci., 38 (1989) 403.
[85] R.T. Klingbiel, H. Coll, R.O. James and J. Texter, Colloids Surfaces, 68 (1992) 103.
[86] I.H. Harding and T.W. Healy, J. Colloid Interface Sci., 107 (1985) 382.
[87] M. Deggelmann, T. Palberg, M. Hagenbüchle, E.E. Maier, R. Krause, C. Graf and R. Weber, J. Colloid Interface Sci., 143 (1991) 318.
[88] M. Dittgen and B. Zosel, Colloid Polym. Sci., 269 (1991) 259.
[89] K. Ito, N. Ise, and T. Okubo, J. Chem. Phys., 82 (1985) 5732.
[90] K. Makino, S. Yamamoto, K. Fujimoto, H. Kawaguchi and H. Ohshima, J. Colloid Interface Sci., 166 (1994) 251.
[91] A. Fernández, A. Martín, J. Callejas and R. Hidalgo-Álvarez, J. Colloid Interface Sci., 162 (1994) 257.
[92] E. Donath, P. Kuzmin, A. Krabi and A. Voigt, Colloid Polym. Sci., 271 (1993) 930.
[93] H. Ohshima, J. Colloid Interface Sci., 168 (1994) 269.
[94] H. Ohshima, Adv. Colloid Interface Sci., 62 (1995) 189.
[95] S. S. Dukhin, Adv. Colloid Interface Sci., 36 (1991) 219.
[96] D. Bastos, R. Santos, J. Forcada, F.J. de las Nieves and R. Hidalgo-Álvarez, Colloids Surfaces, A: Physicochem. Eng. Aspects, 92 (137) 1994.

[97] B.J. Marlow and R.L. Rowell, Langmuir, 7 (1991) 2970.
[98] J. H. Prescott, S.-j. Shiau and R. Rowell, Langmuir, 9 (1995) 2071.
[99] A. Martín, M.A. Cabrerizo and R. Hidalgo-Álvarez, Anales Fis., 91 (1995) 100.
[100] S-L. Tsaur and R.M. Fitch, J. Colloid Interface Sci., 115 (1987) 450.
[101] S-L. Tsaur and R.M. Fitch, J. Colloid Interface Sci., 115 (1987) 463.
[102] H.J. Van den Hul and J.W. Vanderhoff, J. Electroanal. Chem., 37 (1972) 161.
[103] R. Hidalgo-Álvarez, F.J. de las Nieves, A.J. van der Linde and B.H. Bijsterbosch, Colloids Surfaces, 21 (1986) 259.
[104] J. Th. G. Overbeek, Adv. Colloid Sci. 3, 97 (1950).
[105] F. Booth, Proc. Roy. Soc. London, Ser. A, 203 (1950) 514.
[106] P.H. Wiersema, A.L. Loeb and J.Th.G. Overbeek, J. Colloid Interface Sci., 22 (1966) 78.
[107] A. S. Russell, P.J. Scales, Ch. Mangeldorf and S. M. Underwood, Langmuir, 11 (1995) 1112.
[108] A.G. van der Put and B.H. Bijsterbosch, J. Colloid Interface Sci., 92 (1983) 499.
[109] Th.J.J. van den Hoven and B.H. Bijsterbosch, J. Colloid Interface Sci., 115: 2 (1987) 559.
[110] Th.J.J. van den Hoven and B.H. Bijsterbosch, Colloids Surfaces, 22 (1987) 187.
[111] F.J. Rubio, J. Non-Equilib. Thermodyn. 17 (1992) 333.
[112] R. Hidalgo-Álvarez, J.A. Moleón, F.J. de las Nieves and B.H. Bijsterbosch, J. Colloid Interface Sci., 149 (1992) 23.
[113] R. de Backer and Q. Watillon, Berichte VI. International Kongress grenzflächen-akt. Stoffe, Carl Hanser Verlag, p. 651 München, 1972.
[114] F.J. Rubio, R. Hidalgo-Álvarez, F.J. de las Nieves, B.H. Bijsterbosch and A.J. van der Linde, Progr. Colloid Polym. Sci., 93 (1993) 341.
[115] R.W. O'Brien, J. Colloid Interface Sci., 110 (1986) 477.
[116] A. Vernhet, M.N. Bellon-Fontaine and A. Doren, J. Chim. Phys., 91 (1994) 1728.
[117] B.V. Derjaguin, G.P. Sidorenko, E.A. Zubashchenko and E.V. Kiseleva, Kolloidn. Zh., 9 (1947) 335.
[118] J.L. Anderson, Physicochem. Hydrodynam., 1 (1980) 51.
[119] D.C. Prieve, J.L. Anderson, J.P. Ebel and M.E. Lowell, J. Fluid Mech., 148 (1984) 247.
[120] D.C. Prieve and R. Roman, J. Chem. Soc. Faraday Trans. 2, 83 (1987) 1287.
[121] J.P. Ebel, J.L. Anderson and D.C. Prieve, Langmuir, 4 (1988) 396.
[122] J.L. Anderson and D.C. Prieve, Langmuir, 7 (1991) 403.
[123] R.W. O'Brien, D.W. Cannon and W.N. Rowlands J. Colloid Interface Sci., 173 (1995) 406.
[124] M. Kosmulski and E. Matijevic, J. Colloid Interface Sci., 150 (1992) 291.
[125] P.O. Staffeld and J.A. Quinn, J. Colloid Interface Sci., 130 (1989) 69.
[126] P.O. Staffeld and J.A. Quinn, J. Colloid Interface Sci., 130 (1989) 88.
[127] H.J. Keh and T.Y. Huang, Collloids Surfaces A. Physicochem. Eng. Aspects, 92 (1994) 51.
[128] S.S. Dukhin and V.N. Shilov, Dielectric Phenomena and the Double Layer in Disperse Systems and Polyelectrolytes. Wiley, New York, 1974.
[129] E.H.B. Delacey and L.R. White, J. Chem. Soc. Faraday Trans. 2, 77 (1981) 2007.
[130] M.M. Springer, A. Korteweg and J. Lyklema, J. Electroanal. Chem., 153 (1983)

55.
[131] B.R. Midmore, R.J. Hunter and R.W. O'Brien, J. Colloid Interface Sci., 120 (1987) 210.
[132] J. Kijlstra, H.P. van Leeuwen and J. Lyklema, J. Chem. Soc. Faraday Trans., 88: 2 (1992) 3441.
[133] I.A. Razilov, G. Pendze and S.S. Dukhin, Colloid J., 56 (1994) 612.
[134] D.E. Dunstan and L.R. White, J. Colloid Interface Sci., 152 (1992) 308.
[135] L.A. Rosen, J.C. Baygents and D.A. Saville, J. Chem. Phys., 98 (1993) 4183.
[136] R. Barchini and D.A. Saville, J. Colloid Interface Sci., 173 (1995) 86.
[137] F. Carrique, L. Zurita and A.V. Delgado, Colloids Surfaces, A: Physicochem. Eng. Aspects. 92 (1994) 9.
[138] D.A. Saville, Colloids Surfaces, A: Physicochem. Eng. Aspects, 92 (1994) 29.
[139] J.C. Baygents, Colloids Surfaces, A: Physicochem. Eng. Aspects, 92 (1994) 67.
[140] A.S. Russell, P.J. Scales, Ch.S. Mangeldorf and L.R. White, Langmuir, 11 (1995) 1553.
[141] A.G. van der Put and B.H. Bijsterbosch, J. Colloid Interface Sci., 75 (1980) 512.
[142] B.R. Midmore, R.J. Hunter and R.W. O'Brien, J. Colloid Interface Sci., 120: 1 (1987) 210.
[143] L.A. Rosen and D.A. Saville, J. Colloid Interface Sci., 140 (1990) 82.
[144] B.R. Midmore and R.W. O'Brien, J. Colloid Interface Sci., 123: 2 (1988) 486.
[145] B.R. Midmore, D. Diggins and R. J. Hunter, J. Colloid Interface Sci., 129 (1989) 153.
[146] D.E. Dunstan and L.R. White, J. Colloid Interface Sci., 152 (1992) 297.
[147] D.E. Dunstan, J. Chem. Soc. Faraday Trans., 89 (1993) 521.
[148] R.W. O'Brien, J. Fluid Mech. 190 (1988) 71.
[149] R.W. O'Brien, B.R. Midmore, A. Lamb and R.J. Hunter, Faraday Discuss. Chem. Soc., 90 (1990) 1.
[150] R.O. James, J. Texter and P.J. Scales, Langmuir, 7 (1991) 1993.
[151] M. Loewenberg and R. W. O'Brien, J. Colloid Interface Sci., 150 (1992) 158.
[152] V.E. Shubin, R.J. Hunter and R.W. O'Brien, J. Colloid Interface Sci., 159 (1993) 174.
[153] R.W. O'Brien, D.W. Cannon and W.N. Rowlands, J. Colloid Interface Sci., 173 (1995) 406.
[154] F.N. Desai, H.R. Hammad and K.F. Hayes, Langmuir, 9 (1993) 2888.
[155] P.J. Debye, J. Chem. Phys., 1 (1933) 13.
[156] Booth F., Proc. R. Soc. Lond. A, 203 (1950) 533.
[157] J. Stone-Masui and A. Watillon, J. Colloid Interface Sci., 28 (1968) 187; 34 (1970) 327.
[158] I.G. Watterson and L.R. White, J. Chem. Soc. Faraday 2, 77 (1981) 1115.
[159] R.W. McDonogh and R.J. Hunter, J. Rheology, 27 (1983) 189.
[160] S.A. Ali and M. Sengupta, J. Colloid Interface Sci., 113 (1986) 172.
[161] A. Delgado, F. González-Caballero, M.A. Cabrerizo and I. Alados, Acta Polymerica (1987) 66.
[162] A. Chabalgoity, A. Martín, F. Galisteo and R. Hidalgo-Álvarez, Progr. Colloid Polym. Sci., 84 (1991) 416.
[163] S.M. Kontush, S.S. Dukhin and O.I. Vidov, Colloid J., 56 (1994) 579.
[164] S. Levine, J.R. Marriott, G. Neale and G.N. Neale, J. Colloid Interface Sci., 52

(1975) 136.
[165] A. van der Linde and B.H. Bijsterbosch, Colloids Surfaces, 41 (1989) 345.
[166] J. Aitken, Trans. Roy. Soc. Edimburgh, 32 (1883) 239.
[167] Y. Pawar, Y.E. Solomentsev and J.L. Anderson, J. Colloid Interface Sci., 155 (1993) 488.
[168] W.J. Lechnick and J.A. Shaeiwitz, J. Colloid Interface Sci., 102 (1984) 71.
[169] W.J. Lechnick and J.A. Shaeiwitz, J. Colloid Interface Sci., 104 (1985) 456.
[170] D.C. Prieve and R. Roman, Ann. N.Y. Acad. Sci., 404 (1983) 253.
[171] R.W. O'Brien, J. Colloid Interface Sci., 113 (1986) 81.
[172] J. Lyklema, S.S. Dukhin and V.N. Shilov, J. Electroanal. Chem. 143 (1983) 1.
[173] C. Ballario, A. Bonincontro and C. Cametti, J. Colloid Interface Sci., 54 (1976) 415; 72 (1979) 304.
[174] L.K.H. van Beek, Prog. Dielectrics, 7 (1967) 69.
[175] G. Schwarz, J. Phys. Chem., 66 (1962) 2636.
[176] J.M. Schurr, J. Phys. Chem., 68 (1964) 2407.
[177] H.P. Schwan, G. Schwarz, J. Mackurk and H. Pauly, J. Phys. Chem., 66 (1962) 2626.
[178] J. Lyklema, M.M. Springer, V.N. Shilov and S.S. Dukhin, J. Electroanal. Chem., 198 (1986) 19.
[179] L.A. Rosen and D.A. Saville, J. Colloid Interface Sci., 149 (1992) 542.
[180] R.W. O'Brien, Adv. Colloid Interface Sci., 16 (1982) 281.
[181] P.A. Saville, J. Colloid Interface Sci., 91 (1983) 34.
[182] L.P. Voegtli and C.F. Zukoski, J. Colloid Interface Sci., 141 (1991) 92.
[183] R.W. O'Brien, J. Colloid Interface Sci., 81 (1981) 234.
[184] A. Watillon and J. Stone-Masui, J. Electroanal. Chem., 37 (1972) 143.
[185] C.F. Zukoski IV and D.A. Saville, J. Colloid Interface Sci., 114 (1986) 45.
[186] C.F. Zukoski and D.A. Saville, J. Colloid Interface Sci., 107 (1985) 322.
[187] C.F. Zukoski and D.A. Saville, J. Colloid Interface Sci., 114 (1986) 32.
[188] C.F. Zukoski and D.A. Saville, J. Colloid Interface Sci., 132 (1989) 320.
[189] D.A. Saville, J. Colloid Interface Sci., 91 (1983) 34.
[190] M.R. Gittings and D.A. Savillle, Langmuir, 11 (1995) 798.
[191] R.W. O'Brien and W.T. Perrins, J. Colloid Interface Sci., 99 (1984) 10.
[192] V.E. Shubin, M.P. Sidorova, O.S Chechik and N.A. Sakharova, J. Colloid, 53 (1991) 168.
[193] B.R. Midmore and R.W. O'Brien, J. Colloid Interface Sci., 123 (1988) 486.
[194] B.R. Midmore, D. Diggins and R.J. Hunter, J. Colloid Interface Sci., 129 (1989) 153.
[195] T. Okubo, J. Colloid Interface Sci., 125 (1988) 380.
[196] A. Rutgers, Physica, 5 (1938) 13.
[197] J. Hermans, Phil. Mag., 25 (1938) 426.
[198] J. Enderby, Proc. Royal Soc. (Lond.) A, 207 (1951) 329.
[199] A.J. Babchin, R.S. Chow and R.P. Sawatzky, Adv. Colloid Interface Sci., 30 (1989) 111.
[200] F.N. Desai, H.R. Hammad and K.F. Haynes, Langmuir, 9 (1993) 2888.
[201] E. Yeager, J. Bugosh, F. Hovorka and J. McCarthy, J. Chem. Phys., 17 (1949) 411.
[202] E. Yeager, H. Dietrick and F. Hovorka, J. Acoust. Soc. Am., 25 (1953) 456.

[203] A. Rutgers and J. Vidts, Nature, 165 (1950) 109.
[204] U. Beck, R. Zana and E. Rohloff, Tappi, 61 (1978) 63.
[205] R.O. James, J. Texter and P.J. Scales, Langmuir, 7 (1991) 1993.
[206] R.W. O'Brien, D.W. Cannon and W.N. Rowlands, J. Colloid Interface Sci., 173 (1995) 406.
[207] M. James, R.H. Hunter and R. W. O'Brien, Langmuir, 8 (1992) 420.
[208] F.J. Rubio, J. Non-Equilib. Thermodyn., 18 (1993) 195.
[209] Th. F. Tadros, Colloids Surfaces, 18 (1986) 137.
[210] M. von Smoluchowski, Kolloidzeit, 18 (1916) 190.
[211] W. Krasny-Ergen, Kolloidzeit, 74 (1936) 172.
[212] E.J. Hinch and J.D. Sherwood, J. Fluid Mech., 132 (1983) 337.
[213] E.P. Honing, W.F. J. Pünt and P.H.G. Offermans, J. Colloid Interface Sci., 134 (1990) 169.
[214] J. Yamanaka, H. Matsuoka, H. Kitano and N. Ise, J. Colloid Interface Sci., 134 (1990) 92.
[215] O. Quadrat, L. Mrkvickova and J. Snuparek, J. Colloid Interface Sci., 123 (1987) 353.
[216] F.S. Chan, J. Blanchford and D. Goring, J. Colloid Interface Sci., 22 (1966) 378.
[217] J.E. Seebergh and J.C. Berg, Colloids Surfaces, A: Physicochem. Eng. Aspects, 100 (1995) 139.
[218] R. Zimhel and G. Lagaly, Colloids Surfaces, 22 (1987) 225.
[219] J.W.S. Goossens and A. Zembrod, Colloid Polym. Sci., 257 (1979) 437.
[220] J.H. Prescott, S. Shiau and R.L. Rowell, Langmuir, 9 (1993) 2071.
[221] S. Sasaki, Colloid Polym. Sci., 262 (1984) 406.
[222] J.W.S. Goossens and A. Zembrod, J. Dispersion Sci. Tech., 2 (1981) 255.
[223] B.M. Verdegan and M.A. Anderson, J. Colloid Interface Sci., 158 (1993) 372.
[224] H.J. van den Hul, J. Colloid Interface Sci., 92 (1983) 217.
[225] R. Zimehl, G. Lagaly and J. Ahrens, Colloid Polym. Sci., 268 (1990) 924.
[226] M. Von Smoluchowski, Z. Phys., 17 (1917) 557.
[227] N. Fuchs, Z. Phys., 89 (1934) 736.
[228] B.V. Derjaguin and L.D. Landau, Acta Physicochem. URSS, 14 (1941) 633.
[229] E.J.W. Verwey and J.Th.G. Overbeek, Trans. Faraday Soc., 42B (1946) 117.
[230] E.J.W. Verwey and J.Th.G. Overbeek, Theory of the Stability of Lyophobic Colloids. Elsevier, Amsterdam, 1948.
[231] O. Stern, Z. Elektrochem., 30 (1924) 508.
[232] J. Lyklema J. Colloid Interface Sci., 58 (1977) 242.
[233] B. Vincent, B.H. Bijsterbosch and J. Lyklema J. Colloid Interface Sci., 37 (1970) 171.
[234] J.Th.G. Overbeek, Adv. Colloid Interface Sci., 16 (1982) 17.
[235] E. Matijevic, K.G. Mathal, R.H. Ottewill and M. Kerker, J. Phys. Chem., 65 (1961) 826.
[236] H. Reerink and J.Th.G. Overbeek, Discuss Faraday Soc., 18 (1954) 74.
[237] R.M. Jayasuriya, M.S. El-Aasser and J.W. Vanderhoff, J. Polym. Sci. Chem. Ed., 23 (1985) 2819.
[238] R.H. Ottewill and J.N. Shaw, Discuss. Faraday Soc., 42 (1966) 154.
[239] J. Gregory, Adv. Colloid Interface Sci., 2 (1969) 397.

[240] D.C. Prieve and W.B. Russel, J. Colloid Interface Sci., 125 (1988) 1.
[241] R.L. Schild, M.S. El-Aasser, G.W. Poehlein and J.W. Vanderhoff, Emulsion Latexes and Dispersions. Dekker, New York, 1978.
[242] A. Watillon and A.M. Joseph-Petit, A.C.S. Symposium on Coagulation Coagulant Aids, 61, 1961.
[243] A.S.G. Curtisy and L. Hocking, Trans. Faraday Soc., 66 (1970) 138.
[244] A. Kotera, K. Furusawa and K. Kudo, Kolloid Z. Z. Polym., 240 (1970) 837.
[245] B. Goldstein and B.H. Zimm, J. Chem. Phys., 54 (1971) 4408.
[246] H. Krapp and G. Walter, J. Colloid Interface Sci., 39 (1972) 421.
[247] B.H. Bijsterbosch, Colloid Polym. Sci., 256 (1978) 343.
[248] R.A. Robinson and R.H. Stokes, Electrolyte Solutions. Butterworth, London, 1970.
[249] LL.A. Spielman, J. Colloid Interface Sci., 33 (1970) 562.
[250] E.P. Honig, G.J. Roebersen and P.H. Wiersema, J. Colloid Interface Sci., 36 (1971) 97.
[251] M.C. Herman and K.D. Papadopoulos, J. Colloid Interface Sci., 136 (1990) 385.
[252] A.M. Lenhoff, Colloids Surfaces, A: Physicochem. Eng. Aspects, 87 (1994) 49.
[253] M. Kostoglou and A.J. Karabelas, J. Colloid Interface Sci., 171 (1995) 187.
[254] Z. Adamczyk and P. Warszynski, Adv. Colloid Interface Sci., 63 (1996) 41.
[255] H. Ohshima, Adv. Colloid Interface Sci., 53 (1994) 77.
[256] J. Lyklema, Adv. Colloid Interface Sci., 2 (1968) 65.
[257] B. Vincent, Adv. Colloid Interface Sci., 4 (1974) 193.
[258] Th.F. Tadros in: Th.F. Tadros (Ed.), Effect of Polymer on Dispersion Properties. Academic Press, 1982.
[259] R. Evans and D.H. Napper, Kolloid Z. Z. Polym., 251 (1973) 329.
[260] D.W.J. Osmond, B. Vincent and F.A. Waite, Colloid Polym. Sci., 253 (1975) 676.
[261] E.L. Markor, J Colloid Sci., 6 (1951) 492.
[262] D.H. Napper, Polymeric Stabilization of Colloidal Dispersion. Academic Press, 1983.
[263] R.H. Ottewill, J. Colloid Interface Sci., 58 (1977) 357.
[264] B. Vincent, J. Edwards, S. Emmett and A. Jones, Colloids Surfaces, 18 (1986) 261.
[265] K. Tajima, M. Koshinuma and A. Nakamura, Colloid Polym. Sci., 270 (1992) 759.
[266] M.B. Einarson and J. Berg, J. Colloid Interface Sci., 155 (1993) 165.
[267] A. Marmu, J. Colloid Interface Sci., 72 (1979) 41.
[268] Q. Wang, J. Colloid Interface Sci., 145 (1991) 99.
[269] A.M. Sung and I. Piirma, Langmuir, 10 (1994)1393.
[270] C.J. Van Oss, M.K. Chaudhury and R.J. Good, Chem. Rev., 88 (1988) 927.
[271] S. Bárány, A.A. Baran, I. Solomentseva and L. Velichanskaya, American Chem. Soc., Chap. 31 (1994) 406.
[272] J. Skvarla, J. Colloid Interface Sci., 155 (1993) 506.
[273] S. Rawson, K. Ryan and B. Vincent, Colloids Surfaces, 34 (1988/89) 89.
[274] G.J. Fleer, J.M.H.M. Scheutjens and B. Vincent, ACS Symp, Ser., 240 (1984) 245.
[275] G.J. Fleer, J.M.H.M. Scheutjens and M.A. Cohen-Stuart, Colloids Surfaces, 31 (1988) 1.
[276] Th.F. Tadros and A. Zsednai, Colloids Surfaces, 49 (1990) 103.
[277] J.E. Seebergh and J.C. Berg, Langmuir, 10 (1994) 454.
[278] J.A. Maroto and F.J. de las Nieves, Colloids Surfaces A, 96 (1995) 121.

[279] J.A. Maroto and F.J. de las Nieves, Prog. Colloid Polym. Sci., 98 (1995) 89.
[280] A.M. Islam, B.Z. Chowdhry and M.J. Snowden, Adv. Colloid Interface Sci., 62 (1995) 109.
[281] H. Kihira and E. Matijevic, Adv. Colloid Interface Sci., 42 (1992) 1.
[282] B. Alince, J. Petlicki and T.G.M. van de Ven, Colloids Surfaces, 59 (1991) 265.
[283] H. Kihira, N. Ryde and E. Matijevic, Colloids Surfaces, 64 (1992) 317.
[284] S. Harley, D.W. Thompson and B. Vincent, Colloids Surfaces, 62 (1992) 163.
[285] H. Kitano, S. Iwai, N. Ise and T. Okubo, J. Am. Chem. Soc., 109 (1987) 6641.
[286] H. Nihira, N. Ryde and E. Matijevic, J. Chem. Soc. Faraday Trans., 88 (1992) 2379.
[287] H. Nihira and E. Matijevic, Langmuir, 8 (1992) 2855.
[288] N. Ryde and E. Matijevic, J. Chem. Soc. Faraday Trans., 90 (1994) 167.
[289] F. Dumont, G. Amerycks and A. Watillon, Colloids Surfaces, 51 (1990) 171.
[290] H. Lichtenfeld, H. Sonntag and Ch. Durr, Colloids Surfaces, 54 (1991) 267.
[291] M. Okubo, K. Ichikawa, M. Tsujihiro and Y. He, Colloid Polym. Sci., 268 (1990) 791.
[292] M. Okubo, Y. He and K. Ichikawa, Colloid Polym. Sci., 269 (1991) 125.
[293] S. Kim and C.F. Zukoski, J. Colloid Interface Sci., 139 (1990) 198.
[294] B.E. Rodriguez and E.W. Kaler, Langmuir, 8 (1992) 2376.
[295] R. Hogg, T.W. Healy and D.W. Fuerstenau, J. Chem. Soc., Faraday Trans. I, 62 (1966) 1638.
[296] J.G. Rarity and K.J. Randle, Opt. Acta, 31 (1984) 26.
[297] J.G. Rarity and K.J. Randle, J. Chem. Soc. Faraday Trans. I, 81 (1985) 285.
[298] F. Family and D.P. Landau (Eds.), Kinetics of Aggregation and Gelation. Elsevier/North-Holland, Amsterdam, 1984.
[299] D.H. Sutherland, J. Colloid Interface Sci., 25 (1967) 373.
[300] G.K. von Schulthess and G.B. Benedek, Macromolecules, 13 (1980) 939.
[301] J.E. Martin, J. P. Wilcoxon, D. Schaefer and J. Odinek, Phys. Rev. A, 41 (1990) 4379.
[302] G. Bolle, C. Cametti, P. Codastefano and P. Tartaglia, Phys. Rev. A, 35 (1987) 837.
[303] H.Y. Lin, H.M. Lindsay, D.A. Weitz, R.C. Ball, R. Klein and P. Meakin, Phys. Rev. A., 41 (1990) 2005.
[304] M. L. Broide and R. J. Cohen, Phys. Rev. Lett., 64 (1990) 2026.
[305] M. Carpineti and M. Giglio, Adv. Colloid Interface Sci., 46 (1993) 73.
[306] J. Stankiewicz, M. Cabrerizo, R. Hidalgo-Álvarez and F. Martínez, Progr. Colloid Polym. Sci., 93 (1993) 359.
[307] R. Jullien, Comments Cond. Mat. Phys., 13 (1987) 177.
[308] M. Von Smoluchowski, Z. Phys. Chem., 92 (1917) 129.
[309] T. Vicsek, Fractal Growth Phenomena. Word Scientific, 1992.
[310] B.B. Mandelbrot, The Fractal Geometry of Nature, Freeman W.H., 1982.
[311] R.M. Ziff, Kinetics of Aggregation and Gelation. Elsevier/North-Holland, 1984.
[312] S. Chandrasekhar, Rev. Mod. Physics, 15 (1943) 1.
[313] R.M. Ziff, M.H. Ernst and E.M. Hendriks, J. Phys. A: Math. Gen., 16 (1983) 2293.
[314] M.H. Ernst, R.M. Ziff and E.M. Hendriks, J. Colloid Interface Sci., 97 (1984) 266.
[315] F. Leyvraz and H.R. Tschudi, J. Phys. A 15, (1982) 1951.
[316] E.M. Hendriks, M.H. Ernst and R.M. Ziff, J. Stat. Phys., 31 (1983) 519.
[317] P.G.J. Van Dongen and M.H. Ernst, Phys. Rev Lett., 54 (1985) 1396.

[318] A.A. Lishnikov, J. Colloid Interface Sci., 45 (1973) 549.
[319] M.H. Ernst in: L. Pietronero and E. Tosatti (Eds.), Fractals in Physics. Elsevier/North-Holland, Amsterdam, 1986.
[320] R.C. Ball, D.A. Weitz, T.A. Witten and F. Leyvraz, Phys. Rev. Lett., 58 (1987) 274.
[321] T.W. Taylor and C.M. Sorensen, Phys. Rev. A, 36 (1987) 5415.
[322] B. Chu, Laser Light Scattering. Academic Press, London, 1991.
[323] R. Pecora, Dynamic Light Scattering. Plenum Press, New York, 1985.
[324] A. Lips, C. Smart and E. Willis, Trans Faraday Soc., 67 (1971) 2979.
[325] T. H. Herrington and B.R. Midmore, J. Chem. Soc. Faraday Trans., 85 (1989) 3529.
[326] J.W. Wirden and J.C. Berg, J. Colloid Interface Sci., 149 (1992) 528.
[327] L.L. Hoekstra, R. Vreeker and W.G.H. Agterof, J. Colloid Interface Sci., 151 (1992) 17.
[328] D.A. Weitz and H. Oliveira, Phys. Rev. Lett., 52 (1984) 1433.
[329] D.W. Schaefer, J.E. Martin, P. Wiltzius and D.S. Cannell, Phys. Rev. Lett., 52 (1984) 2371.
[330] M. Carpineti, F. Ferri, M. Giglio, E. Paganini and U. Perini, Phys. Rev. A, 42 (1990) 7347.
[331] E.G.M. Pelssers, M.C.A. Cohen-Stuart and G.J. Fleer, J. Colloid Interface Sci., 137 (1990) 350.
[332] E.G.M. Pelssers, M.C.A. Cohen-Stuart and G.J. Fleer, J. Colloid Interface Sci., 137 (1990) 362.
[333] M.S. Bowen, M.L. Broide and R.J. Cohen, J. Colloid Interface Sci., 105 (1985) 605.
[334] M.S. Bowen, M.L. Broide and R.J. Cohen, J. Colloid Interface Sci., 105 (1985) 617.
[335] P.G. Cummins, E.J. Staples, L.G. Thompson, A.L Smith and L. Pope, J. Colloid Interface Sci., 92 (1983) 189.
[336] N. Buske, H. Gedan, H. Lichtenfeld, W. Katz and H. Sonntag, Colloid Polym. Sci., 258 (1980) 1303.
[337] A. Elaissari and E. Pefferkorn, J. Chem. Phys., 95 (1991) 2919.
[338] S. Stoll, V. Lanet and E. Pefferkorn, J. Colloid Interface Sci., 157 (1993) 302.
[339] V.K. La Mer, R.H. Smellie and P.K.J. Lee, J. Colloid Interface Sci., 12 (1957) 230.
[340] E. Killman and E. Eisenhauer, in: Th.F. Tadros (Ed.), The Effect of Polymer on Dispersion Properties. Academic Press, 1982.
[341] R. Wolff, Kollöid Z., 150 (1957) 71.
[342] V.K. La Mer and T.W. Haly, Rev. Pure Appl. Chem., 13 (1963) 112.
[343] T. Hanoi and P. Sherman, Emulsion Science. Academic Press, 1968.
[344] M. Kerker, The Scattering of Light and Other Electromagnetic Radiations. Academic Press, 1969.
[345] G.E. Elicabe and L.H. García Rubio, J. Colloid Interface Sci. (1988).
[346] J.W.Th. Lichtenbelt, C. Pathmamanoharan and P.H. Wiersema, J. Colloid Interface Sci., 49 (1974) 281.
[347] P. Walstra and J. Brit, Appl. Phys. 15 (1964) 1545.
[348] H. Schnablegger and O. Gläter, J. Colloid Interface Sci., 158 (1993) 228.
[349] D.E. Koppel, J. Chem. Phys., 57 (1972) 4814.
[350] J.C. Brown and P.N. Pusey, J. Chem. Phys., 62 (1975) 1136.
[351] D.A. Weitz, J.S. Huang, H.Y. Lin and J. Sung, Phys. Rev. Lett., 54 (1984) 1416.
[352] L. Spielman and S.L. Goren, J. Colloid Interface Sci., 26 (1968) 175.

[353] J.G. Harfield, B. Miller, R.W. Lines and T. Godin, in: M.J. Groves (Ed.), Particle Size Analysis, 1978.
[354] R.W. Deblois, C.P. Bean and R.K.A. Wesley, J. Colloid Interface Sci., 61 (1977) 323.
[355] E. Pefferkorn and S. Stoll, J. Colloid Interface Sci., 138 (1990) 261.
[356] A. Fernández Barbero, PhD. Thesis, Universidad de Granada, 1994.
[357] A. Fernández-Barbero, A. Schmitt, M. Cabrerizo-Vílchez and R. Martínez-García, Physica A (in Press).
[358] J. Cahill, P.G. Cummins, E.J. Staples and L.G. Thompson, J. Colloid Interface Sci., 117 (1987) 406.
[359] L. Goren, J. Colloid Interface Sci., 36 (1971) 94.
[360] J. Cahill, P.G. Cummins, E.J. Staples and L.G. Thompson, Colloids Surfaces, 18 (1989) 189.
[361] H. Gedan, H. Lichtenfeld, H. Sonntag and H, J. Krug, Colloids Surfaces, 11 (1984) 199.
[362] W.I. Higuchi, R. Okada, G.A. Sterter and A.P Lenberger, J. Pharm. Sci., 52 (1963) 49.
[363] B.A. Mathews and C.T. Rhodes, J. Pharm. Sci., 57 (1969) 557.
[364] A. Lips and E.J. Willis, J. Chem, Soc, Faraday Trans., 69 (1973) 1226.
[365] W. Hatton, P. McFadyen and A.L. Smith, J. Chem, Soc, Faraday Trans. 70 (1974) 665.
[366] M.L. Broide and R.J. Cohen, J. Colloid Interface Sci., 105 (1985) 605.
[367] M.L. Broide and R.J. Cohen, J. Colloid Interface Sci., 105 (1985) 617.
[368] K. Higashitani, M Kondo and A. Matacle, J. Colloid Interface Sci., 142 (1991) 204.
[369] M. Thorn and M. Seesselberg, Phys. Rev. Lett., 72 (1994) 3622.
[370] E. Pefferkorn and R. Varoqui, J. Chem. Phys., 91 (1989) 5679.
[371] C. Aubert and D.S. Cannel, Phys. Rev. Lett., 56 (1986) 738.
[372] P. Meakin, Phys. Rev. A 32 (1985) 453.
[373] P. Meakin, Z. Chen and J.M. Deutch, J. Chem. Phys., 82 (1985) 3786.
[374] P. Wiltzius, Phys. Rev. Lett., 58 (1987) 710.
[375] D.A. Weitz and M.Y. Lin, Phys. Rev. Lett., 57 (1986) 2037.
[376] A. Elaissari and E. Pefferkorn, J. Colloid Interface Sci., 141 (1991) 522.
[377] J.E. Martin, Phys. Rev. A 36 (1987) 3415.
[378] Z. Zhou and B. Chu, J. Colloid Interface Sci., 143 (1991) 356.
[379] B.J. Olivier and C.M. Sorensen, J. Colloid Interface Sci., 134 (1990) 139.
[380] J. P. Wilcoxon, J. E. Martin and D.W. Schaefer, Phys. Rev. A, 39 (1989) 2675.
[381] P. Meakin and F. Family, Phys. Rev. A, 38 (1988) 2110.
[382] A. Fernández-Barbero, M. Cabrerizo-Vílchez, R. Martínez-García and R. Hidalgo-Álvarez, Phys. Rev. E (in Press).
[383] V. Lowry, M.S. E-Aasser, J.W.Vanderhoff, A. Klein and C.A. Silebi, J. Colloid Interface Sci., 112 (1986) 521.
[384] J.T. Long, Engineering for Nuclear Fuel Reprocessing. Gordon and Breach Science Publishing Inc., New York, (1967) 586.
[385] R.J. Pugh and L. Nishkov, in: Processing of Complex Ores, Ed., 1990, 87.
[386] K. Kang and S. Redner, Phys. Rev. A, 20 (1984) 2833.
[387] F. Hausdorff, Math. Ann., 79 (1919) 157.
[388] See for example, R.J. Hunter, Foundation of Colloid Science, Vol. 1. Clarendon

Press, Oxford University Press, New York, 1987.
[389] M.P. Lyne, Electrostatic Interactions between Interfacial Particles, M.S. Thesis, University of British Columbia, 1989.
[390] B.V. Derjaguin, Kolloid Z., 69 (1934), 155–164.
[391] H.C. Hamaker, Physica, 4 (1937) 1058.
[392] D.F. Williams, Aggregation of Colloidal Particles at the Air–Water Interface, Ph.D Thesis, University of Washington, 1991.
[393] E.J. Clayfield, E.C. Clumb and P.H. Mackey, J. Colloid Interface Sci., 37 (1071) 382.
[394] J.J. Gregory, J. Colloid Interface Sci., 83 (1981) 138.
[395] M.L. Gee and J.N. Israelachvili, J. Chem. Soc. Faraday Trans. 86 (1990) 4049.
[396] H.K. Christenson and P.M. Claesson, Science, 239 (1988) 390.
[397] A.W. Adamson, Physical Chemistry of Surfaces. Wiley-Interscience, 1990.
[398] W.A. Gifford and L.E. Scriven, Chem. Eng. Sci., 26 (1971) 287.
[399] D.Y.Chan, J.D. Henry and L.R.J. White, J. Colloid Interface Sci., 79 (1981) 410.
[400] Nicholson, D. and Parsonage, N.G., Computer Simulation and the Statistical Mechanics of Adsorption, 1982, Ch. 8, Academic Press, New York.
[401] J.N. Israelachvili and R.M. Pashley, Nature, 300 (1982) 341.
[402] D.F. Williams and C.J. Berg, J. Colloid Interface Sci., 152 (1992) 218.
[403] D.W. Heermann, Computer Simulation Methods in Theoretical Physics, Second Edition, Springer-Verlag, 1990.
[404] P. Meakin, Phys. Rev. A, 38 (1988) 4799.
[405] P. Meakin and M. Muthukumar, J/ Chem. Phys., 91 (1989) 3212.
[406] T.A. Witten Jr. and L.M. Sander, Phys. Rev. Lett., 47 (1981) 1400.
[407] M. Kolb, R. Botet and R. Jullien, Phys. Rev. Lett., 51 (1983) 1123.
[408] P. Meakin, Phys. Rev. Lett., 51 (1983) 1119.
[409] R. Jullien R. and M. Kolb, J. Phys. A: Math. Gen., 17 (1984) 639.
[410] W.D. Brown and R.C. Ball, J. Phys. A: Math. Gen., 18 (1985) 517.
[411] R. Jullien, CCACAA, 65 (1992) 215.
[412] P.Meakin, CCACAA, 65 (1992) 237.
[413] R. Botet and R. Jullien, J. Phys. A., 19 (1986) 907.
[414] R. Jullien R. and R. Botet, Aggregation and Fractal Aggregates, World Scientific, Singapore, 1987.
[415] R. Jullien, J. Phys. A, 19 (1986) 2129.
[416] T. Vicsek and F. Family, Phys. Rev. Lett., 52 (1984) 1669.
[417] M. Kolb, Phys. Rev. Lett., 53 (1984) 1653.
[418] R. Botet and R. Jullien, J. Phys. A: Gen., 17 (1984) 2517.
[419] P. Meakin, T. Vicsek and F. Family, Phys. Rev. B, 31 (1985) 564.
[420] F. Family, P. Meakin and F. Vicsek, J. Chem. Phys., 83 (1985) 4144.
[421] P. Pieranski, Phys. Rev. Lett., 45 (1980) 569.
[422] A.J. Hurd and D.W. Shaefer, Phys. Rev. Lett., 54 (1985) 1043.
[423] D.J. Robinson and J.C. Earnshaw, Langmuir, 9 (1993) 1436.
[424] D.J. Robinson and J.C. Earnshaw, Phys. Rev. A, 46 (1992) 2045.
[425] D.J. Robinson and J.C. Earnshaw, Phys. Rev. A, 46 (1992) 2055.
[426] D.J. Robinson and J.C. Earnshaw, Phys. Rev. A, 46 (1992) 2065.
[427] J. Stankiewicz, M.A. Cabrerizo and R. Hidalgo-Álvarez, Phys. Rev. E, 47 (1993)

2663.
[428] A.E. Gonzalez, Phys. Lett. A, 171 (1992) 293.
[429] A.E. Gonzalez, J. Phys. A: Math. Gen., 26 (1993) 4215.
[430] A.E. Gonzalez, Phys. Rev. E, 47 (1993) 2923.
[431] A.E. Gonzalez, Phys. Rev. Lett., 71 (1993) 2248.
[432] T. Sintes, R. Toral and A. Chakrabarti, Phys. Rev. A, 46 (1992) 2039.
[433] T. Sintes, R. Toral and A. Chakrabarti, Phys. Rev. E, 50 (1994) 2967.
[434] T. Sintes, R. Toral and A. Chakrabarti, Phys. Rev. E, 50 (1994) 3330.
[435] M.D. Haw, M. Sievwright, W.C.K. Poon and P.N. Pusey, Adv. Colloid Interface Sci., 62 (1995) 1.
[436] M.D. Haw, M. Sievwright, W.C.K. Poon and P.N. Pusey, Physica A, 217 (1995) 231.
[437] W. Schaertl and H. Sillescu, J. Colloid Interface Sci., 155 (1993) 313.
[438] K. Danov, R. Aust, F. Durst and U. Lange, J. Colloid Interface Sci., 175 (1995) 36.
[439] P.A. Kralchevsky and K. Nagayama, Langmuir, 10 (1994) 23.
[440] P.A. Kralchevsky, C.D. Dushkin, V.N. Paunov, N.D. Denkov and K. Nagayama, Progr. Colloid Polym Sci., 98 (1995) 12.
[441] D.J. Robinson and J.C. Earnshaw, Phys. Rev. Lett., 71 (1993) 715.
[442] J.C. Earnshaw and D.J. Robinson, Phys. Rev. Lett., 72 (1994) 3682.
[443] J.C. Earnshaw and D.J. Robinson, Physica A, 214 (1995) 23.